ISSN 1018-5593

Commission of the European Communities

nuclear science and technology

Natural analogue and microstructural studies in relation to radionuclide retardation by rock matrix diffusion in granite

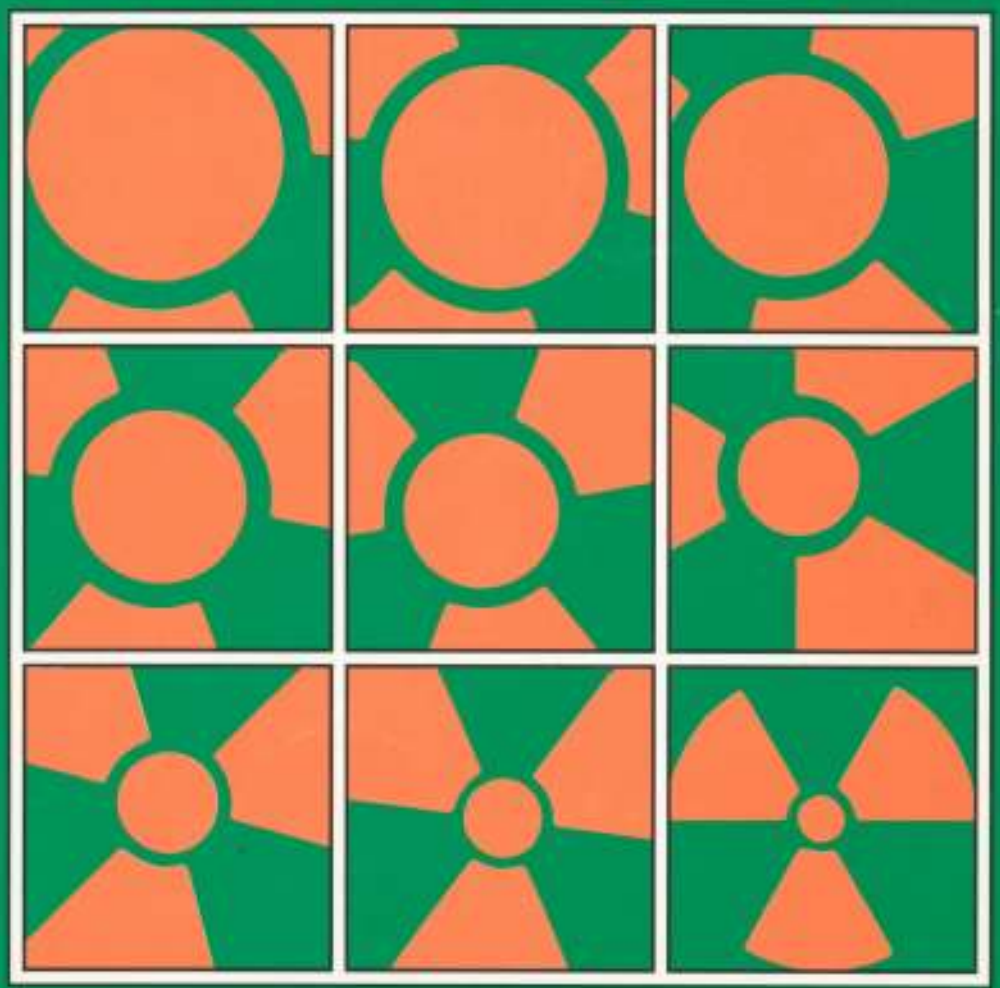

Report

EUR 14352 EN

Commission of the European Communities

nuclear science and technology

Natural analogue and microstructural studies in relation to radionuclide retardation by rock matrix diffusion in granite

M. Montoto,[1] M. J. Heath,[2] A. Rodríguez Rey,[1]
V. G. Ruiz de Argandoña,[1] L. Calleja[1] and B. Menéndez[1]

[1] **Group of Petrophysics, Department of Geology**
University of Oviedo, E-33005 Oviedo

[2] **Earth Resources Centre, University of Exeter,**
North Park Road, Exeter EX4 4QE,
United Kingdom

Final report

Contract FI1W/0143

Work carried out under cost-sharing contract with
the European Atomic Energy Community in the framework of its third
R&D programme on 'Management and storage of radioactive waste'
Part A, Task 4: 'Geological disposal studies'

Publication of this report has been supported by the Dissemination of Scientific and Technical Knowledge Unit,
Directorate-General for Information Technologies and Industries, and Telecommunications,
Commission of the European Communities, Luxembourg

Directorate-General
Science, Research and Development

1992

EUR 14352 EN

Published by the
COMMISSION OF THE EUROPEAN COMMUNITIES

Directorate-General XIII
Information Technologies and Industries, and Telecommunications

L-2920 Luxembourg

Cataloguing data can be found at the end of this publication

Luxembourg: Office for Official Publications of the European Communities, 1992

ISBN 92-826-4961-X

Printed in Luxembourg

TABLE OF CONTENTS

1. SUMMARY

In radionuclide transport models, it is commonly assumed that radionuclides migrating in solution along fractures will diffuse into pores within the rock matrix adjacent to fractures, and that by this diffusion, coupled with sorption onto the pore walls, radionuclides will be retarded relative to the water flow.

The objective of this study has been observe diffusion-related phenomena in rocks and thus to assess the effectiveness of diffusion as a retardation mechanism. This has been attempted principally by examining the microstructure and by determining the extent of disequilibrium in the uranium-238 decay series in crystalline rock adjacent to fractures. These studies have been supported by detailed geochemical and petrophysical analyses.

The project has been undertaken jointly by the Department of Geology, University of Oviedo, Spain, and the Earth Resources Centre (formerly the Department of Geology), University of Exeter, UK. It is hoped that the results of the study will have helped in resolving a major area of uncertainty in existing radionuclide retardation models.

The work undertaken has been concerned with five major areas of study:

(1) Microstructural analysis using microscopy and digital image processing techniques;

(2) Determination of the physical properties of samples;

(3) Determination of the dynamic properties of samples;

(4) Uranium series disequilibrium studies;

(5) Geochemical analysis.

The work carried out in each of these areas is described in this final report. Samples of granite have been collected from: the El Berrocal natural analogue study site near Madrid, Spain; the Stripa test mine, Sweden; the Underground Research Laboratory, Whiteshell, Canada; and from the Feldslabor Grimsel, Switzerland. Additional samples have been collected from the Gondomar, Morgadanes and El Escorial granites in Spain.

Granite blocks and cores intersected by hydrogeologically active fractures have been selected for study. Each rock sample has been cut to provide a series of rock slices at increasing distance from the fracture, the first slice including the fracture surface itself. These slices have been studied using uranium series, geochemical and petrophysical techniques in order

to observe changes in key rock properties as the fracture is approached. Results for cores drilled through a fracture surface of a granite block collected from a shallow mine adit at El Berrocal in central Spain are described here along with those from deep cores obtained from El Berrocal, Stripa, Whiteshell and Grimsel. Values for U, Th, and selected trace metals, iron oxidation, and U-234/U-238 and Th-230/U-234 ratios are compared with open porosity, water content, void index, velocity of longitudinal waves and dry density for each rock slice.

The El Berrocal sample block is of shallow origin (20 - 30 m depth) and has suffered de-stressing following the erosion of overlying rocks. The selected fracture shows clear evidence of water movement, while the groundwaters have been found to contain as much as 60 ppb uranium. In such an environment, deep penetration of uranium into the rock matrix by free diffusion might be expected. Such free diffusion does not appear to have taken place, however, there being a clearly-defined zone extending only 35 mm into the rock to which diffusion from the fracture surface appears to have been limited. Beyond this zone of uranium enrichment, and extending up to 100 mm from the fracture surface, is a zone of uranium depletion. Analysis of a deep core of El Berrocal granite has revealed a similar zone of enhanced uranium mobility extending some 80 mm into the rock. Results obtained from deep (350 m) samples of Stripa granite show a similar pattern, with a zone of marked uranium enrichment extending only 25 mm from the fracture surface. In the case of deep Whiteshell samples (250 m, 320 m), the zone of enhanced uranium mobility extends some 50 mm from the fracture, in both altered and unaltered rock.

In each of the rocks studied, the zone of enhanced uranium mobility is characterised by microstructural alteration in the rock adjacent to fractures. The zone of microstructural alteration commonly extends beyond the zone of enhanced uranium mobility, diffusion appearing to have taken place where the physical properties have changed most, but the microstructural alteration is itself confined to a narrow zone extending up to 100 mm from the fracture.

These results suggest that, in some granitic rocks, rock matrix diffusion may not be as effective a mechanism for radionuclide retardation as early diffusion models implied, and that not all of the rock may be available for diffusion. This will be particularly important where the flow of groundwater is confined to narrow channels in which flow velocity is high and access by nuclides to the walls of fractures is restricted. The geochemical and petrophysical characterization of rock adjacent to fractures has also been shown to yield valuable information and provide a useful insight into the controls of diffusion processes.

2. OBJECTIVES AND OUTLINE OF RESEARCH

In early radionuclide transport models, it was assumed that radionuclides migrating in solution along fractures would diffuse into water held in pores within the rock matrix adjacent to fractures (the 'diffusion porosity' of Norton and Knapp (1977)), and would thus be retarded relative to the flow of water. For many nuclides, this retardation would be enhanced by sorption onto the pore walls. In the retardation models developed in the UK, for example, the main limit to diffusion of radionuclides into the rock adjacent to fractures was the fracture separation (S), the penetration depth of the nuclides being S/2 (Lever et al., 1982). It was also assumed in the models developed by Grisak and Pickens (1981) that free diffusion into the rock matrix would occur to a depth controlled by the spacing of major fractures, though it was acknowledged that this assumption placed some limitations on the applicability of the model. Similarly, in the Swedish diffusion model, it was assumed that non-sorbing nuclides could diffuse into the rock matrix to the extent that they "saturate the rock sections between the fractures" (KBS, 1983). The possibility that there existed adjacent to fractures a zone to which diffusion might be restricted, or that the pores adjacent to fractures might be clogged by the products of alteration and/or mineralisation, were not incorporated into these models. It was recognised by Neretnieks (1980), however, that retardation could be limited if all of the rock matrix were not available for diffusion. Hadermann and Roesel (1985) also envisaged a system in which diffusion was limited to a narrow, damaged zone of microfracturing extending only a few centimetres adjacent to fractures, while doubts about the effectiveness of rock matrix diffusion as a retardation mechanism led to its removal from the Finnish radionuclide migration model (Peltonen, 1985). The uncertainties of the diffusion concept, and the need for further experimental validation, were also acknowledged in the Swiss research programme (NAGRA, 1985).

The experimental validation of diffusion models is normally based upon the determination of diffusion coefficients for samples of intact rock collected away from the influence of fractures, thus ignoring the possible effects of the fractures themselves on diffusion. Additionally, the properties (notably the porosity) of the samples used in such experiments will probably have been changed significantly by removal of the confining pressures to which they were subjected in the ground, thus rendering diffusion coefficients unreliable.

The objective of the study has been to assess the effectiveness of diffusion as a mechanism for the retardation of radionuclides. The approach adopted has involved examination of the microstructure and the extent to which the uranium-238 decay series is in disequilibrium in rock adjacent to fractures.

Previous studies have only examined the uranium series and geochemical characteristics of rock samples; the microstructure and physical properties of the rock have not been included. The effects on porosity and potential diffusion of fracture-related phenomena have also been considered, with particular regard to stress-relief effects and to pore-clogging by the products of alteration, mineralisation and precipitation.

It is hoped that the study will have contributed to the Spanish programme of research into the suitability of crystalline rocks for the long term isolation of high level radioactive waste, and that the results of the study will have helped to resolve a major area of uncertainty in existing radionuclide retardation models.

3. GEOLOGICAL FRAMEWORK

In radionuclide transport models, it is commonly assumed that (1) water-conducting fractures can be modelled as parallel-walled slots and that (2) diffusion (at least of non-sorbing species) takes place freely into the rock adjacent to fractures, in accordance with experimentally-determined diffusion coefficients, until the pores become saturated. Both of these assumptions are questionable on geological grounds, with serious implications for diffusion models.

It is now widely recognised that water movement in fractures takes the form of channel flow, in which water moves along discrete channels, much (or even most) of the fractures being tightly closed (e.g. Neretnieks et al., 1987). Evidence of channelling is sometimes found in the distribution of mineralization and iron staining on fracture surfaces, but channelling is usually very difficult to characterise, particularly as it is so variable in form, even locally. Where water flow is controlled by channelling, diffusion will be limited to that which can take place through the walls of channels, not through the fracture walls as a whole.

The possibility that an increase in porosity accompanies the removal of samples from depth, and that diffusivity values obtained from those samples might consequently be unreliable (that is, overestimated), was investigated by Skagius and Neretnieks (1986) who applied mechanical stress to samples before carrying out diffusion measurements in order to simulate real repository depths. Porosities were indeed found to be reduced in the stressed samples compared with those tested under atmospheric pressure. The authors considered that the observed reduction in diffusivity was not significant, but it should be recognised that, once a rock has suffered the microstructural effects of de-stressing, it is unlikely that re-stressing it

will restore it to its original microstructural state.

Observation of the results of fracture-controlled geological processes suggests that, even where highly reactive, high temperature, high pressure fluids are involved, mineralisation and/or alteration is commonly confined to a narrow zone (perhaps only a few centimetres wide) adjacent to the fracture. Similarly, patterns of iron staining in granite may give an indication of how much of the fracture surface is available for diffusion. Commonly, at least near the surface, a zone of iron deposition penetrating up to about 10 cm, sometimes very variable in width and form, is observed either side of a water-conducting fracture.

Clearly, the factors controlling such geological processes are many and complex, and not all of the processes involved will be of importance in a repository environment. Nevertheless, prima facie evidence suggests that diffusion might be limited, at least in some cases (and the extreme variability of granite must be emphasised), to a zone of rather limited extent adjacent to water-conducting fractures.

Uranium series disequilibrium work by Smellie et al. (1986) on deep granite cores from Sweden (Gotemar granite from Krakemala, 318 m deep) and Switzerland (Bottstein granite, 618 m deep) has also suggested that diffusion might be limited. The penetration of radionuclides from fractures into the rock matrix was found to be very limited (1-3 cm), and it was suggested that "this measure could act as an upper limit in migration models". Smellie's group also suggested the possibility that hydro-thermal enhancement of the porosity around fractures might be a pre-requisite for deep penetration of radionuclides into the rock matrix. The presence of hydrothermal clay minerals would also increase the potential for sorption. The mineralization/alteration history of a granite appears, therefore, to exert an important control on the potential for diffusion and sorption.

Interestingly, Smellie et al. (1986) found no evidence for uranium series disequilibrium in samples of Grimsel granite (which were free of alteration adjacent to fractures), a feature they interpreted as indicating an absence of any water-rock interaction, even though the fracture studied was believed to be water-conducting. In later work on Grimsel granite, equilibrium was indicated by both U-234/U-238 and Th-230/U-234 activity ratios, though a possible excess of Th-230 over U-234 was noted between 3 cm and 6 cm from the fracture (Alexander et al., 1990).

Later work on the same section of Bottstein granite core studied by Smellie et al. (1986) has shown that the potential for rock matrix diffusion may be much greater than originally suggested, with uranium migration affecting a zone extending at

least 20 cm from the fracture studied (Alexander et al., 1988). This suggests that the assumptions made about rock matrix diffusion in the Swiss radionuclide migration models may be too conservative, though the authors acknowledged that the rock had suffered hydrothermal alteration that might have eased the entry of groundwater into the rock. In a thorough discussion of the Swiss natural analogue work presented by Alexander et al. (1990), it was concluded that a diffusion limit of 5 cm from fractures would probably be realistic, and that 1 cm would be "sufficiently conservative".

Work by Gascoyne and Cramer (1987) on granite from the Lac de Bonnet batholith in Manitoba suggests that the exchange of radionuclides between water flowing in fractures and the rock adjacent to those fractures may be limited to a zone a few centimetres in width. At distances greater than a few centimetres from the fracture studied, uranium depletion was found to have occurred, but the disequilibrium evidence suggested that this depletion was associated with alteration processes operating more than one million years ago. Later work on the samples from 150-250 m depth in the same granite by Ivanovich et al. (1987) concluded that the main locations for actinide exchange are fracture surfaces where there is evidence for both uranium uptake and removal depending upon oxidation conditions (which are reflected in iron oxidation states). Hydrothermal alteration was found to have caused iron enrichment and uranium depletion in the rock adjacent to fractures; later uranium remobilisation accompanied the introduction of oxidising waters within the last 300,000 years.

In all of the studies undertaken to date, the difficulty of interpreting the geochemical and uranium series data has been emphasised, as the processes operating in the rock adjacent to fractures are many and complex, and often produce opposing effects. It has been one of the aims of the present study to aid interpretation of the observed uranium series characteristics and geochemistry by providing microstructural and petrophysical insight into the processes operating in the rock.

4. WORK UNDERTAKEN

The main purpose of the study has been to determine whether or not the diffusion depth in rock adjacent to fractures is sufficiently limited to undermine the validity of existing diffusion models. To this end, the study has focused on the rock adjacent to water-conducting fractures and has followed two main lines of investigation: (A) an examination of the microstructure and physical properties of the rock; and (B) measurement of geochemical changes and the extent to which the U-238 decay series has been disrupted by the diffusion of members of the decay

chain towards or away from the fracture.

It was intended initially that six different techniques would be applied in pursuit of the study's objectives:

(1) Porosity and permeability determinations;
(2) Microstructural analysis, microscopy and digital image processing;
(3) Mineralogical and petrographical studies;
(4) Uranium series disequilibrium studies;
(5) Mossbauer studies; and
(6) In situ stress determinations.

It became clear as the project progressed that the initial work plan was over-ambitious, and a number of areas were subsequently removed from the programme. Of particular importance were the permeability determinations. After an extensive review of the available techniques and equipment, it was concluded that, for reasons of cost and the need for special expertise, permeability determinations were not a feasible part of the project. For similar reasons, in situ stress determinations have not been carried out, though existing data have been reviewed. Finally, owing to the temporary decommissioning of the Mossbauer system in Exeter, iron oxide chemistry has been studied using geochemical methods rather than Mossbauer spectroscopy.

4.1. SAMPLES.

4.1.1. Sample locations.

To assist in the successful interpretation of the data obtained from the study, samples have been collected from crystalline rock sites which are well-characterised in terms of their structure (notably fracture characteristics), petrography, stress history, hydrogeology and hydrogeochemistry. It was originally planned to obtain samples from the Project IPES ("Instalación Piloto Experimental Subterránea") underground laboratory planned for the Duero Valley (ENRESA, 1987), but the subsequent suspension of Project IPES required that samples were obtained from other well-characterised locations. The study has, therefore, focused on four major sites:

(1) El Berrocal Natural Analogue Study Site, Spain;
(2) Stripa Mine, Sweden;
(3) Underground Research Laboratory (URL), Whiteshell, Canada;
(4) Feldslabor Grimsel (FLG), Switzerland.

El Berrocal has been the main focus of the study. Stripa samples were the first to be obtained and have been used for technique development and comparative purposes. The samples from Whiteshell and Grimsel have also provided comparative data.

Additional samples were collected for technique development purposes from Gondomar (granodiorite) and Morgadanes (granite) in Galicia, NW Spain, and from El Escorial (adamellite) near Madrid.

4.1.2. Sample descriptions.

4.1.2.1. El Berrocal Granite, Spain.

The El Berrocal granite has been the main focus of the study, both block and core samples having been employed. Two blocks were collected in January 1990 from material recently excavated from the mine adit (samples EB1 and EB2). Precise details about the original location of these blocks were not available, but the samples were known to have been derived from the near-surface environment at a depth of approximately 20 - 30 m. Each block was bounded on one face by a natural fracture; in each case, the fracture surface was iron stained and the rock adjacent to the fracture showed alteration and a zone of red staining extending some 30 - 40 mm into the rock.

A core (sample EB3), 70 mm in diameter, was also obtained from a vertical borehole in the drift at a depth of a few tens of metres.

The El Berrocal batholith is enclosed in the Galaico-Castellana zone of the Hesperian Massif of central Spain (Lotze, 1945). The granite is a late synkinematic to post-kinematic Hercynian intrusion; the granite is intensely fractured with two dominant fracture strikes, N20° -40°E and N110°E. A detailed petrographic description of the El Berrocal granite has been presented by Arribas (1964), ENRESA (EC contract FI1W.230) and Perez del Villar et al. (1989).

4.1.2.2. Stripa Granite, Sweden.

Stripa granite samples were the first deep samples obtained and were used for technique development and comparative purposes. Two cores were obtained from borehole DBH 5, a vertical borehole drilled in the floor of the 'Extensometer Drift', 346 m below the surface. Complete U series, geochemical and petrophysical data were obtained for sample ST6, a core intersected by a fracture 6.29 m below the top of the borehole (i.e., at a depth of 352.90 m below surface). Other development work was carried out on samples ST5 (350.18 - 350.60 m depth) and ST7 (352.90 - 353.87 m).

A detailed description of the geology of the Stripa mine has been given by Wollenberg et al. (1980); the hydrogeology has been described by Gale et al (1987), and the geochemistry and isotope chemistry by Nordstrom et al. (1985).

4.1.2.3. Whiteshell Granite, Canada.

Two 60 mm diameter core samples were obtained from the Underground Research Laboratory (URL) at Whiteshell, Manitoba. The first sample (WS1) was obtained from borehole HC-27 at a depth below the borehole collar of 16.41 - 16.61 m, which is within "fracture zone 2" a few centimetres from a highly permeable rubble zone. The fracture studied was derived from a depth of approximately 250 m. Alteration was clearly visible at both ends of the core, and sample WS1 is considered to represent relatively 'altered' material.

The second Whiteshell sample (WS2) was obtained from borehole 209-069-PH3 at a depth below collar of 84.20 - 84.61 m. This borehole intersects a series of permeable vertical fractures seen as roof drips in Room 209 close to the locations of excavation response experiments and geophysical tests. The fracture studied was derived from a depth of approximately 320 m. The core had only one natural fracture surface and showed little alteration. Sample WS2 represents relatively 'unaltered' material.

4.1.2.4. Grimsel Granite, Switzerland.

Core samples (60 mm diameter) were obtained from borehole BO/VE 84.011, a horizontal hole drilled parallel to the ventilation drift at the Grimsel rock laboratory (Feldslabor Grimsel, or FLG). The FLG is situated within the Juchlistock Massif at an elevation of approximately 1730 m; the depth of the laboratory varies between about 300 m and 500 m beneath an irregular surface topography. Sample GR1 was a core intersected by a natural fracture at a depth of 27.0 m; sample GR2 was intersected by a fracture at a depth of 62.27 m. Both cores appeared to be unaltered.

4.1.2.5. Gondomar, Morgadanes and El Escorial Granites, Spain.

Some of the early technique development work was carried out on block material from Gondomar (granodiorite) and Morgadanes (granite) in Galicia, NW Spain, and from El Escorial (adamellite) near Madrid.

4.1.3. Sample preparation.

The project has been concerned with gaining an understanding of processes operating in the rock adjacent to fractures. The samples selected have, therefore, been granite cores or cored blocks intersected by fractures. These cores have been cut to enable changes in the rock close to fractures to be investigated. Each core has been divided into two parts (one from each side of the fracture), one part being set aside for porosity

determinations, the other being cut longitudinally for microstructural analysis and radioactive disequilibrium/ geochemical work (Figure 1).

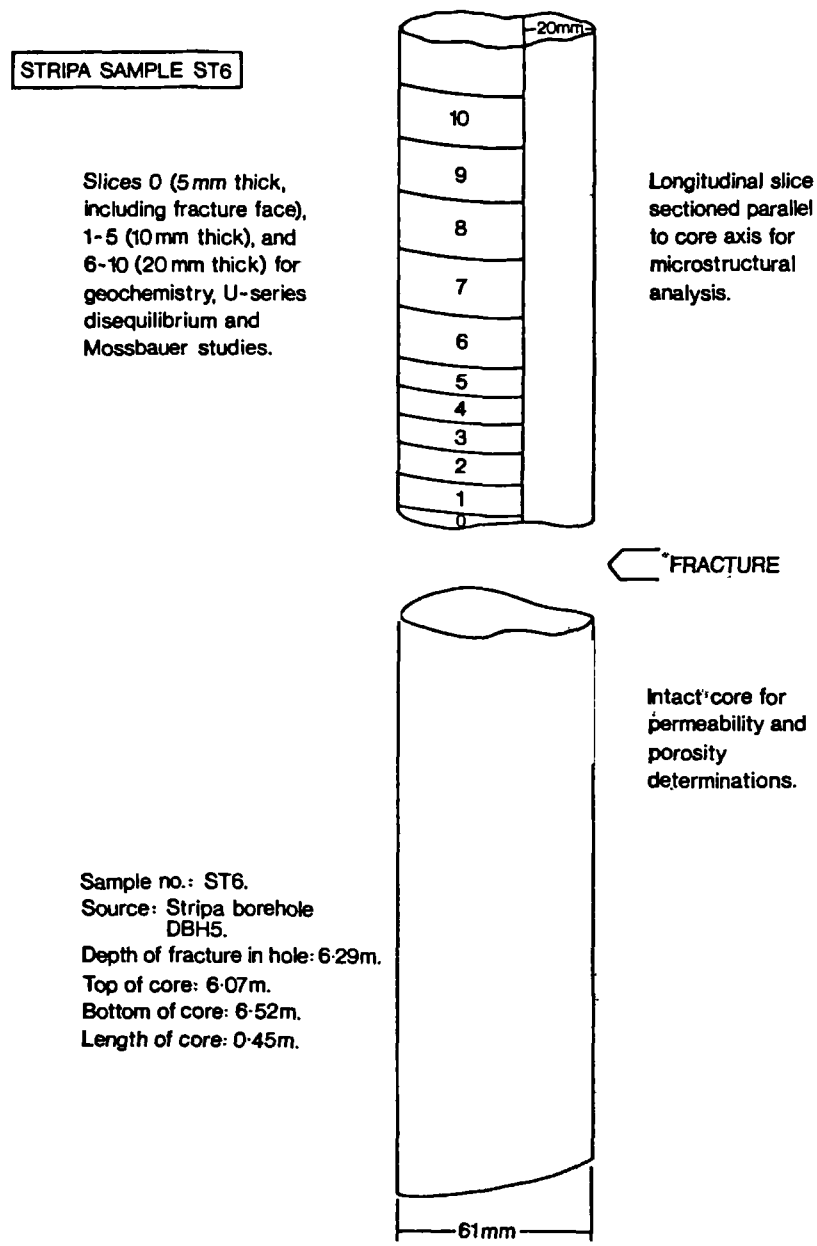

Fig. 1.- Cutting of a typical core for microstructural, radioactive disequilibrium and geochemical studies.

For the microstructural work, thin sections were prepared from each of a series of slices to enable microstructural changes to be studied as the fracture is approached. For the radioactive disequilibrium/ geochemical work, each core was cut parallel to the fracture surface to produce a series of slices. The first slice, 5mm thick, includes the fracture surface itself; a series of other slices were also cut, generally 10-20 mm in thickness, allowing the rock to be studied at increasing distance from the fracture. Between each slice, 1-3 mm of rock was lost during sawing (the thickness of the saw blade).

Samples from El Berrocal, the main focus of the study, included cores (50 mm in diameter and 120-130 mm long) obtained from a block of intact rock the upper surface of which was formed by a hydrogeologically-active fracture (Figure 2). Each core was divided into two longitudinal halves and subsequently cut into slices (Figure 2).

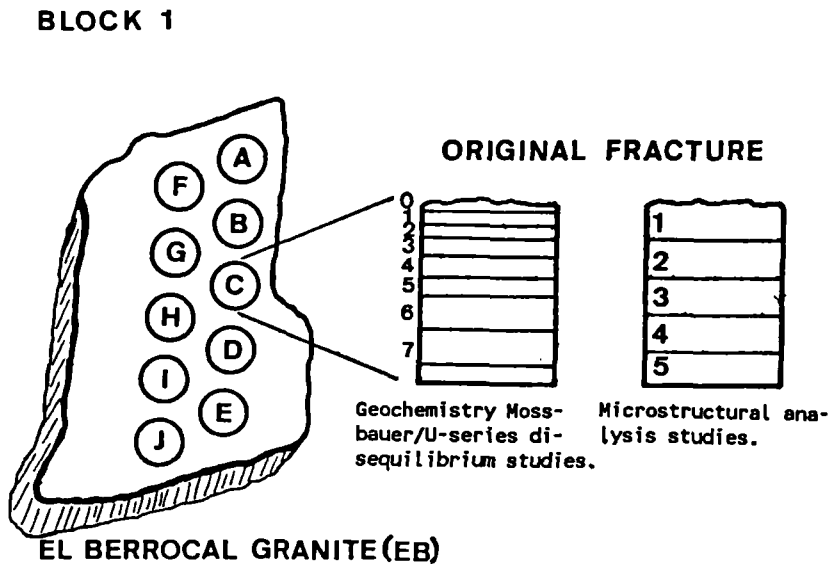

Fig. 2.- Scheme of the El Berrocal granite block (EB1) and sample distribution for microstructural, radioactive disequilibrium and geochemical studies (core references are: EB1A, EB1B, etc).

4.2. MICROSTRUCTURAL ANALYSIS AND DIGITAL IMAGE PROCESSING.

Thin sections have been studied by optical (including transmission, reflected light and fluorescence) microscopy and

scanning electron microscopy, and the microstructure of the rock adjacent to fractures and the availability of pores for diffusion have been analysed using digital image processing techniques and multi-image analysis. Particular attention has been paid to the interconnectivity of pores and to their nature adjacent to fractures. The applicability of acoustic microscopy to the study has also being investigated.

4.2.1. Studies aimed at perfecting methods for the preparation of samples for petrographic characterisation by microscopic techniques.

Methods for preparing samples for petrographic examination by microscopic techniques have been studied, with particular reference to the impregnation of samples with fluorescent resins for fluorescence optical microscopy. Two aspects have been of particular interest: improvement in the use of resins, and the use of new resins.

In order to improve the impregnation method, an existing technique was redesigned (Figure 3). The equipment consists of a cylindrical vessel (3) into which the sample is placed. The cylinder is then closed by operating a piston (2) and is evacuated to 0.01 torr via the outlet tube (5), thus drawing the resin into the sample by suction. The piston is held under a pressure of 2.5 tonnes for a period of 15 minutes to enhance penetration of the fluorescent resin into the interior of the sample. Finally, the vacuum is released, the sample is withdrawn using the handle (1), and the resin is allowed to polymerise.

The use of new resins, the viscosity and surface tension of which might allow improved impregnation, has also been studied.

4.2.2. Studies of the suitability of acoustic microscopy for the petrographic characterisation of rocks.

4.2.2.1. Scanning acoustic microscopy.

The applicability of acoustic microscopy to the petrographic characterisation of rocks has been assessed. The work has been carried out at the Department of Materials of the University of Oxford in collaboration with Dr. G. A. D. Briggs. The results have recently been published (Rodriguez-Rey et al., 1990). The study represents one of the first attempts to apply Scanning Acoustic Microscopy (SAM) to the study of rocks. Other previous studies, though not totally devoted to rocks, are those of Ilett et al. (1984), Briggs (1985) and Hoppe and Bereiter-Hahn (1985).

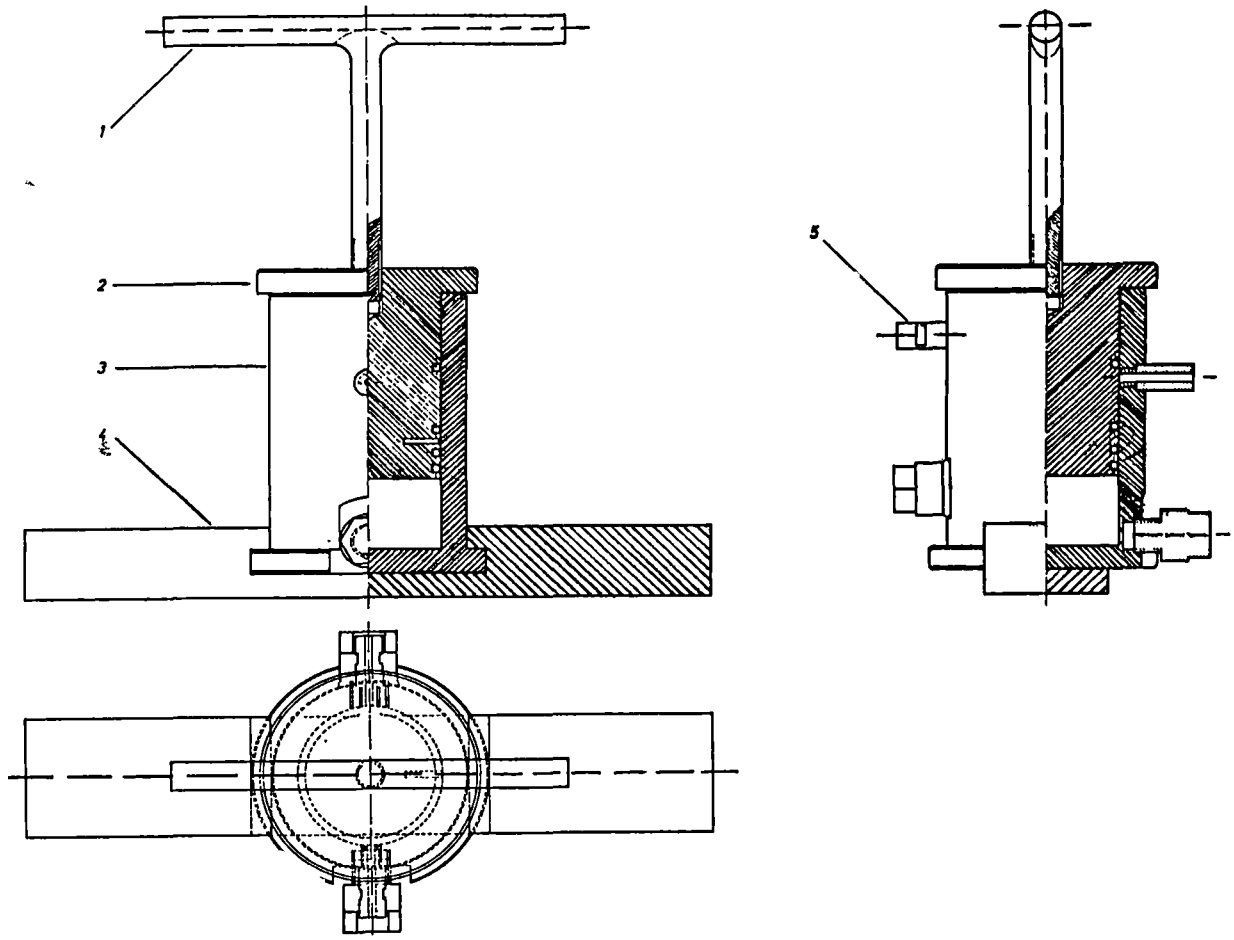

Fig. 3.- Equipment for the impregnation of rock samples for fluorescence light microscopy. Scale 1:2.8.

The aim of this research has been to assess the usefulness of SAM in providing new and different petrographic information which could complement that provided by other microscopy techniques. The advantage of SAM is that acoustic images depend upon the contrast in physical properties (density, mechanical properties, thermoelastic coefficients, etc.) which vary more widely between different materials than the optical properties

that form the basis for optical microscopy. This enables petrographic information related to mechanical properties, degree of alteration etc. to be obtained.

4.2.2.2. Information provided by scanning acoustic microscopy.

The type of information that can be obtained by applying SAM to the study of rocks is illustrated by work carried out on samples of El Escorial granite from Spain.

The specimens studied were flat-polished fluorescein-impregnated thin sections, 30 μm thick, specially prepared for study by different microscopy techniques, including polarizing microscopy, fluorescence microscopy, scanning electron microscopy and scanning acoustic microscopy.

Information provided by SAM can be described under the following headings:

- textural characteristics;
- crack detection;
- intragranular information.

Textural characteristics.

The images obtained by SAM provide considerable information on rock samples. Textural characteristics, such as grain size and shape, are clearly visible. In the case of polymineralic rocks, the strong contrast seen in the image arises from differences in the elastic properties of the different minerals present. This contrast changes according to the distance between the lens and the specimen surface.

In SAM, it is essential to understand the effect on contrast of 'defocus', which occurs when the specimen is moved above or below the focal plane of the lens ($z = 0$). By convention, when the specimen is moved closer to the lens, the distance between this position and the focal plane (z) is said to correspond to a defocus of $-z$. In practice very little contrast is usually found by operating the microscope at focus, as two regions of a specimen with different elastic properties will often produce similar images at $z = 0$; the contrast begins to appear for negatives values of z.

In monomineralic rocks, or monomineralic aggregates, the origin of the contrast lies in the anisotropy of the elastic properties of the same mineral. Again, the contrast changes with defocus. This property makes SAM complementary to SEM, in which grain boundaries in monomineralic (and some polymineralic) aggregates are not visible owing to similar secondary electron emission. Features not visible under reflected light polarizing

microscopy are also sometimes revealed by SAM.

Crack detection.

Very fine cracks not visible under optical microscopy can be detected by SAM, particularly when the specimen is defocused a little towards the lens. Under optical microscopy, a crack narrower than the wavelength of light cannot be detected. Under SAM, cracks finer than the wavelength of acoustic waves can, however, be detected at much lower magnifications than would be necessary to detect the cracks using SEM, thus enabling large areas to be examined for defects much more efficiently than would otherwise be possible.

Figure 4 shows several images of an area of another polished thin section of the granite of El Escorial observed using different techniques: polarising microscopy, fluorescence optical microscopy, scanning electron microscopy and scanning acoustic microscopy. Regarding cracks, the most comprehensive information is provided by SAM, more cracks being visible than in the other images at the same magnification. These 'new cracks' are extremely fine and can only be seen at very high magnification under scanning electron microscopy. Information about sub-surface geometry of the cracks can also be obtained.

The images shown in Figure 5 correspond to the same area of a polished thin section of the granite of El Escorial observed by acoustic microscopy. The difference in elastic properties of the three minerals present (quartz, plagioclase and biotite) renders textural features visible; this is most prominent when the specimen is moved closer to the lens (negative defocus). As defocus value changes, contrast reversals occur.

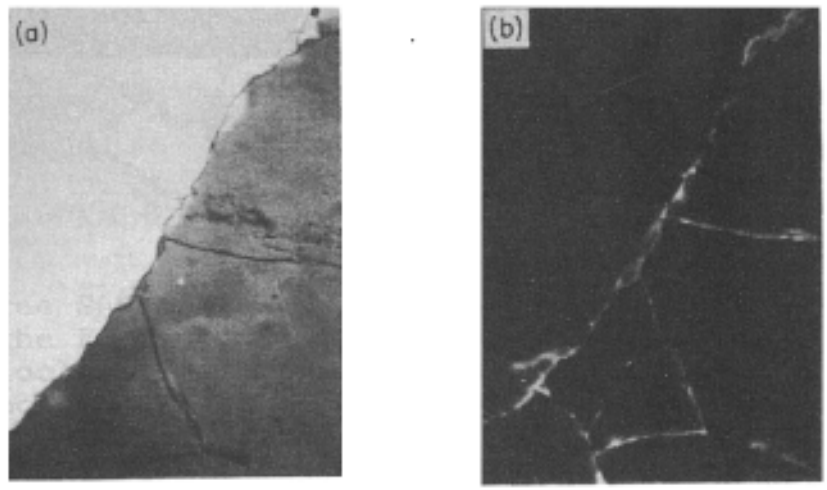

Fig 4.- Caption overleaf.

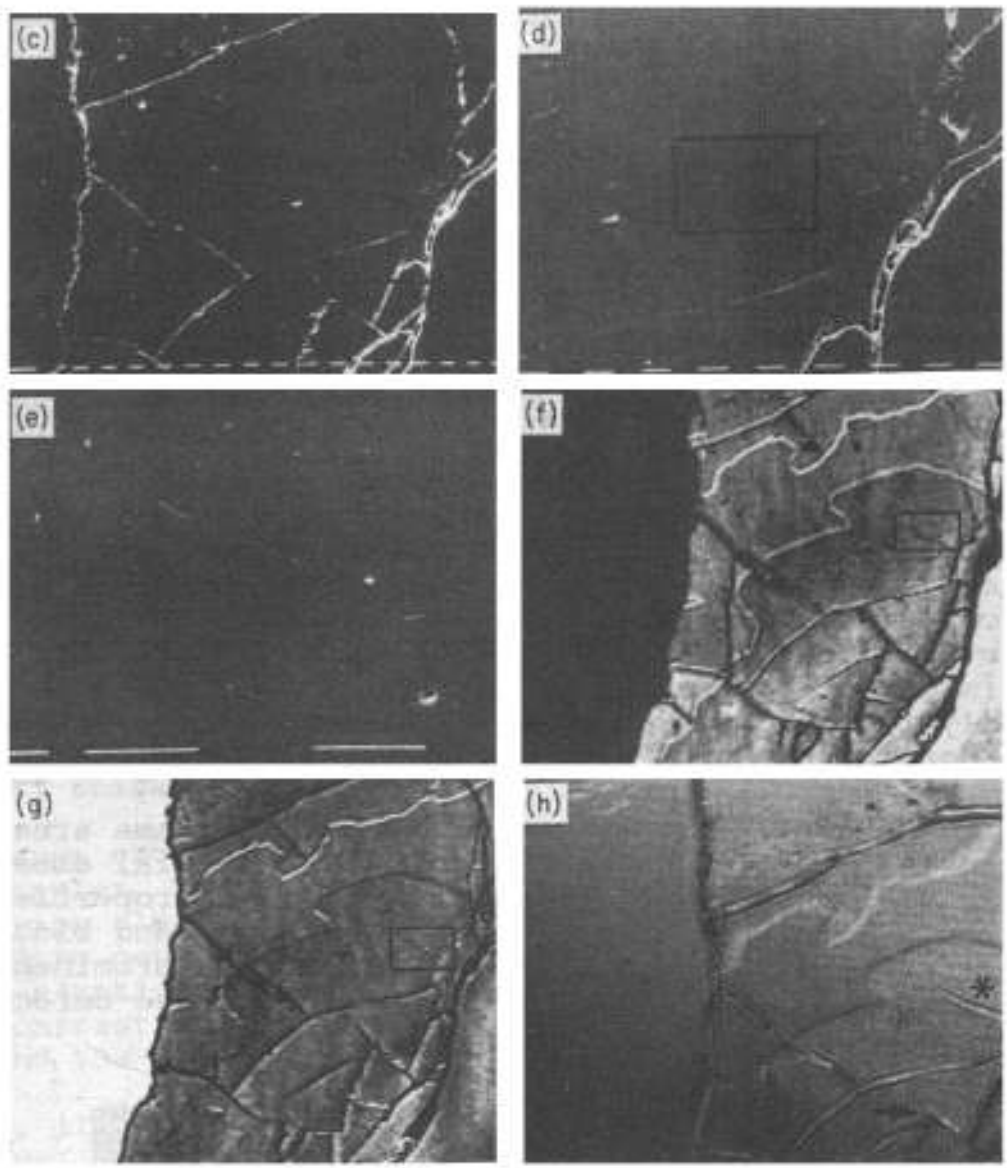

Fig. 4.- Caption overleaf.

Fig. 4.- An area of a fluorescein-impregnated, polished thin section of El Escorial granite, showing a boundary between two grains of quartz, observed under very different microscopic techniques: (a) transmitted-light polarizing microscopy allows the two grains to be distinguished and their textural characteristics to be studied. (b) reflected-light fluorescence microscopy reveals the micro-crack network. (c), (d), (e) scanning electron microscopy is well suited to the study of cracks but the textural characteristics of the rock are not readily identified. (f), (g), (h) the images from SAM provide comprehensive information about the specimen: the two grains are clearly distinguished (the contrast reverses with defocus in (g) and (h). This technique gives more information than any other about microcracks, more cracks being visible at the same magnification; the marked crack in (f) is extremely fine and can only be seen at very large magnification under SEM (e). (After Rodríguez-Rey et al. 1990).

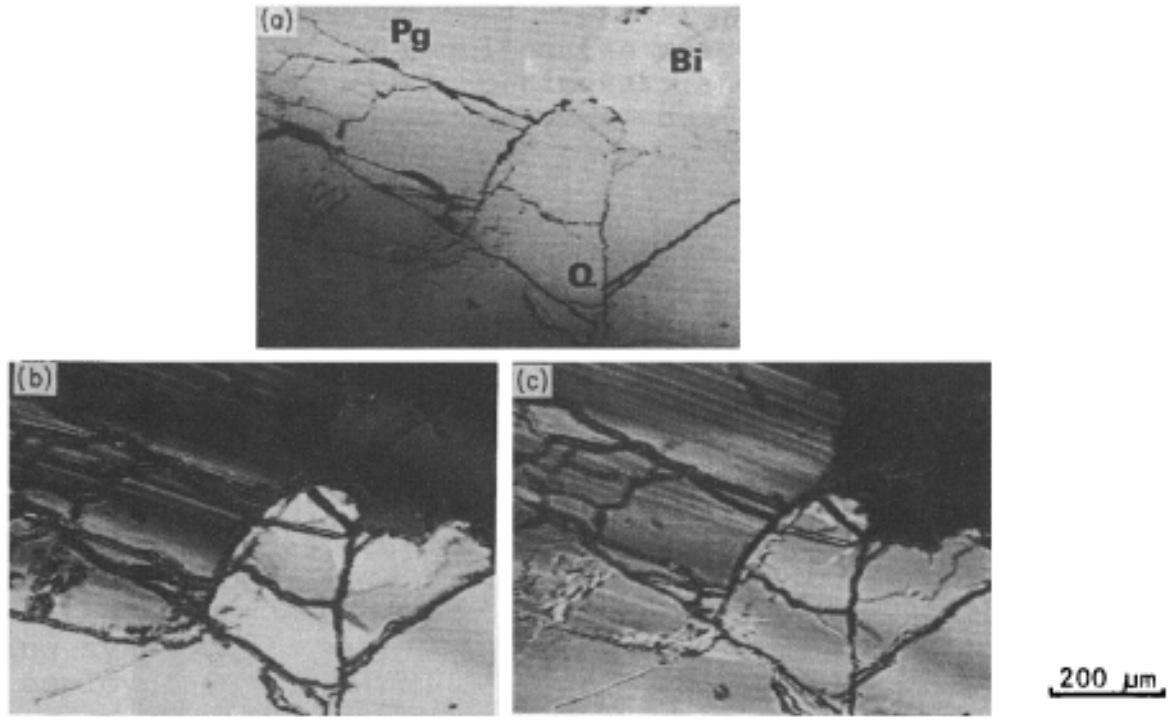

Fig. 5.- Three SAM images of the same area of a polished thin section of the El Escorial granite showing three different minerals: Plagioclase (Pg) top left, Biotite (Bi) top right, and Quartz (Q) bottom. Textural characteristics of rock (grain boundaries, microcrack network, etc) can be identified. Polysynthetic twinning in the plagioclase crystal and exfoliation fractures in the biotite are visible. The contrast changes with varying defocus. (a) z= 0 µm, (b) z= - 4 µm, (c) z= - 6 µm. 400 MHz. (After Rodríguez-Rey et al. 1990).

Intragranular information: subdomains in deformed mineral grains.

The stress experienced by many rocks during their history can be 'recorded' in the structures of deformed rock-forming minerals within rocks. Quartz grains, in particular, commonly show irregular, wavy or segmented, undulose (mosaic) extinction under transmitted-light polarizing microscopy. Acoustic microscopy is very useful in revealing the subgrain structure of these deformed grains. As the SAM image arises in the surface layer (the depth of the wavelength of Rayleigh waves), the image obtained is clearer than that obtained by transmitted light polarising microscopy, where the effect of the thickness of the section may obscure the image.

Figure 6 compares the images obtained by transmitted-light polarising microscopy and scanning acoustic microscopy. The subdomains within the grain of quartz can be easily identified under SAM as they show different contrast which can be enhanced by changing the defocus.

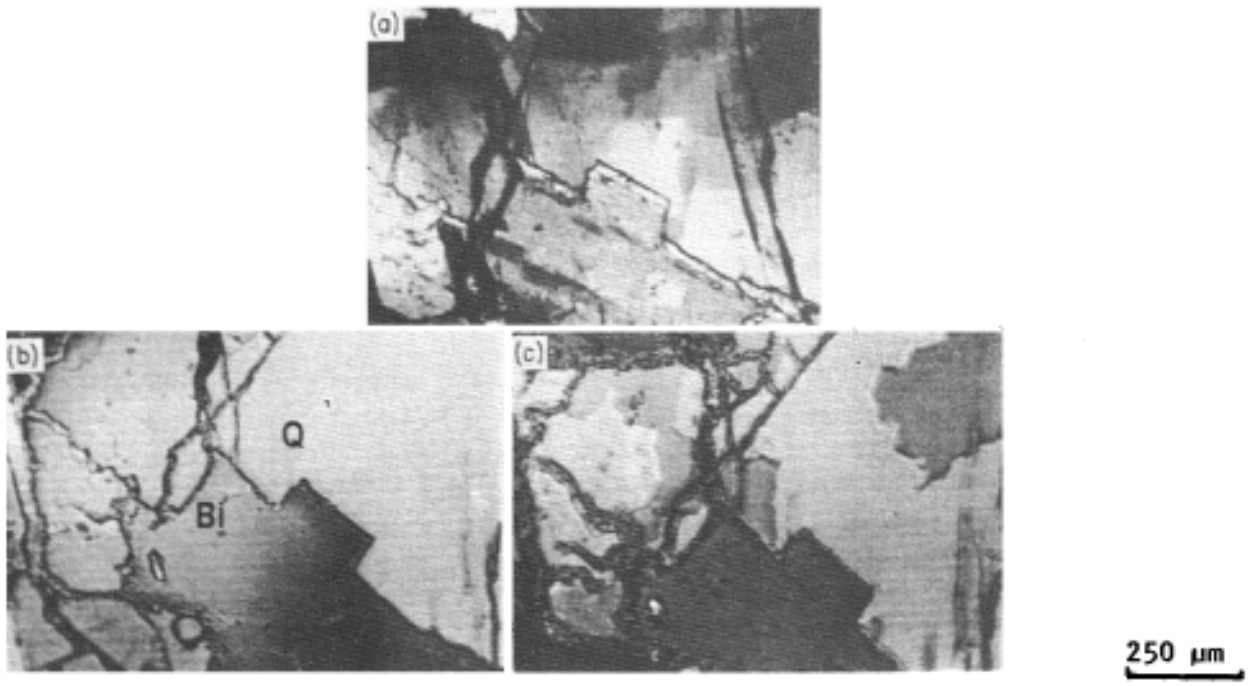

Fig. 6.- An area of a polished thin section of El Escorial granite. Under SAM ((b) and (c)), subareas with different optical extinction are clearly visible while under transmitted light polarizing microscopy (a) the effects of the specimen thickness make these subareas difficult to distinguish. (After Rodríguez-Rey et al. 1990).

4.2.3. An appraisal of new parameters for the quantitative petrographic characterisation of rocks.

The applicability and usefulness of the textural coefficient (TC) of Howarth and Rowlands (1987) to the quantitative petrographic characterisation of rocks has been assessed. The TC is a non-dimensional quantitative measure of rock texture that describes the form, orientation and degree of interpenetration of the grain mass and the grain packing density.

In addition to its usefulness as a descriptive parameter, the TC is of great practical interest. Howarth and Rowlands (1987) studied the relation between TC and the mechanical resistance and 'drillability' (both by rotary and percussion techniques) of 11 rock types displaying very different properties (sandstones, marbles and igneous rocks), and obtained a good statistical correlation between TC and mechanical properties. Sandstones, for example, with low TC values, are easily drilled, while igneous rocks, with high TC values, are difficult to drill. TC can thus be used to estimate the resistance and drillability of rocks.

The determination of TC requires the measurement, in thin section, of the length, width, perimeter, angular orientation and area of each grain, and the percentage of grains and matrix. These measurements enable the form of each grain to be described in terms of the aspect ratio and the form factor. The parameters describing the form of the grain mass in terms of TC can then be calculated. Orientation data for each grain provide an orientation factor for the whole grain mass. Finally, the packing density is determined.

4.2.4. Development and application of digital image processing techniques for the determination of the textural coefficient.

Howarth and Rowlands (1987) developed a digital image processing procedure specifically to measure the textural characteristics required for the calculation of TC. A digital image processing system for the measurement of the same parameters has been employed in this project. The system consists of:

- Zeiss Standard Universal microscope;
- Digitiser: Hamamatsu C-1000 camera with analog/digital converter;
- IBM S/1 computer;
- Visual display system: Ramtek colour monitor and Grundig monochrome monitor.

The software for the system is written in EDL and runs under an EDX operating system. The IMAGO program pack, developed in

Oviedo specifically for the analysis of petrographic microscopy images, has been modified and used for the calculation of TC.

The system has been used for the determination of TC on samples of Gondomar granodiorite. Grain characteristics have been measured on images obtained from thin sections by polarising optical microscopy. Each thin section was divided into zones using a grid system. To enable the characterisation of individual grains, two or more images were obtained from each zone with different angles between the nicol prisms (Figures 7 and 8). Images were digitised to a size of 256 x 256 pixels distinguished in 256 levels of grey.

The first stage of analysis consists of the extraction of grain boundaries from the image. Only those boundaries that lie totally within the image are included. Figure 9 shows the grain boundaries of the sections shown in Figures 7 and 8. From the image showing the grain boundaries, the program calculates the area and perimeter of each grain. Additionally, from the axes of the ellipse that encloses each grain, the length and width of grains are determined; the orientation of each grain is calculated from the angle the major axis of the ellipse makes with the horizontal.

The value of TC obtained by this technique (2.14) compares well with that obtained manually (2.18), confirming the suitability of the technique for use in these studies. The values obtained show considerable variation, not only in different directions within the sample (parallel to 100, 101 and 001), but also in the same direction:

100: 2,14	010: 1,76	001: 1,38
1,81	1,42	1,48
1,81	1,28	1,65

4.2.5. Results of microstructural investigations.

Microstructural studies have been carried out on samples of El Berrocal and Stripa granite.

4.2.5.1. El Berrocal granite.

The El Berrocal batholith is enclosed in the Galaico-Castellana zone of the Hesperian Massif of central Spain (Lotze, 1945). The granite is a late synkinematic to post-kinematic Hercynian intrusion. The granite is fractured with two dominant fracture strikes, N20°-40°E and N110°E.

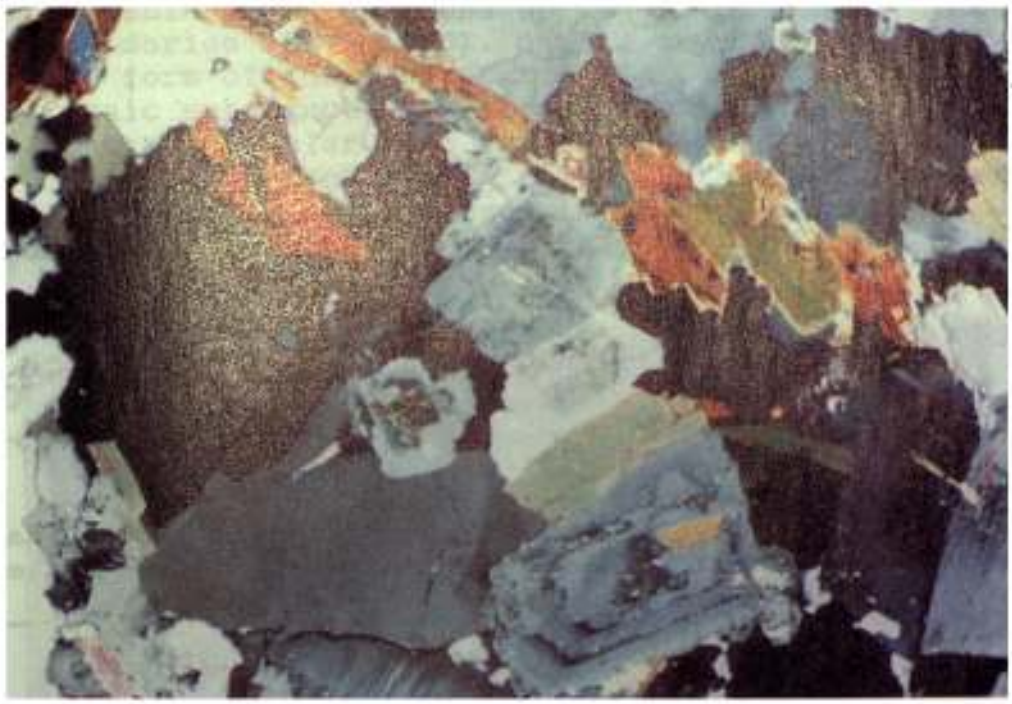

7

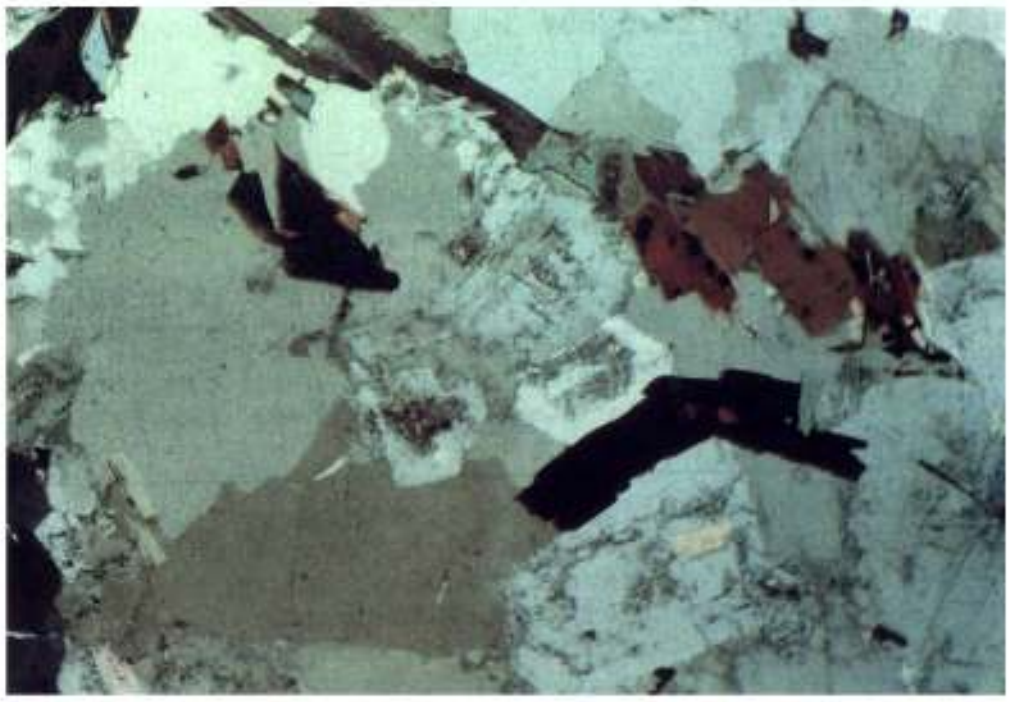

8

0.5 mm

Figs. 7 and 8.- Photomicrographs of the Gondomar granodiorite with nichols crossed at two different angles.

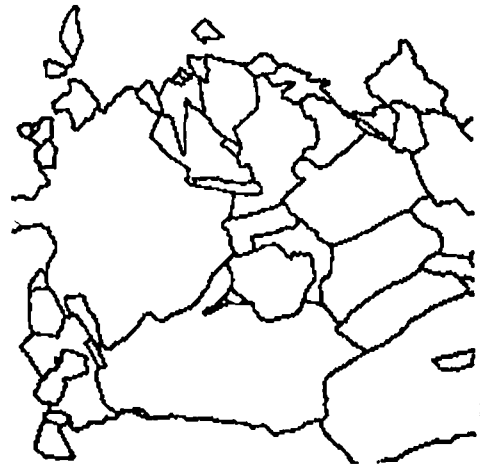

Fig. 9.- Digital image of the grain boundaries of an image of the Gondomar granodiorite used in the calculation of the TC (textural coefficient) of Howarth and Rowlands.

Petrographic analysis.

A detailed petrographic description of the El Berrocal granite has been presented by Arribas (1964), ENRESA (EC contract FI1W-230) and Perez del Villar et al. (1989). Further petrographic analysis has been carried out in connection with the present study.

The rock is an allotriomorphic (with a certain hypidiomorphic tendency), heterogranular, medium to course grained granite. In places, the rock is porphyritic, with large crystals of K-feldspar (up to 8 mm long in section).

The mineralogical composition of the granite is presented in Table I. According to the classification of Streckeisen (1974), the rock is an alkali granite.

TABLE I

Mineral	%
Quartz	40.7
K-feldspar	19.6
Plagioclase	28.8
Muscovite	8.2
Biotite (chlorite)	2.7

TABLE I.- Mineral composition of El Berrocal sample EB1.

Quartz appears as aggregates of clearly allotriomorphic crys-

tals of variable size (sections up to 4.8 mm long), often with sutured boundaries (Figure 10). Quartz crystals show deformation in the form of anomalous extinction, sometimes showing growth- mosaic substructure. There is an associated microcrack network of transgranular type (sometimes partly intergranular), in many cases microcracks being filled with leached material derived from weathering processes. Some small intragranular cracks are also developed in some grains.

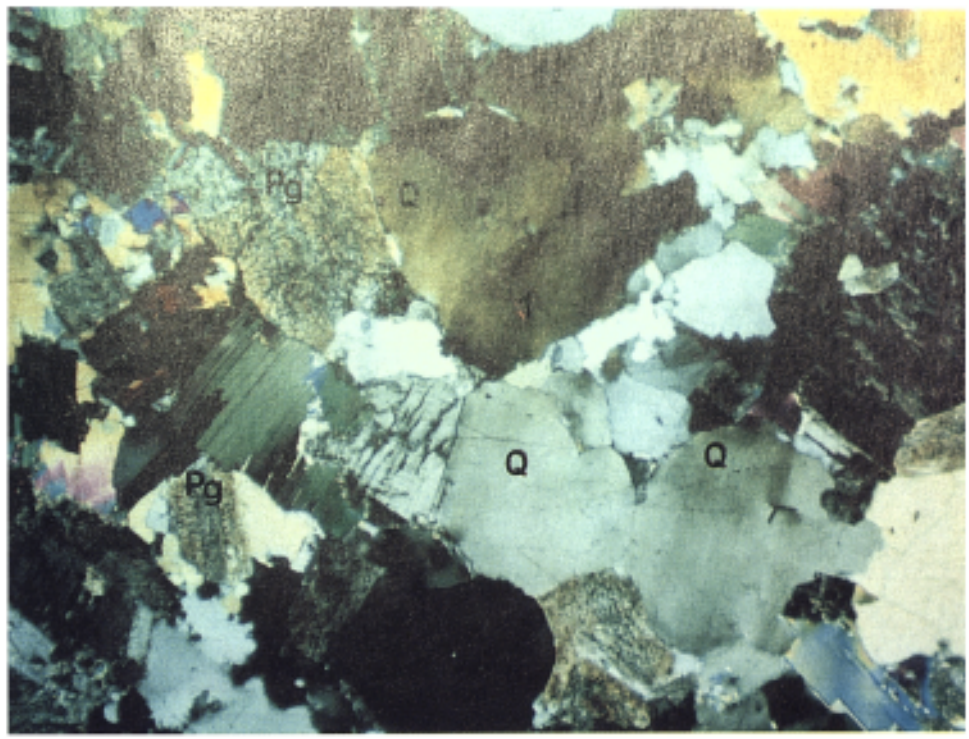

Fig. 10.- General aspect of the rock, with aggregates of allotriomorphic and deformed crystals of quartz (Q) with sutured grains and weathered plagioclases (Pg). A transgranular microcrack (1) network runs through the quartz aggregate (crossed nicols). Berrocal granite.

The K-feldspar (orthoclase and microcline) appears in allotriomorphic to hipidiomorphic crystals, the largest in the rock. The crystals are rather weathered even in the sections furthest from the fracture. Carlsbad twins are frequent as is combined albite-pericline twinning in microcline.

The plagioclase appears in hypidiomorphic crystals, variable in size with sections up to 36 mm long, displaying albite twinning in the form of very fine lamellae; combined albite-Carlsbad twinning is also present. No zonation is visible. The crystals are very weathered.

Muscovite and biotite are present as xenomorphic crystals showing strong deformation in the form of wavy extinction and deformed exfoliation planes. Biotite is usually thoroughly weathered to chlorite (Figure 11).

Andalucite, apatite and zircon are the major accessories present, with sericite, chlorite and epidote as the main weathering products.

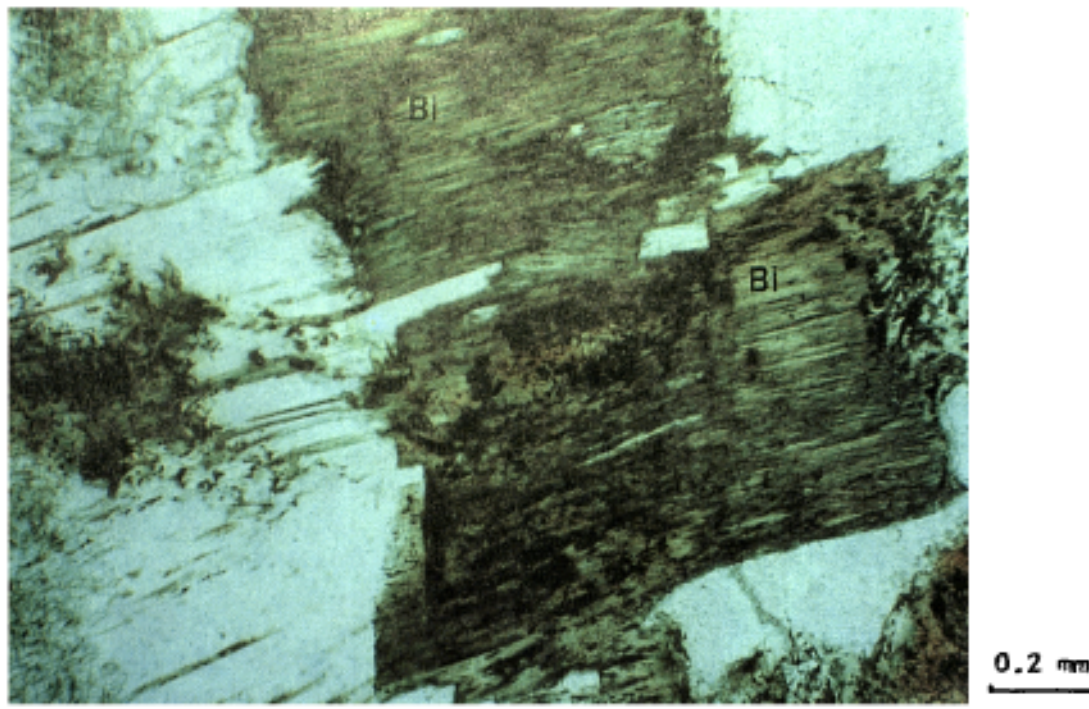

Fig. 11.- Weathered and allotriomorphic crystals of biotite (Bi), with deformed exfoliation planes (parallel nicols). El Berrocal granite.

Microcrack network.

The variation of microcrack density with respect to the distance from the fracture surface has been studied in thin sections obtained from cores EB1A and EB1B by means of reflected-light fluorescence microscopy. Only those fluorescent microcracks were examined as isolated cracks and those filled with alteration products cannot be impregnated with resin.

Quantification of the microcrack density is based upon counting the number of intersections of microcrack surface traces within a set of regularly spaced parallel lines. In this way, a parameter is obtained that represents the total length of microcrack

traces per unit surface area of the thin section.

Values of microcrack density for the different slices of core EB1B are related to the distance from the fracture surface in Figure 12. It can be seen that the section closest to the fracture has the greatest microcrack density. This may be attributable to the greater abundance of weathering products in this slice, preventing the microcracks from being impregnated with resin.

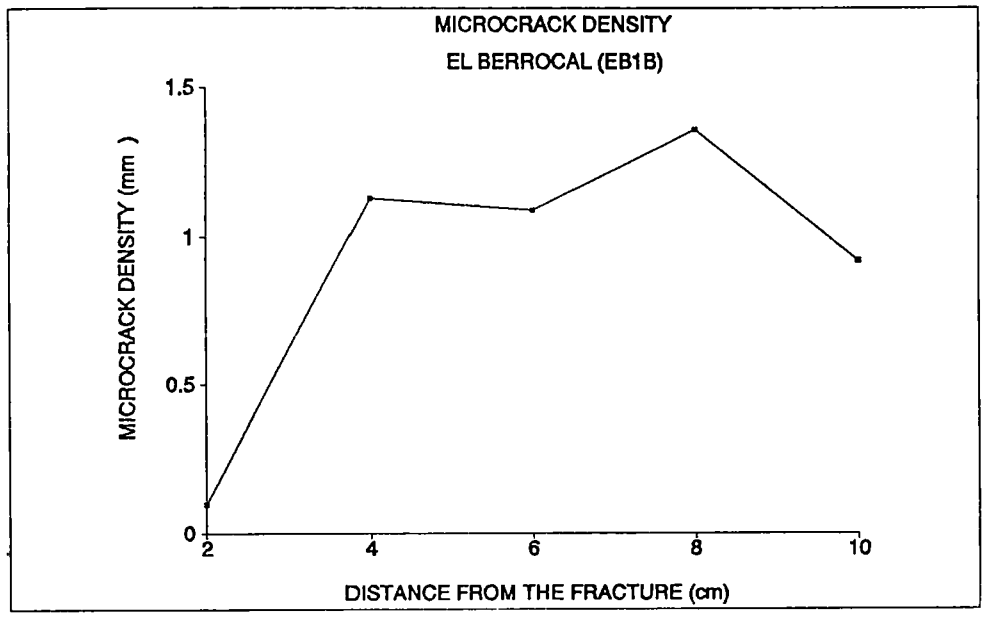

Fig. 12.- Density of microcracks in the series of thin series prepared from core EB1B, plotted as a function of the distance from the fracture. El Berrocal granite.

4.2.5.2. Stripa granite.

The Stripa granite has been studied extensively. Detailed petrographic descriptions of the rock can be found elsewhere (Montoto et al., 1980; Wollenberg et al., 1981). Montoto et al. (1980) studied microfissures of thermal origin in samples from the area of the heater test in the Stripa Mine using optical and electron microscopy and digital image processing techniques to obtain comprehensive quantitative information on the microfractography of the rock in relation to the texture and mineralogy. The following discussion is based upon analysis of thin

sections of sample ST5.

Texturally, the rock is xenomorphic, heterogranular (maximum grain size 2.5 - 3.0 mm), strongly strained, and shows cataclastic features in many areas (Figure 13), with marked deformation of crystals.

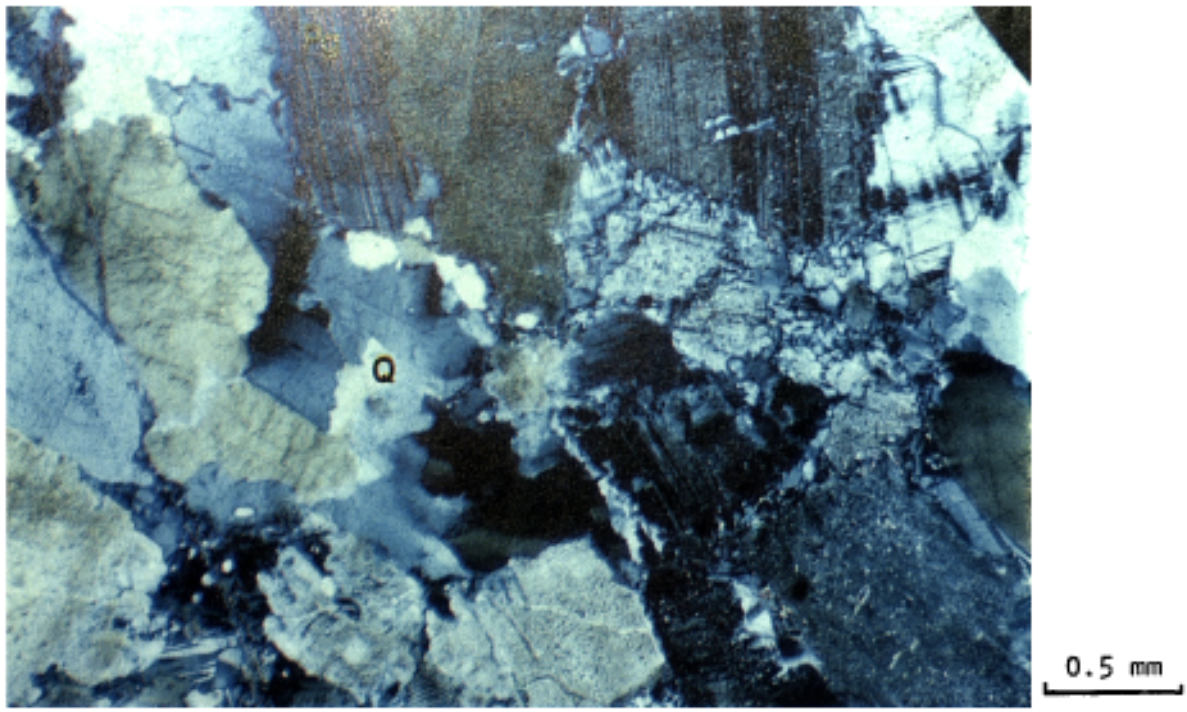

Fig. 13.- General aspect of the rock showing cataclastic texture (rims of comminuted grains between minerals, wavy extinction in quartz (Q) and deformation of albite-twin lamellae in plagioclase (Pg), (crossed nicols). Stripa granite.

The modal composition of sample ST5 is given in Table II. According to the classification of Streckeisen (1974), the rock is a monzogranite.

Quartz appears in aggregates of xenomorphic grains with autophase serrated boundaries and with strongly developed wavy extinction. Intergranular quartz-mica fissures are very common. K-feldspar (microcline), only slightly weathered, also shows evidence of deformation. Plagioclase, in very weathered grains, is often surrounded by a rim of comminuted grains as a result of stress. The albite-twin lamellae also appear deformed and, in some cases, form kink-band structures. Micas (muscovite and biotite) are also very deformed, biotite crystals appearing in ribbon aggregates almost completely transformed to chlorite and

epidote (Figure 14), and commonly filling cracks (Figure 15).

TABLE II

Mineral	%
Quartz	35.9
Plagioclase	35.0
Microcline	22.0
Biotite (chlorite)	3.0
Muscovite	1.8
Accessories (zircon, rutile)	
Secondaries (chlorite, epidote, sericite, clay minerals and calcite)	2.3

TABLE II.- Mineral composition of Stripa sample ST5.

The form factor (FF) of grains has been measured using digital image processing techniques. This parameter takes into account both perimeter (p) and area (a) for each grain using the relationship:

$$FF = p^2/4\pi a$$

The value of FF has been measured separately in thin section prepared from each semi-disc shaped specimen cut from sample ST5. There is no variation in the value of FF measured in the different thin sections. In Figure 16, the distribution of FF values for the total number of grains measured in all the thin sections is shown. The mean value of FF for the whole sample is 1.68. For comparison, the form factor of a circle is 1.00, and that of a square is 1.27: FF increases as the irregularity of the shape of the grain increases.

Microcrack network.

Although many wide cracks are visible under polarising microscopy, most are filled with alteration products (chlorite, epidote and clay minerals). During impregnation, therefore, the fluorescent resin only penetrates into very few, narrow, open (or accessible) cracks. Most of these impregnated cracks are of transgranular type, although they may change to intergranular for part of their path. There are also small intragranular cracks developed in quartz grains.

Fig. 14.- Due to severe deformation biotite crystals appear in ribbon aggregates (crossed nicols). Stripa granite.

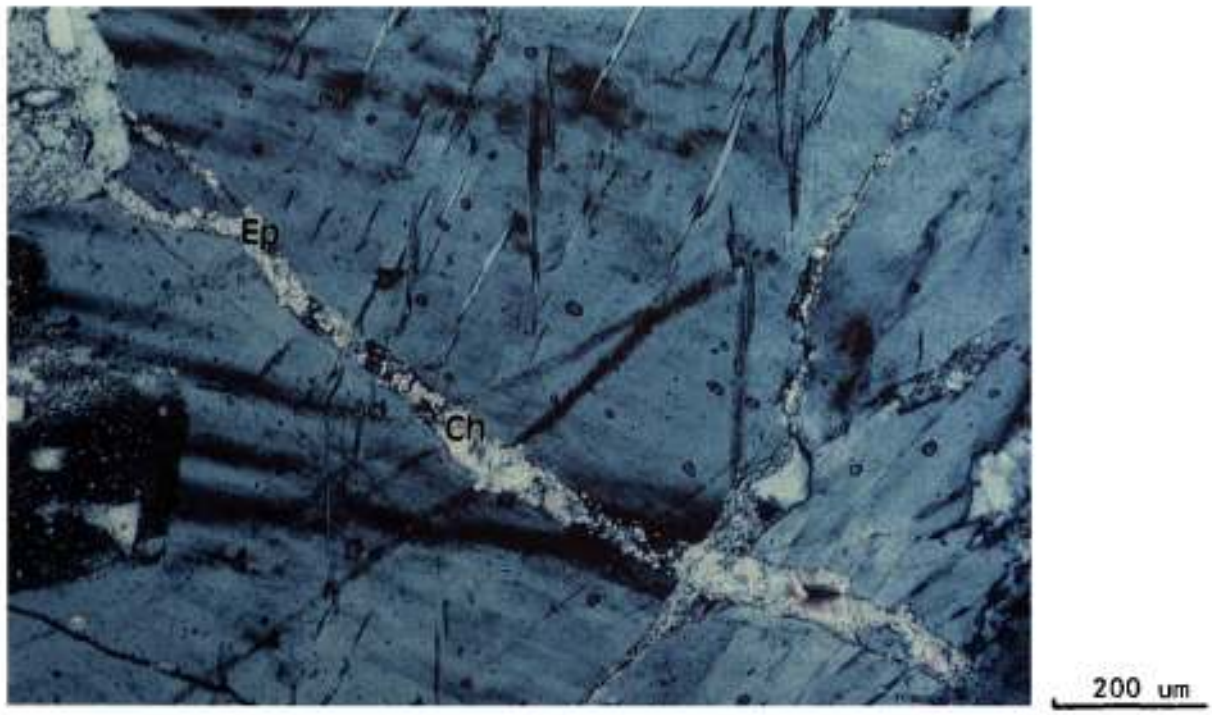

Fig. 15.- Alteration minerals (chlorite and epidote) fill intragranular cracks inside K-feldspar (crossed nicols). Stripa granite.

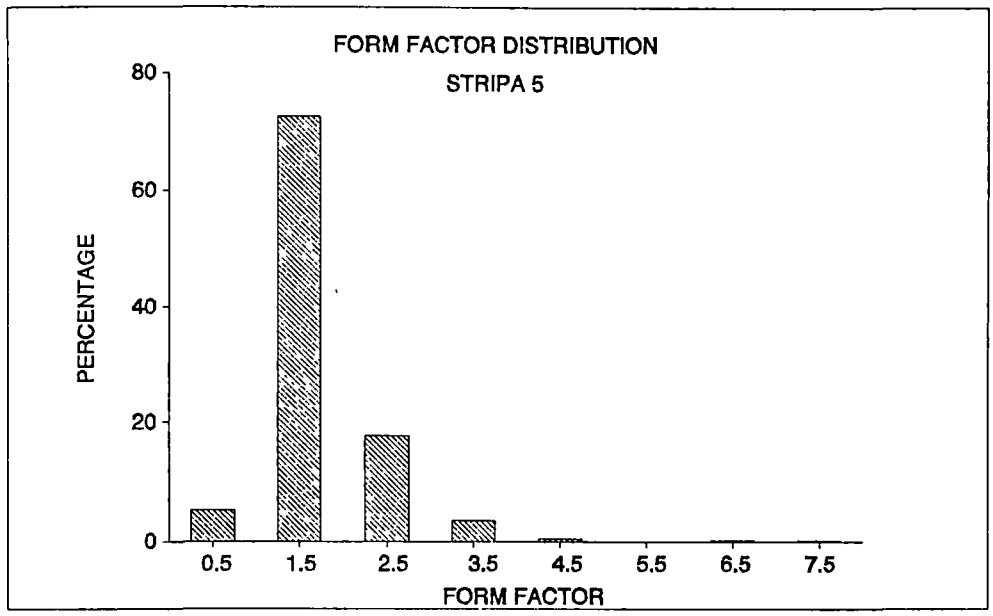

Fig. 16.- Distribution of form factor of grains in ST5 sample. Stripa granite.

The quantification of crack density has been carried out in specimens taken from Stripa sample ST5. A series of thin sections cut from the different semi-disc shaped specimens has been studied under reflected-light fluorescence microscopy.

The linear crack density (LCD) of Bauer and Johnson (1979) has been determined for each sample. This parameter is expressed as the number of cracks per millimetre, and is calculated by counting the number of traces of cracks intersected in two orthogonal directions. Results from one of the sample slices (ST5-E, located 95 mm from the fracture and parallel to it) are very different from those obtained from other samples. In the latter, almost no accessible cracks have been observed. In section ST5-E, however, many open cracks, were observed. The measured LCD was 0.28/mm. Regarding the type of cracks, 12.5% of the traces observed were of intragranular type, 61.6% of transgranular type, and 25.8% were intergranular.

4.3. PHYSICAL PROPERTIES.

Physical properties related to the following petrographic characteristics of the rocks studied have been measured:

- the nature and relative abundance of the mineral grains present;
- the nature of grain boundaries;
- the percentage and nature of voids.

4.3.1. Test methods.

In the measurement of physical properties, techniques suggested by ISRM (1981) and the standard methods of ASTM (1988), RILEM (1980) and CNR-ICR (1981) have been followed. In order to avoid micrographic artifacts, however, drying has been carried out in a oven at 60°C until constant weight is attained, rather than the 105°C recommended in the standard methods.

In accordance with the ISRM methods, the following terms and symbols have been used when describing the physical properties of the rocks studied:

- grains (the solid component of the sample): mass Ms, volume Vs;
- pore water: mass Mw, volume Vw;
- pore air: zero mass, volume Va;
- pores (voids): volume Vv + Vw + Va;
- bulk sample mass: M = Ms + Mw;
- bulk sample volume: V = Vs + Vv.

4.3.2. Key physical parameters.

Dry density (ρ_d).

Dry density, the ratio of the dry bulk sample mass (that is, the mass of the grains, Ms) to its bulk volume (V), has been determined by the saturation and buoyancy techniques (ISRM, 1981):

$\rho_d = Ms / V$ (kg/m^3).

Grain density (ρ_s).

Grain density, the ratio of the mass of grains (Ms) to their volume (Vs), has been determined by the pulverisation method using a volumetric flask (ISRM, 1981):

$\rho_s = Ms / Vs$ (kg/m^3).

Porosity.

Porosity is important in the interpreting the data for other properties, such as permeability, that are related to the movement of fluids within the rock matrix. Two types of porosity can be recognised:

- Accessible (or open) porosity, made up of interconnected pores and fissures that allow fluids to enter the rock matrix;

- Non-accessible porosity, which is essentially related to isolated, unconnected pores and fissures, though mineralised cracks etc. can also be included;

The total porosity is made up of both the accessible and non-accessible porosity.

The **accessible porosity (n_o)** is the ratio of the volume of accessible voids (Vw) to the sample volume (V), expressed as a percentage: o%

$$n_o = (Vw / V) \times 100.$$

The **total porosity (n)** is the total volume of voids (Vv) in relation to the sample volume (V), and is also expressed as a percentage (ISRM, 1981). n has been calculated from the relationship between dry density (ρ_d) and grain density (ρ_s):

$$n = (Vv / V) \times 100;$$

$$n = (\rho_s - \rho_d / \rho_s) \times 100.$$

Degree of saturation (Sr).

Sr, is the ratio of the volume of accessible voids (Vw) to the total volume of voids (Vv), and is calculated as the ration of the two porosities, expressed as a percentage (ISRM, 1981):

$$Sr = (Vw / Vv) \times 100;$$

$$Sr = (n_o / n) \times 100.$$

4.3.3. Hydric properties.

A very important group of physical properties are related to the presence and movement of water within the rock.

Void index (Iv) (Water content after one hour).

The void index is the mass of water contained in a rock sample after a one hour period of immersion, expressed as a percentage of its initial dessicator-dry mass (that is, the grain mass Ms) (ISRM, 1981).

Water content after two days (W_2).

W_2, is the mass of water contained in a rock sample after a two day period of immersion, expressed as a percentage of its initial desiccator-dry mass (Ms).

Saturation water content (Ws).

Water saturation can be achieved by different methods: under vacuum, by free immersion for different periods of time, by boiling etc.. In the present study, water saturation has been achieved under vacuum (10 E-3 torr), following the method of Belikov et al. (1967), the method considered to provide the best results.

Water content in the long term (Wi).

Wi, is defined as the maximum mass of water that can be freely absorbed over a long period of time, and is expressed as a percentage of the dry mass of the rock (that is, its grain mass, Ms) (CNR-ICR, 1981):

Wi = (Pi - Ms) / Ms x 100;
Pi, being the mass of the rock after time 'i'.

In the present study, no increase in water content was observed after 5 days.

Water absorption (Wi(t)).

It is very useful to assess the water content freely absorbed by the rock as a function of time. When determining Wi, therefore, the increase in water content was measured at intervals and expressed with regard to the square root of the time elapsed (Figure 17). The water content is then expressed as a percentage of the maximum water content achievable. Water absorption is very rapid in the first 20 minutes and gradually decreases thereafter.

Water desorption.

In a very similar way, the drying of the rock can be studied by measuring the variation in water content as the sample is allowed to dry under room conditions (20°C, 75% relative humidity). Again, the water content determined at each time interval

is expressed as a percentage of the water content at saturation (Figure 18). Drying takes place very rapidly at first and becomes slower later.

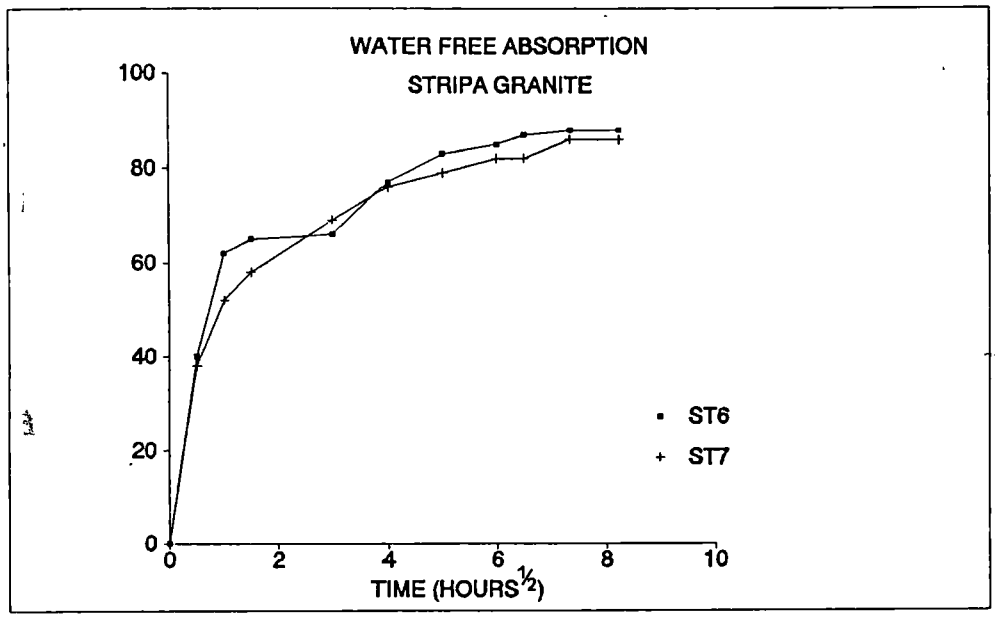

Fig. 17.- Water free absorption expressed as the variation of the degree of saturation with the square root of the time. Stripa granite.

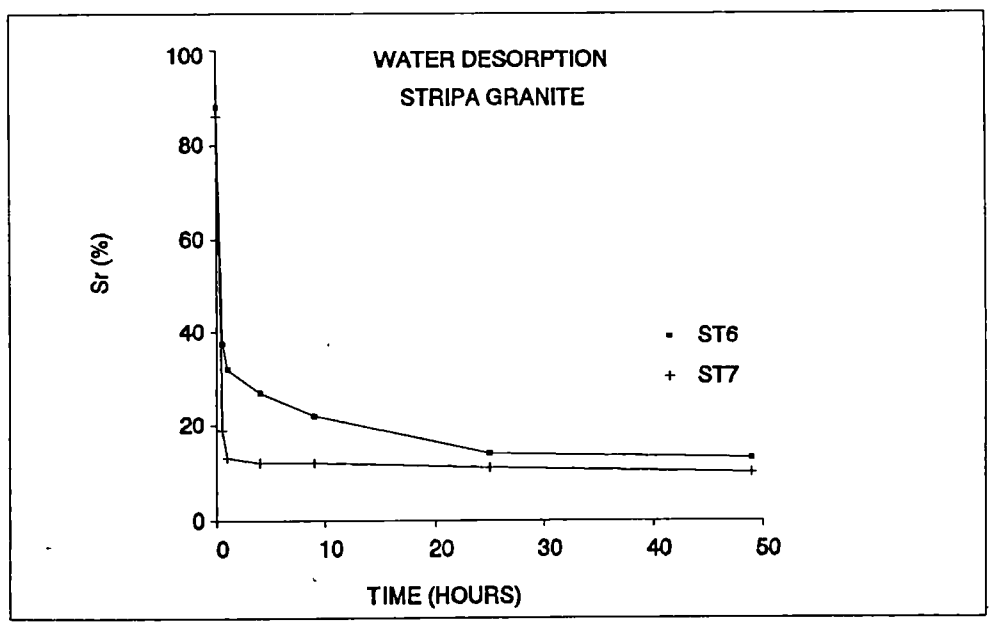

Fig. 18.- Water desorption expressed as the variation of the degree of saturation with the time. Stripa granite.

4.3.4. Variation in physical properties in relation to distance from the fracture surface.

4.3.4.1. El Berrocal granite.

The physical properties of each of the rock slices cut from the five cores (EB1A, EB1B, EB1E, EB1F and EB1J) obtained from sample block EB1 have been determined in order to assess variation in these properties with increasing distance from the fracture. Additionally, mercury porosimetry has been employed to quantify and characterise the rock porosity (Section 4.3.5). The data obtained are presented in Annex 1. In Table III, the mean values obtained for each core are presented with the mean values for the whole set of cores.

The variation in the values of the physical properties determined with distance from the fracture surface varies from property to property. Dry density, total porosity, degree of saturation, and water content after desorption show no well-defined distribution with respect to distance from the fracture.

TABLE III

	EB1A	EB1B	EB1E	EB1F	EB1J	Mean
$\rho d(kg/m^3)$	2625 ± 7	2626 ± 6	2625 ± 8	2627 ± 5	2627 ± 5	2627 ± 4
$\rho s(kg/m^3)$	2661 ± 10	2662 ± 11	2661 ± 12	2663 ± 5	2660 ± 5	2661 ± 1
n_0 (%)	1.22 ± 0.06	1.21 ± 0.18	1.14 ± 0.1	1.25 ± 0.24	1.18 ± 0.08	1.20 ± 0.04
n (%)	1.36 ± 0.17	1.32 ± 0.23	1.34 ± 0.24	1.35 ± 0.31	1.26 ± 0.07	1.33 ± 0.06
Sr (%)	90.11 ± 10	92.21 ± 11.9	85.90 ± 10.04	92.63 ± 6.42	94.20 ± 4.83	91.18 ± 2.71
Ws (%)	0.45 ± 0.05	0.47 ± 0.08	0.44 ± 0.61	0.47 ± 0.09	0.46 ± 0.04	0.46 ± 0.02
Iv (%)	0.36 ± 0.02	0.36 ± 0.04	0.33 ± 0.02	0.36 ± 0.08	0.34 ± 0.03	0.35 ± 0.01
W_2 (%)	0.38 ± 0.03	0.38 ± 0.04	0.34 ± 0.04	0.39 ± 0.09	0.37 ± 0.03	0.37 ± 0.02
W_5 (%)	0.41 ± 0.03	0.40 ± 0.03	0.34 ± 0.04	0.41 ± 0.10	0.38 ± 0.04	0.39 ± 0.02
W_d (%)	0.10 ± 0.02	0.12 ± 0.03	0.10 ± 0.02	0.11 ± 0.02	0.10 ± 0.02	0.11 ± 0.02

ρd: Dry density; n_0: Accesible porosity; n: Total porosity
Sr: Degree of saturation; Ws: Saturation water content; Iv: Void index
W_2: Two days water content; W_5: Five days water content; Wd: Water content after desorption.

Table III.- Physical properties of the intact rock for each core, as well as the mean value for the whole set of cores. (95% confidence interval).

The void index, open porosity, water content after five days, and saturation water content, however, all decrease as the distance from the fracture increases. The variation in the void index, expressed as a percentage of the value obtained from the rock slice immediately adjacent to the fracture, is shown in Figure 19a; the solid line joins mean values obtained from slices at the same distance from the fracture. Also shown are the values obtained for accessible porosity (Figure 19b), water content after five days (Figure 20a) and saturation water content (Figure 20b).

Water absorption and desorption have been determined as a function of time for all sample cores; results for core EB1A are shown in Figures 21 and 22. Variation in the mean values of water absorption and desorption for rock slices obtained from the same distance from the fracture in each of the five cores from block EB1 is plotted as a function of time in Figures 23 and 24. Water absorption is very fast in the first 15 minutes and gradually decreases thereafter. There is no apparent relation between absorption behaviour and distance from the fracture. Desorption was also found to take place very rapidly at first and to become slower later. Again, the distance from the fracture does not appear to influence the desorption behaviour in this or the other cores.

The results for core EB3 are presented in Annex 2 with mean values in Table IV.

TABLE IV

Dry density, ρ_d (kg/m^3)	2619 ± 5.1
Grain density, ρ_s (kg/m^3)	2659 ± 3
Accessible porosity, n_o (%)	1.38 ± 0.06
Total porosity, n (%)	1.57 ± 0.15
Degree of saturation, Sr (%)	89.19 ± 5.64
Saturation water content, Ws (%)	0.53 ± 0.02
Void index, Iv (%)	0.41 ± 0.03
Water content after 2 days, W_2 (%)	0.42 ± 0.03
Water content after 5 days, W_5 (%)	0.48 ± 0.02
Water content after desorption, W_d (%)	0.03 ± 0.003

TABLE IV.- Mean values of physical properties of the intact rock for sample EB3. The maximum error corresponds to a confidence interval of 95%.

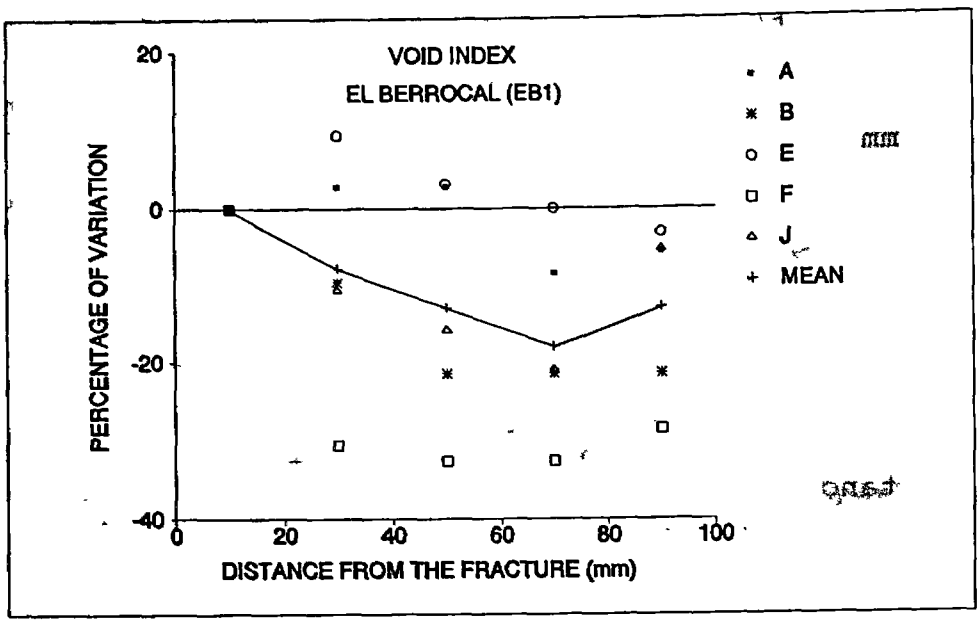

a

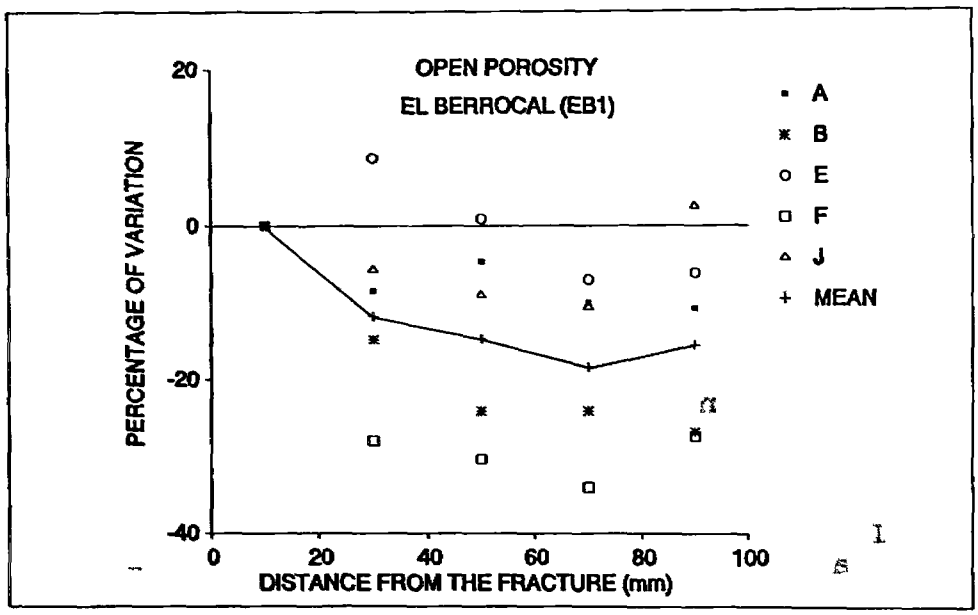

b

Fig. 19.- Variation of the a) void index, b) open porosity, with regard to the distance to the rock fracture, for all the studied slices (A, B,.. stand in for EB1A, EB1B,...; M: mean values for the slices located at the same distance from the fracture). El Berrocal granite, block 1.

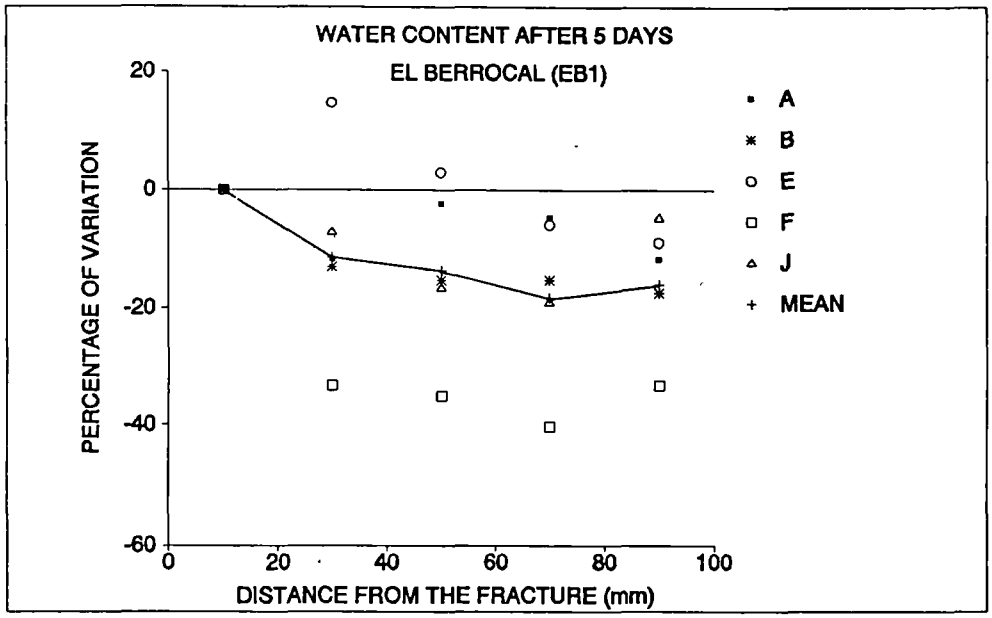

a

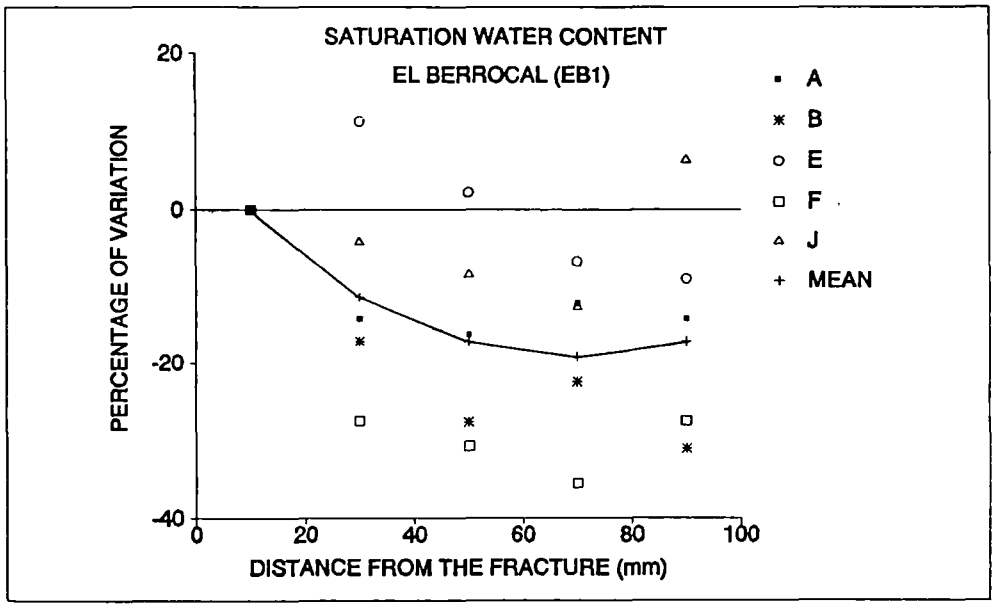

b

Fig. 20.- Variation of the a) water content after 5 days, b) saturation water content, with regard to the distance to the rock fracture, for all the studied slices (A, B,.. stand in for EB1A, EB1B,...; M: mean values for the slices located at the same distance from the fracture). El Berrocal granite, block 1.

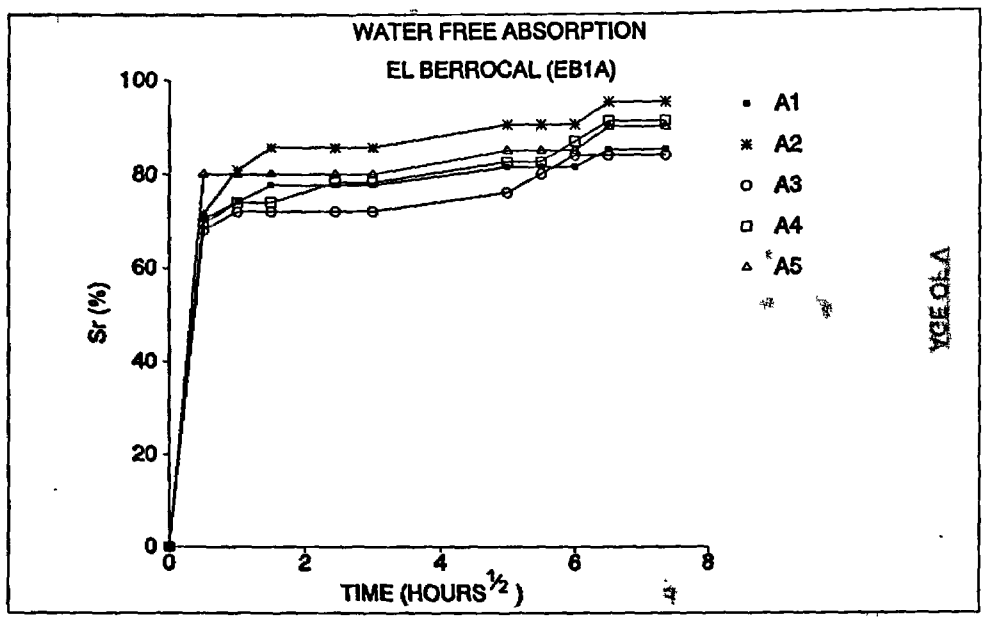

Fig. 21.- Water free absorption expressed as the variation of the saturation degree with the square root of the time for the different slices (A1, A2, etc) from El Berrocal core EB1A.

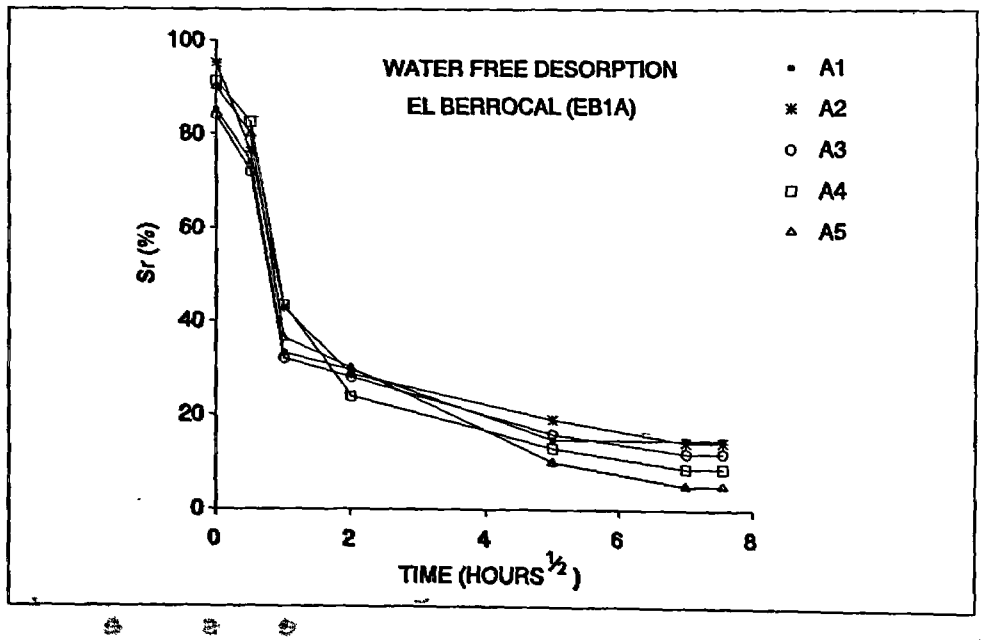

Fig. 22.- Water desorption expressed as the variation of the saturation degree with the square root of the time for the different slices (A1, A2, etc) from El Berrocal core EB1A.

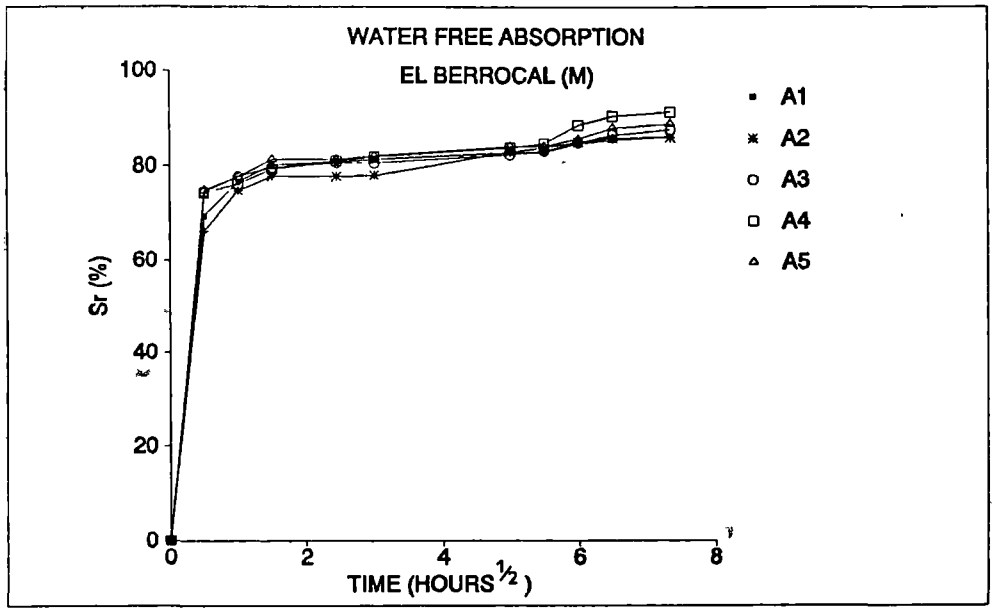

Fig. 23.- Water free absorption expressed as the variation of the degree of saturation with the square root of the time. (Mi = (EB1Ai + EB1Bi + EB1Ei + EB1Fi + EB1Ji)/5; EB1Ai, EB1Bi ..., are the slices of the different cores located at the same distance from the fracture. El Berrocal granite.

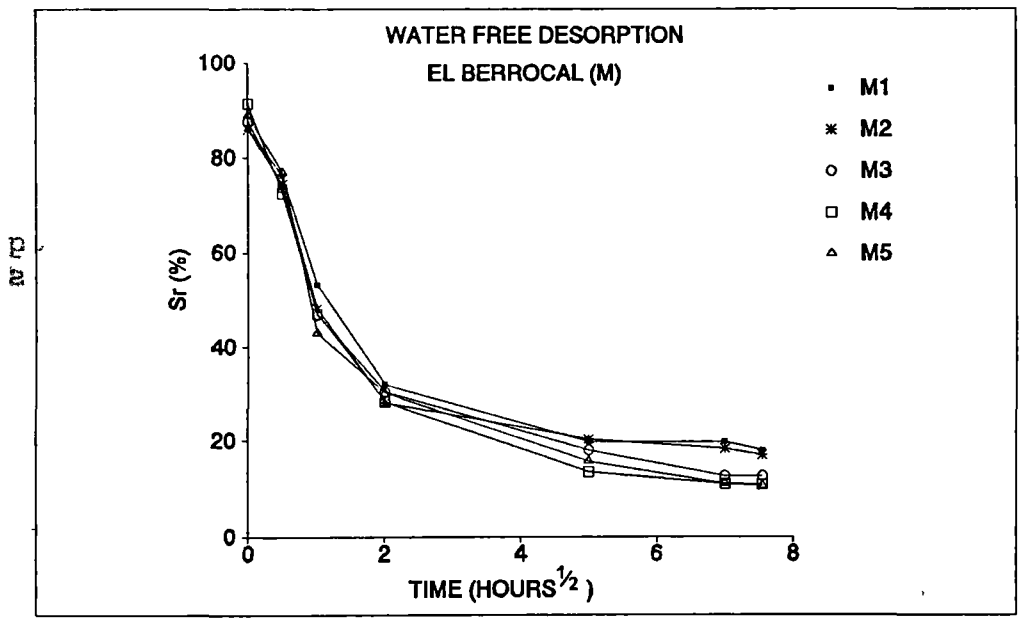

Fig. 24.- Water desorption expressed as the variation of the degree of saturation with the square root of the time. (Mi = (EB1Ai + EB1Bi + EB1Ei + EB1Fi + EB1Ji)/5; EB1Ai, EB1Bi ... are the slices of the different cores located at the same distance from the fracture. El Berrocal granite.

The results of water absorption/desorption studies (Figure 25 and 26) reveal a similar variation to that of samples EB1. Values of open porosity, void index, water content after 2 and 5 days, and saturation water content, however, do seem to show a systematic variation: there is an initial decrease with increasing distance from the fracture up to a distance of approximately 160 mm from the fracture (slice EB3F), values increasing thereafter (Figures 27a - 27e). This pattern is attributed to variation in microfracture density, which first decreases with increasing distance from the main fracture and then increases slightly, the increase being associated with the presence of a macrofracture, as illustrated in Figure 28. The water content after desorption shows a similar variation (Figure 29), but the values are very low, varying between 0.07% and 0.02%.

For the calculation of total porosity (n) in sample EB3, a grain density (ρ_s) value of 2.659 kg/m^3 has been used, as determined in blocks EB1 and EB2.

4.3.4.2. Stripa granite.

The physical properties of 7 semi-disc shaped specimens cut from two cores of Stripa granite (ST6 and ST7) have been determined. Five measurements of each parameter have been carried out on each specimen. The full results are presented in Annex 3. The mean value of each parameter calculated for each sample core is presented in Table V.

Some of the measured physical properties vary erratically with distance from the fracture (Figure 30). Dry density (Figure 30a) shows a very irregular pattern for both ST6 and ST7, there being no clear relation with distance from the fracture surface. The same is true for total porosity (Figure 30b), degree of saturation (Figure 30c), and for water content after desorption (Figure 30d).

In the case of the void index (Figure 30e) and accessible porosity (Figure 30f), ST6 shows a decrease in the value of each property with increasing distance from the fracture, while values for ST7 vary irregularly.

Water content after two days (Figure 30g), water content after five days (Figure 30h), and saturation water content (Figure 30i) show a clear decrease with increasing distance from the fracture, however, in both samples ST6 and ST7.

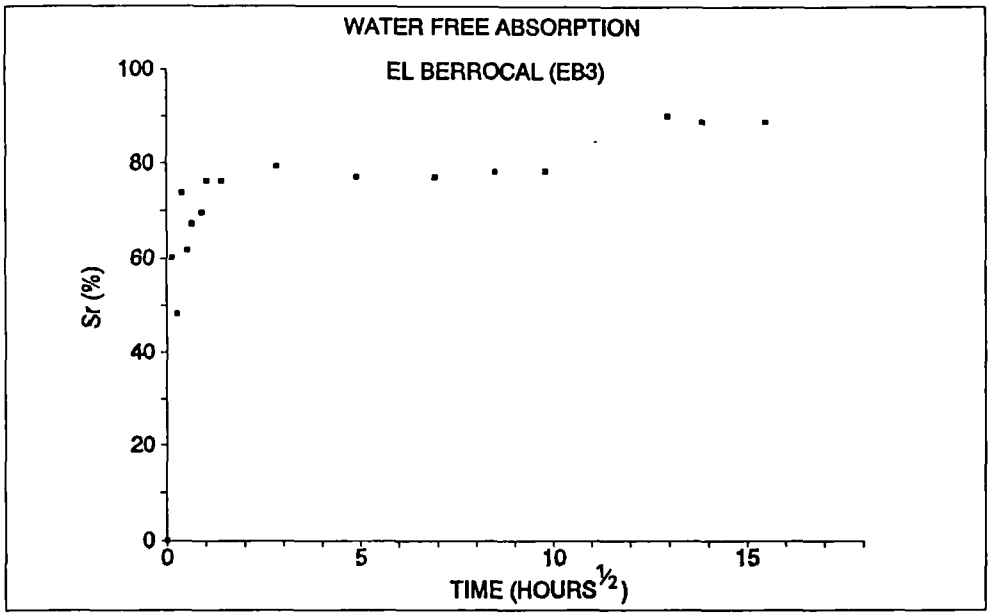

Fig. 25.- Water free absorption; mean values of the different slices. El Berrocal granite, core EB3.

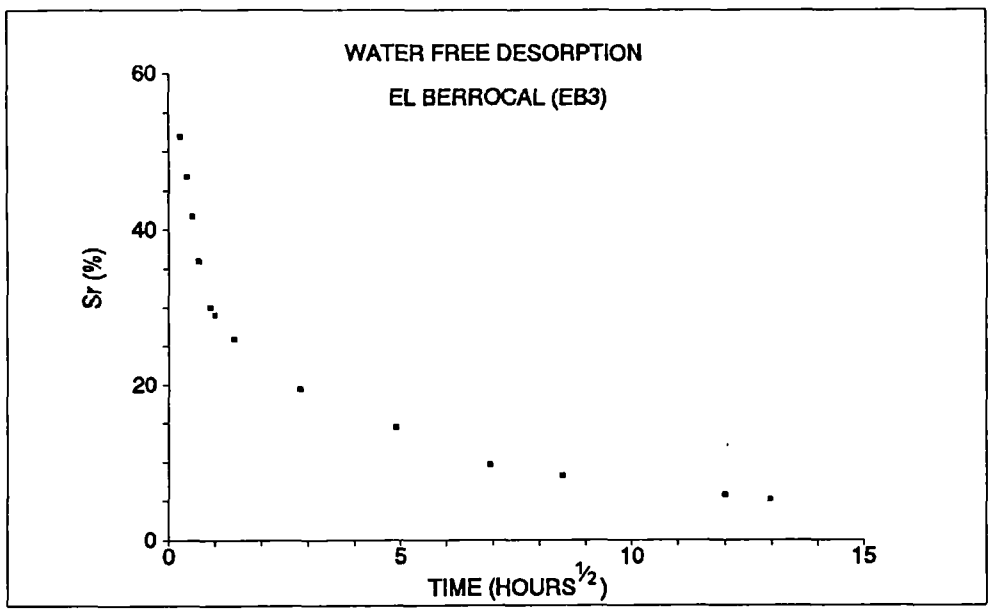

Fig. 26.- Water desorption; mean values of the different slices. El Berrocal granite, core EB3.

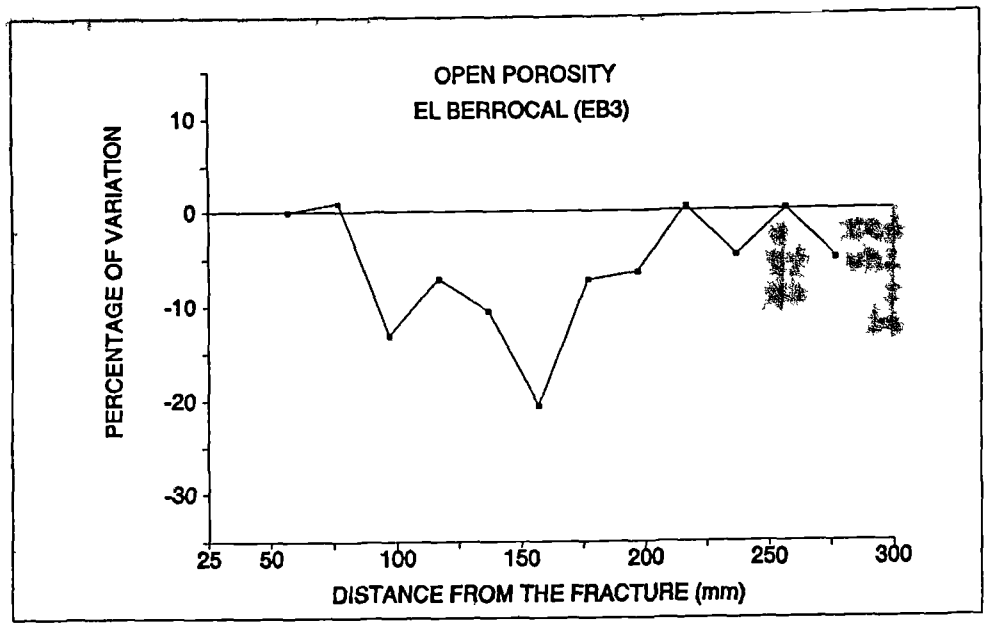

a

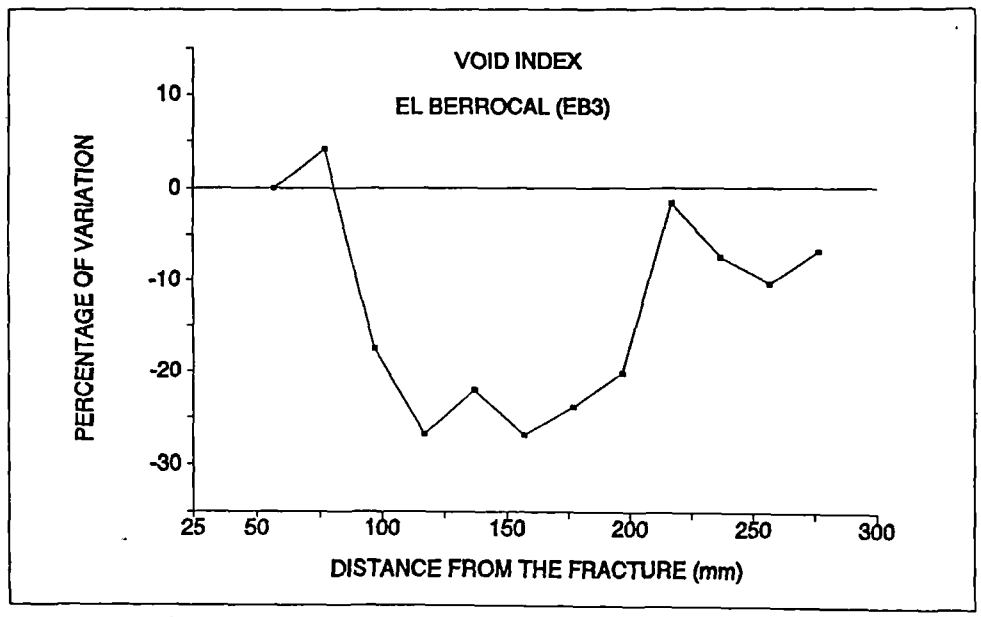

b

Fig. 27.- Variation of the properties with regard to the distance to the main fracture: a) open porosity, b) void index. El Berrocal granite, core EB3.

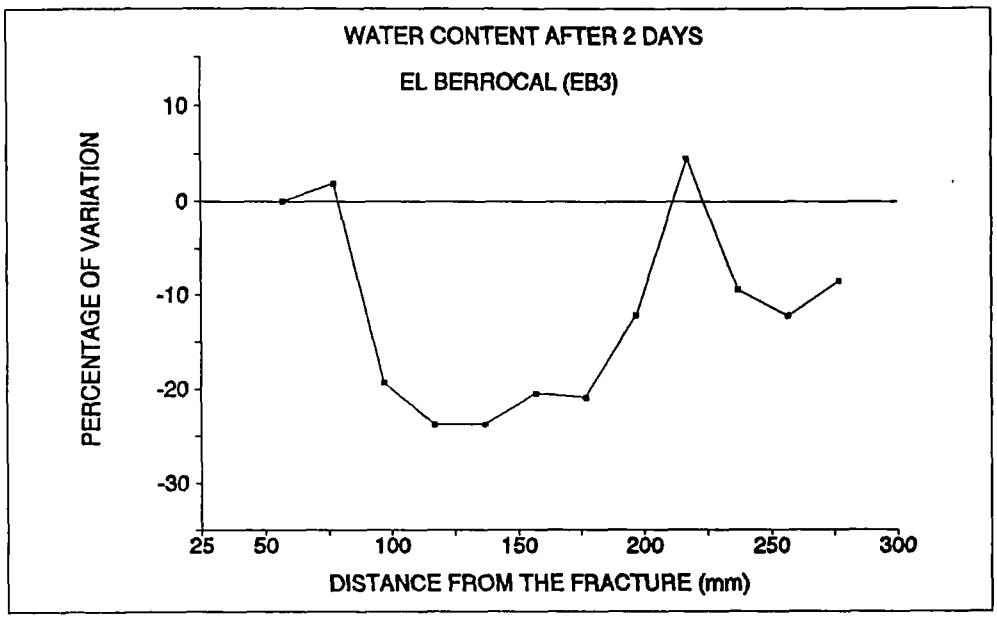

c

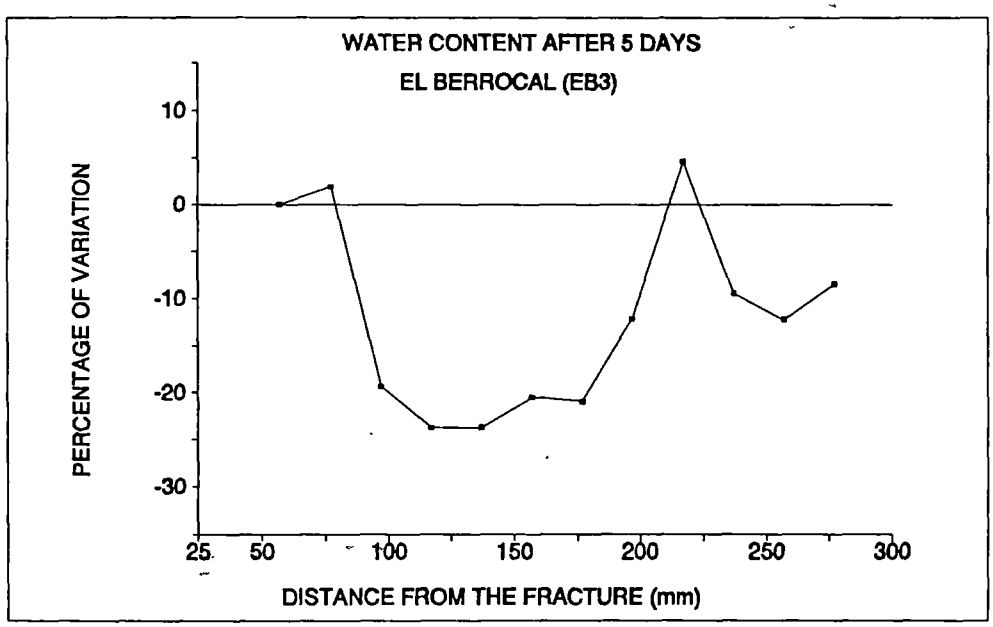

d

Fig. 27.- Variation of the properties with regard to the distance to the main fracture: c) water content after 2 days, d) water content after 5 days. El Berrocal granite, core EB3.

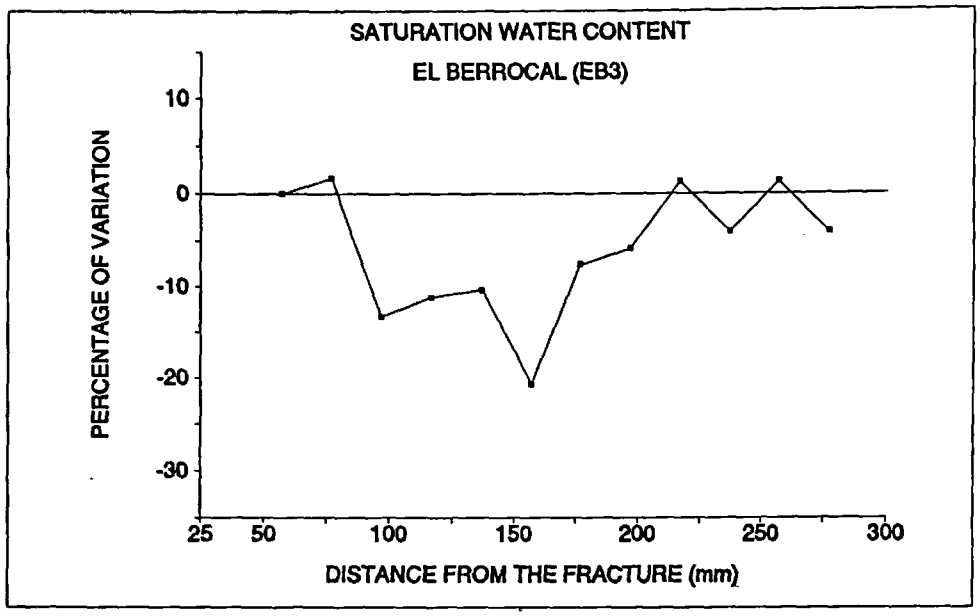

e

Fig. 27.- Variation of the properties with regard to the distance to the main fracture: e) saturation water content. El Berrocal granite, core EB3.

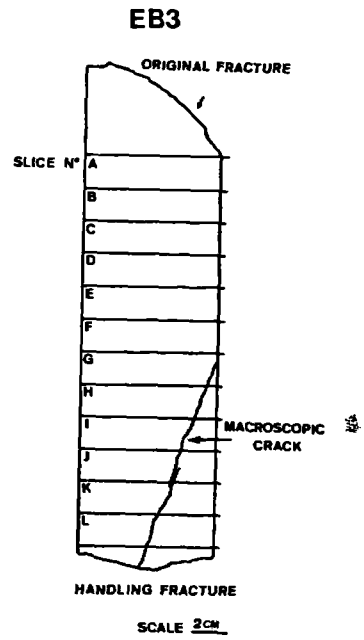

Fig. 28.- Cutting of core for microstructural studies. El Berrocal granite, core EB3.

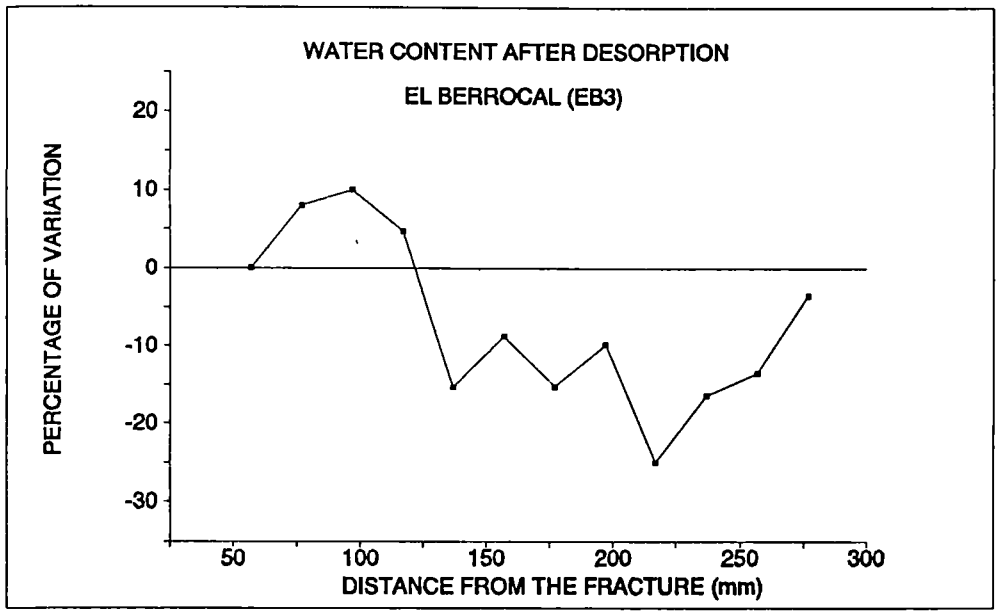

Fig. 29.- Variation of the water content after desorption with regard to the distance from the fracture. El Berrocal granite, core EB3.

TABLE V

	ST-6	ST-7
Dry density, ρd (kg/m^3)	2624 ± 2.68	2624 ± 3.09
Grain density, ρs (kg/m^3)	2638 ± 3.20	2638 ± 2.26
Accesible porosity, n_0 (%)	0.39 ± 0.03	0.37 ± 0.03
Total porosity, n (%)	0.52 ± 0.10	0.52 ± 0.11
Degree of saturation, Sr (%)	76.74 ± 12.68	74.36 ± 15.34
Saturation water content, Ws (%)	0.15 ± 0.02	0.14 ± 0.01
Voind index, Iv (%)	0.11 ± 0.02	0.09 ± 0.01
Two days water content, W_2 (%)	0.13 ± 0.01	0.12 ± 0.01
Five days water content, W_5 (%)	0.13 ± 0.01	0.12 ± 0.01
Water content after desorption, W_d (%)	0.01 --	0.002 --

Table V.- Physical properties of the intact rock for samples ST6 and ST7. The maximun error corresponds to an interval of confidence of 95%.

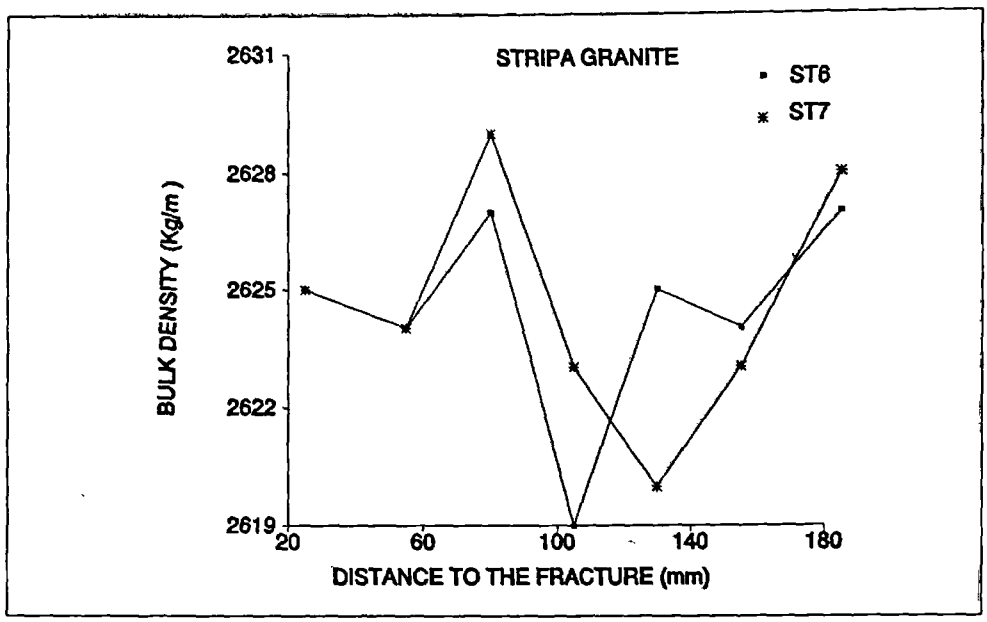

a

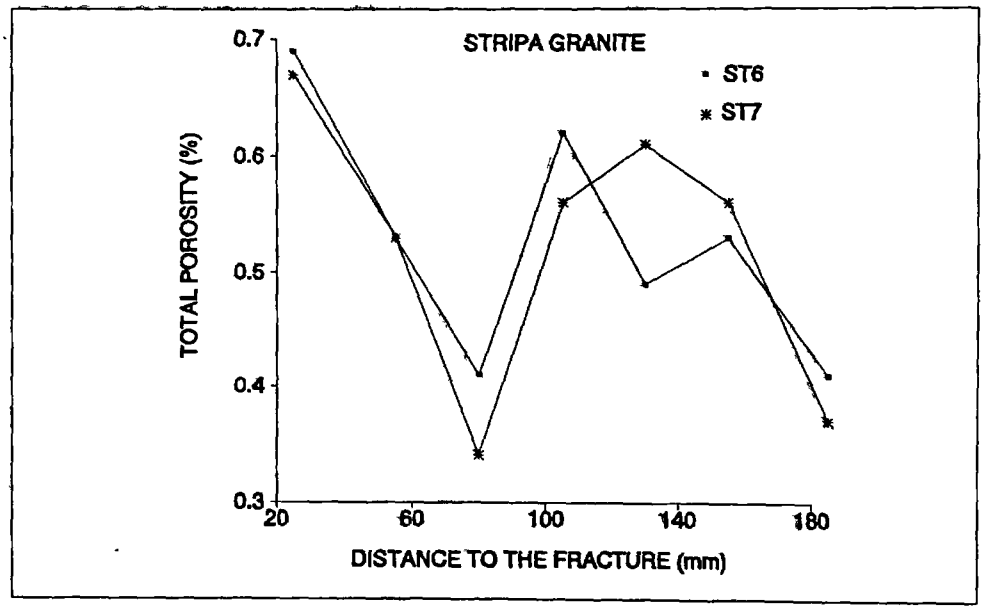

b

Fig. 30.- Variation of the properties with regard to the distance to the rock fracture: a) dry density, b) total porosity. Stripa granite.

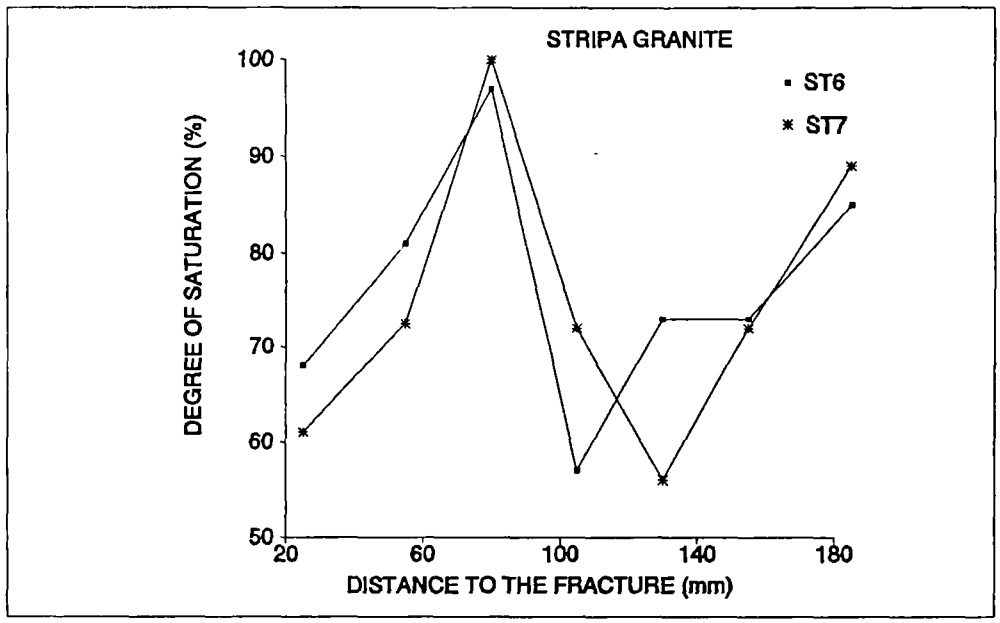

c

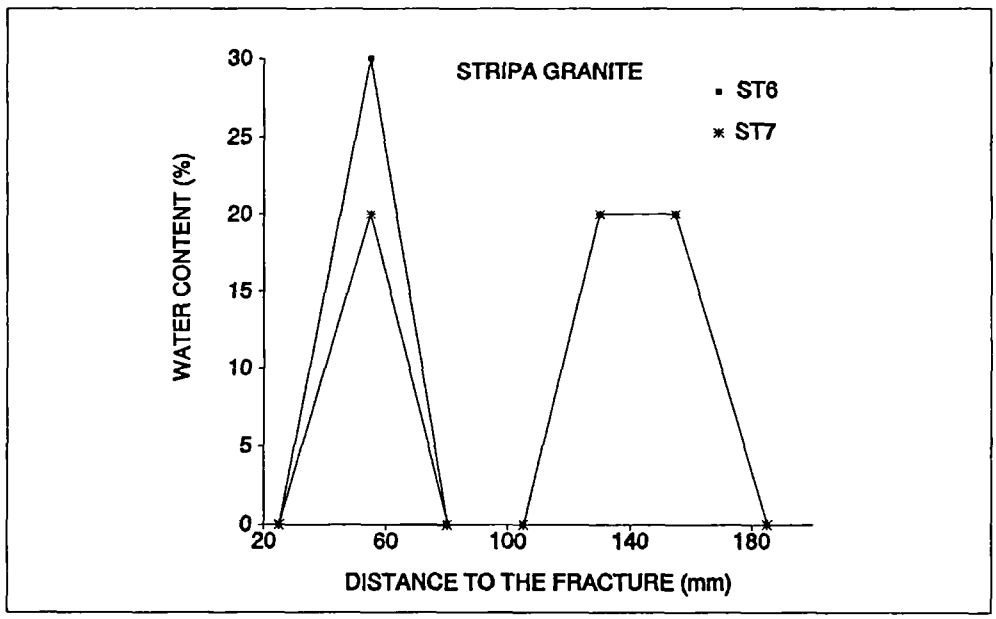

d

Fig. 30.- Variation of the properties with regard to the distance to the rock fracture: c) degree of saturation, d) water content after desorption. Stripa granite.

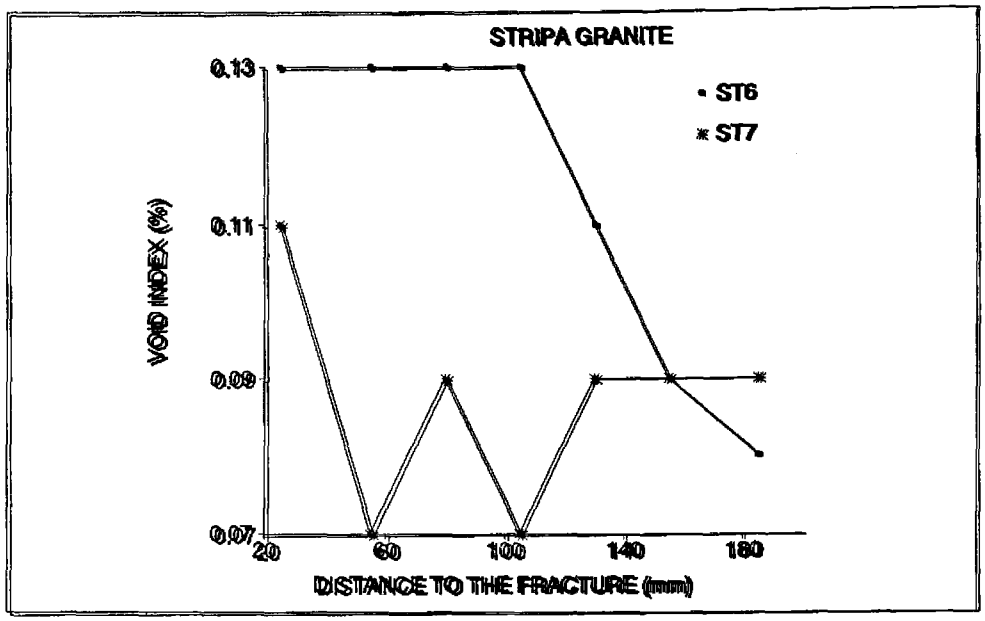

e

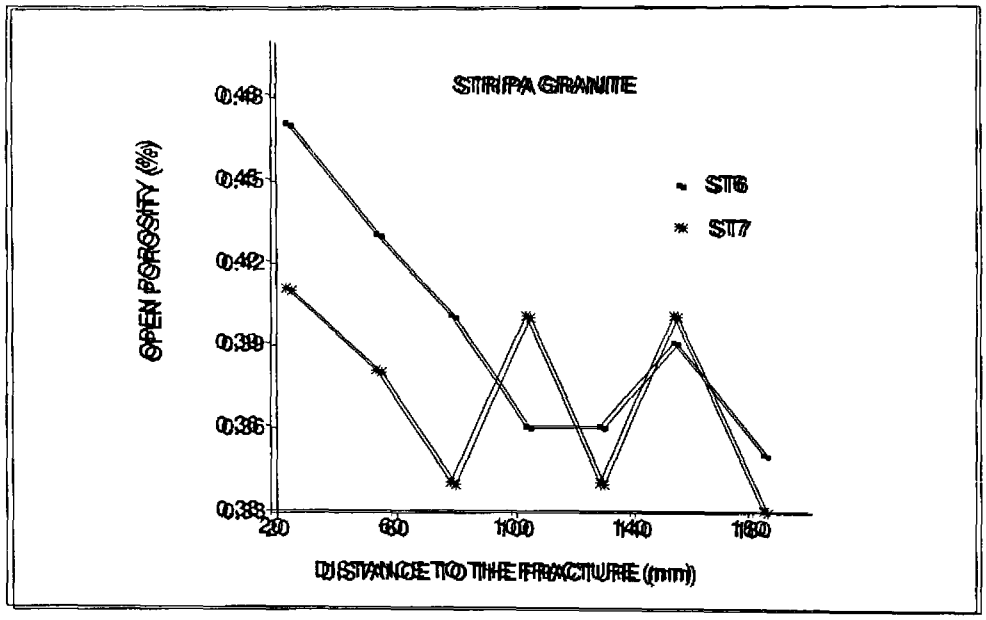

f

Fig. 30.- Variation of the properties with regard to the distance to the rock fracture: e) void index, f) open porosity. Striipa granite.

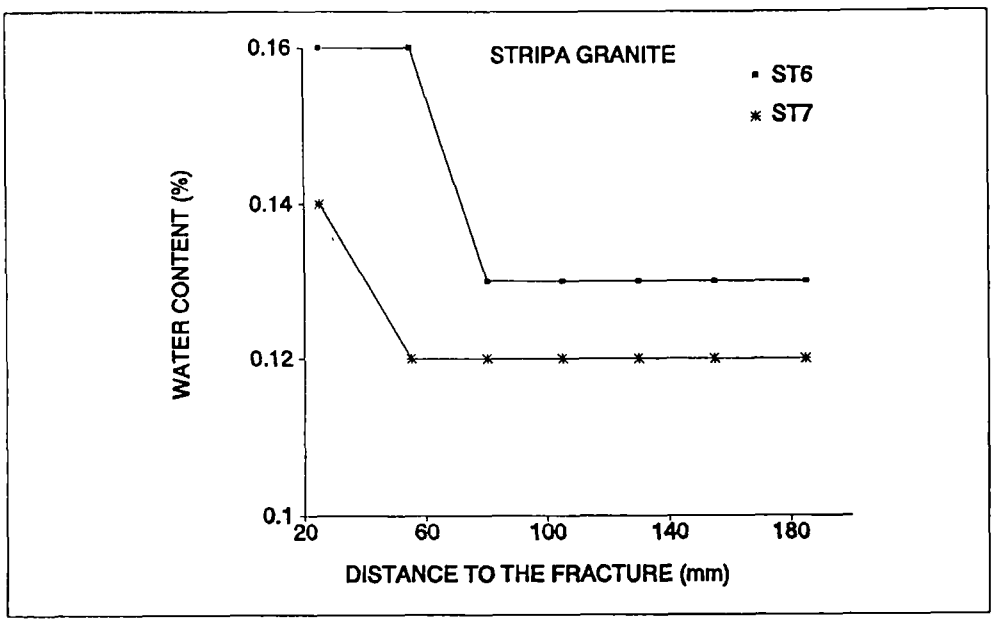

g

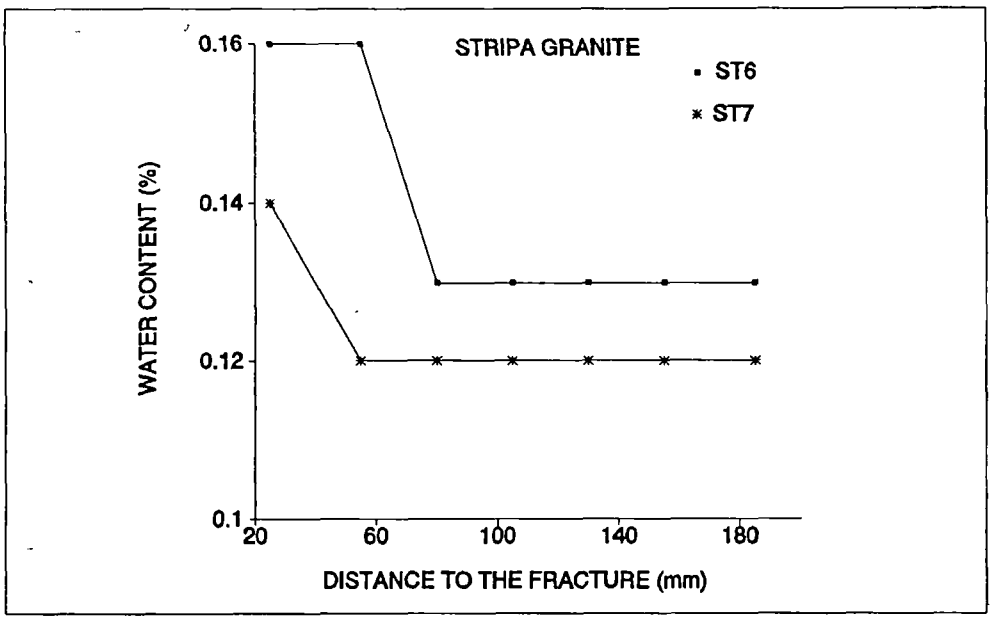

h

Fig. 30.- Variation of the properties with regard to the distance to the rock fracture: g) water content after 2 days, h) water content after 5 days. Stripa granite.

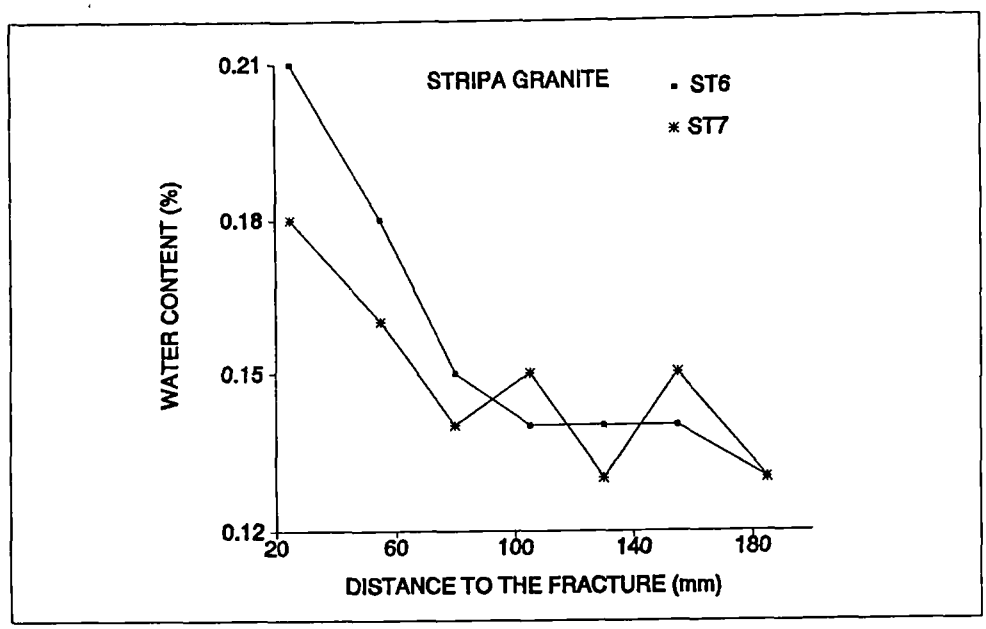

Fig. 30.- Variation of the properties with regard to the distance to the rock fracture: i) saturation water content. Stripa granite.

4.3.4.3. Whiteshell granite.

The physical properties of two cores of Whiteshell granite (WS1 and WS2) have been determined; the cores were cut into a series of slices as shown in Figures 31 and 32. Full results are presented in Annex 4. The mean values of each parameter calculated for each sample core is presented in Table VI.

Water absorption and desorption are plotted as a function of time in Figure 33 (a,b) (WS1) and Figure 34 (a,b) (WS2). Open porosity, void index, water content after 2 and 5 days, saturation water content and water content after desorption show a clear decrease with increasing distance from the fracture in sample WS1 (Figures 35a - 35f) up to a distance of about 50 mm, after which values are more constant (though in some cases rather erratic). For sample WS2 (Figures 36a - 36f), however, there is no clear relation between physical properties and distance from the fracture, although both porosity and saturation water content increase with increasing distance from the fracture up to a distance of 120 mm, and then decrease.

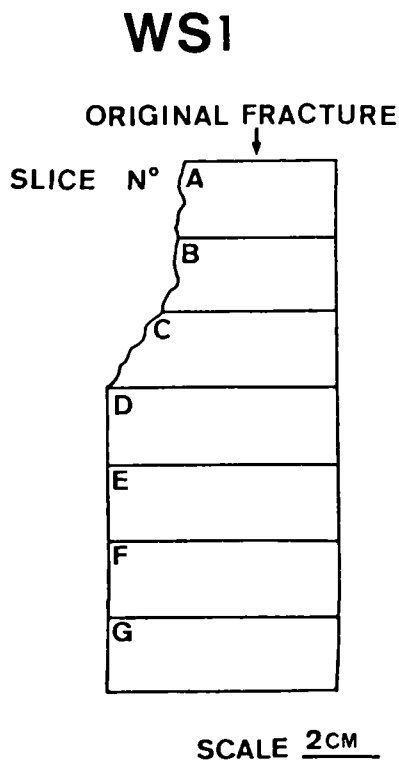

Fig. 31.- Cutting of core for microstructural studies. Whiteshell granite, core WS1.

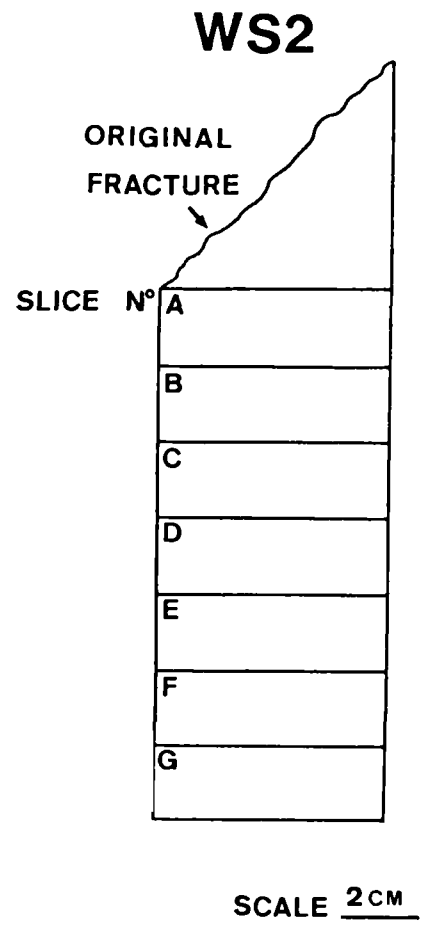

Fig. 32.- Cutting of core for microstructural studies. Whiteshell granite, core WS2

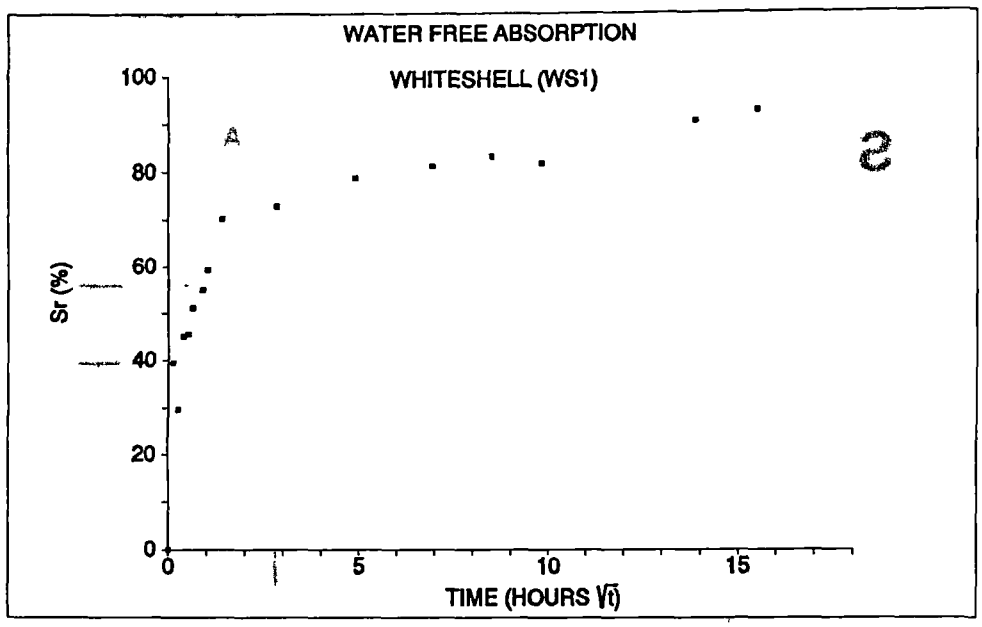

Fig. 33 a.- Water free absorption; mean values of the different slices. Whiteshell granite, core WS1.

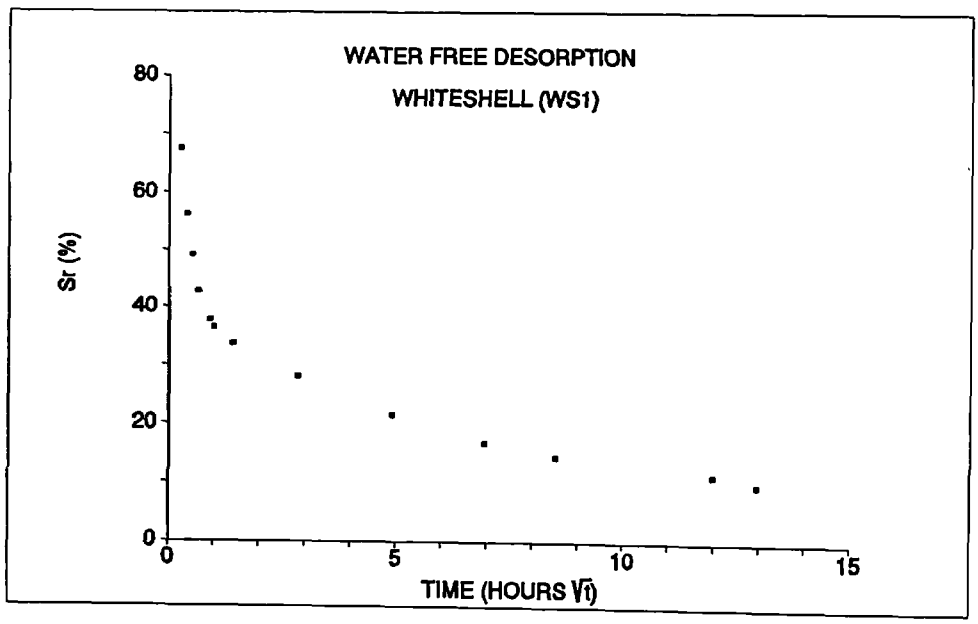

Fig. 33 b.- Water desorption; mean values of the different slices. Whiteshell granite, core WS1.

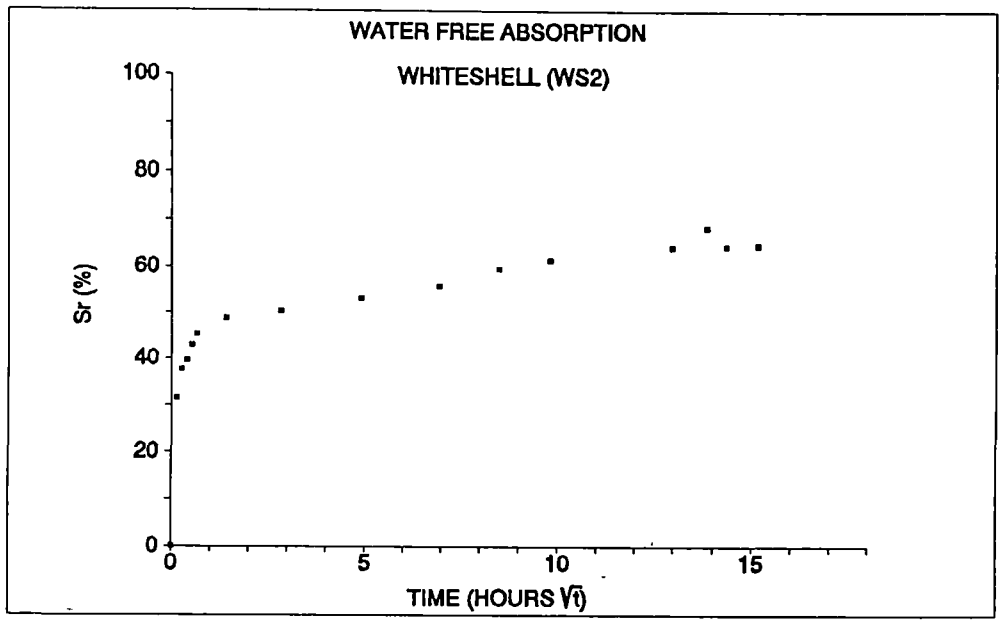

Fig. 34 a.- Water free absorption; mean values of the different slices. Whiteshell granite, core WS2.

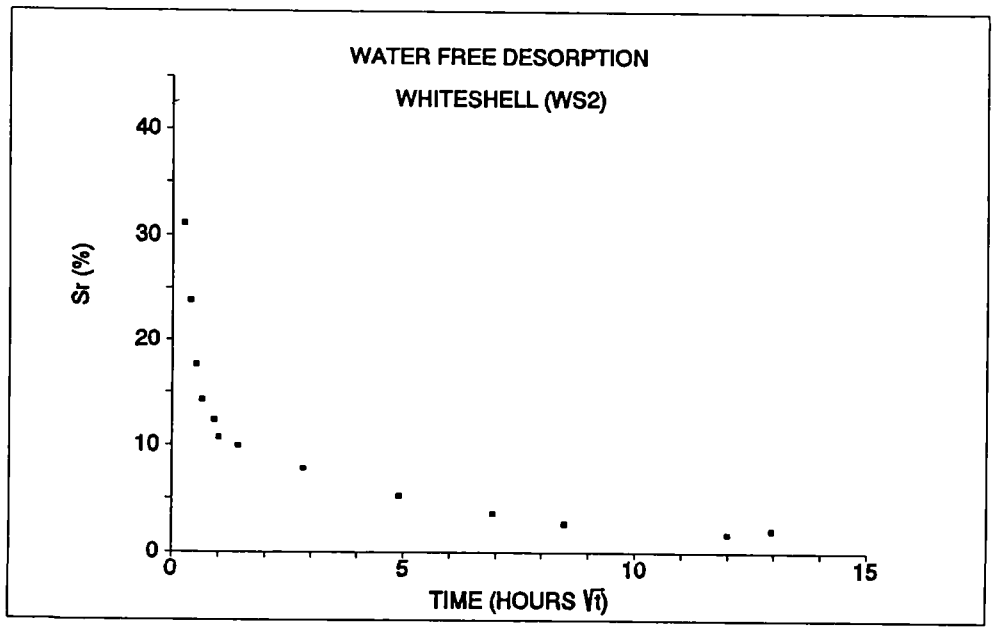

Fig. 34 b.- Water desorption; mean values of the different slices. Whiteshell granite, core WS2.

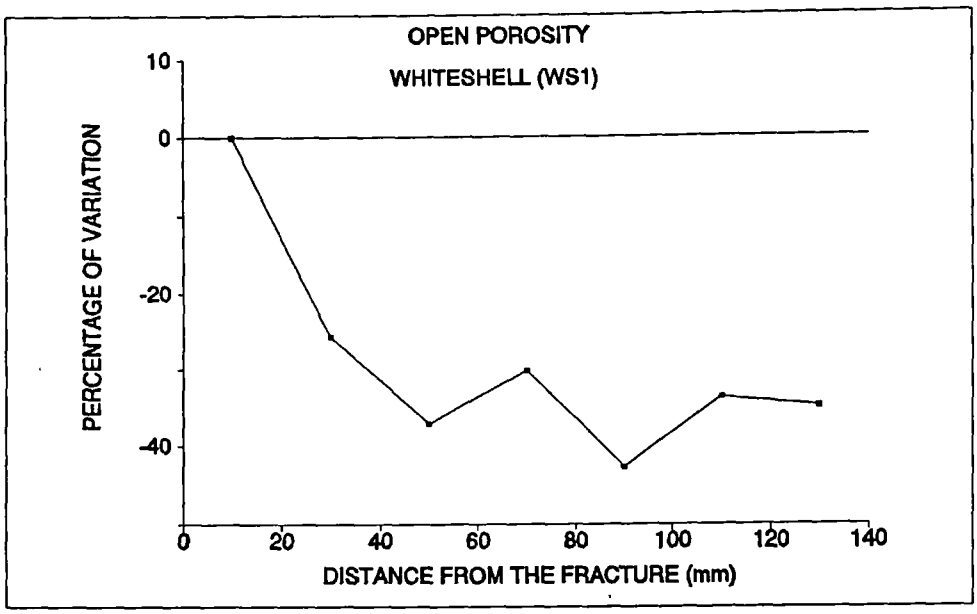

a

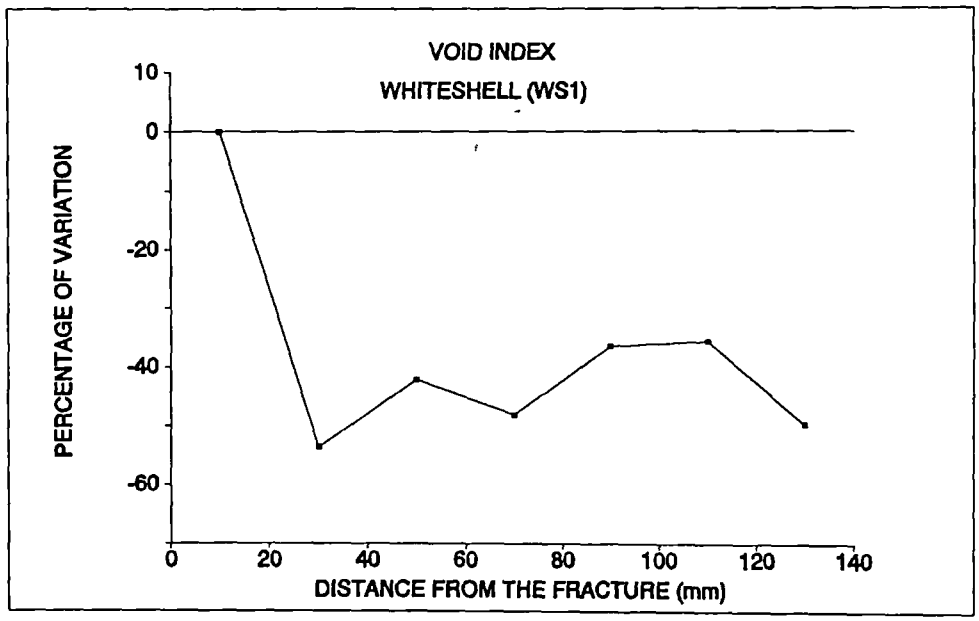

b

Fig. 35.- Variation of the properties with regard to the distance to the main fracture: a) open porosity, b) void index. Whiteshell granite, core WS1.

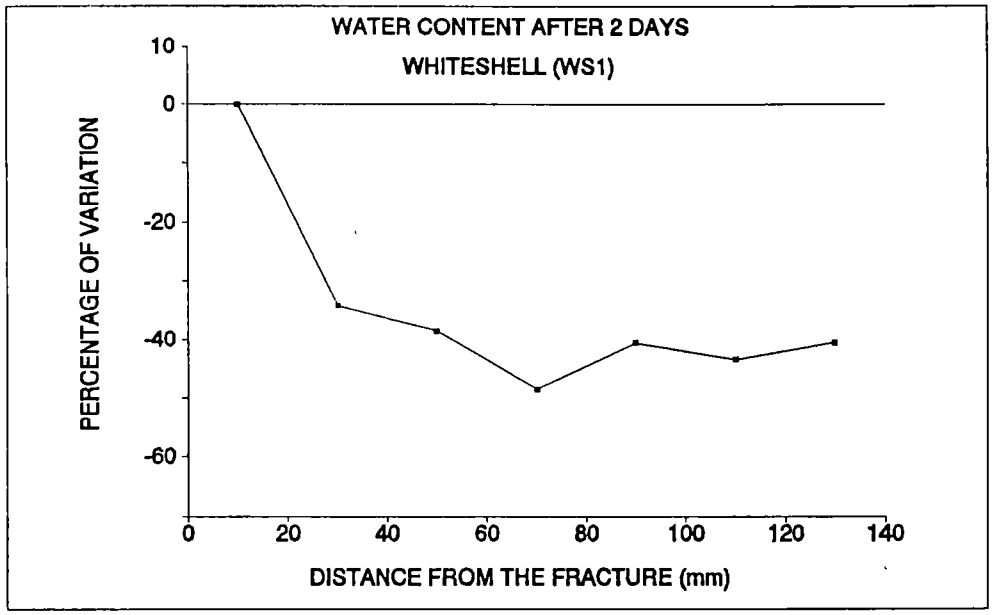

c

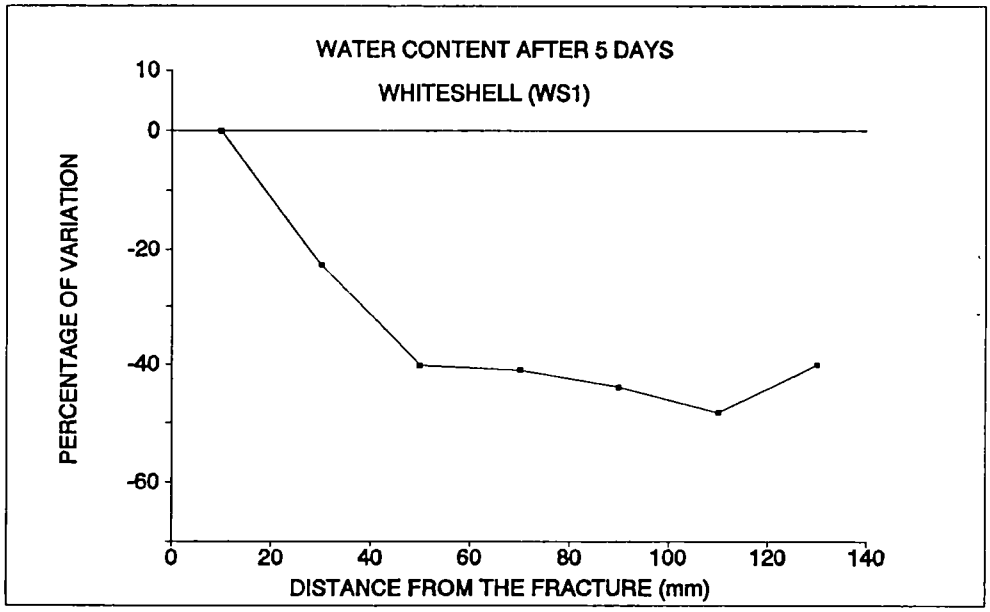

d

Fig. 35.- Variation of the properties with regard to the distance to the main fracture: c) water content after 2 days, d) water content after 5 days. Whiteshell granite, core WS1.

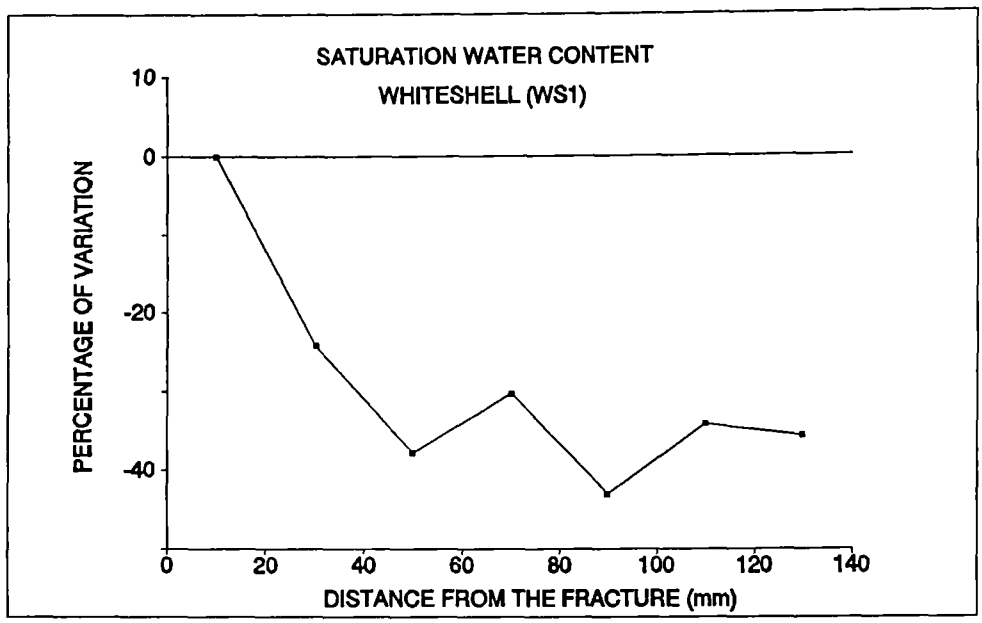

e

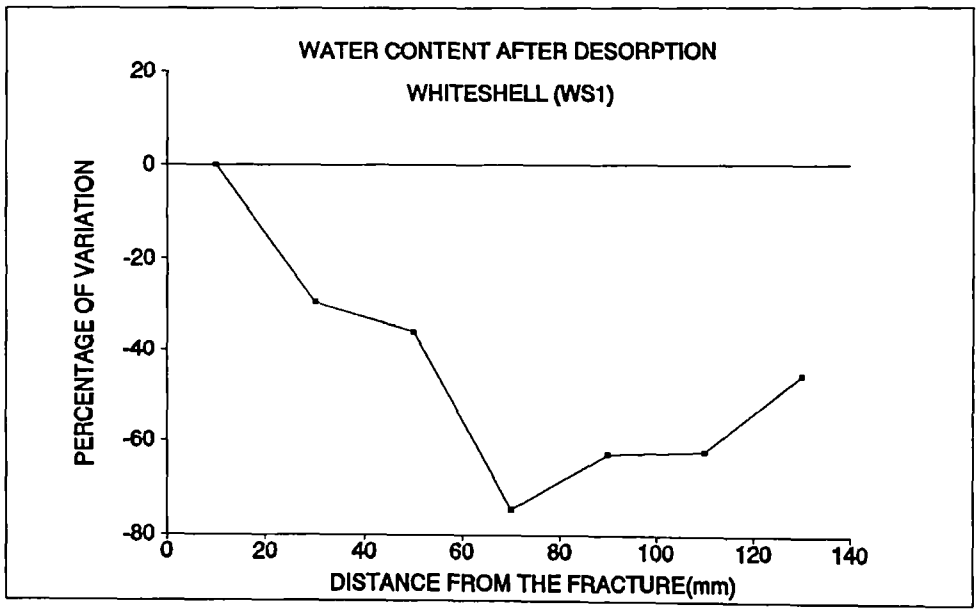

f

Fig. 35.- Variation of the properties with regard to the distance to the main fracture: e) saturation water content, f) water content after desorption. Whiteshell granite, core WS1.

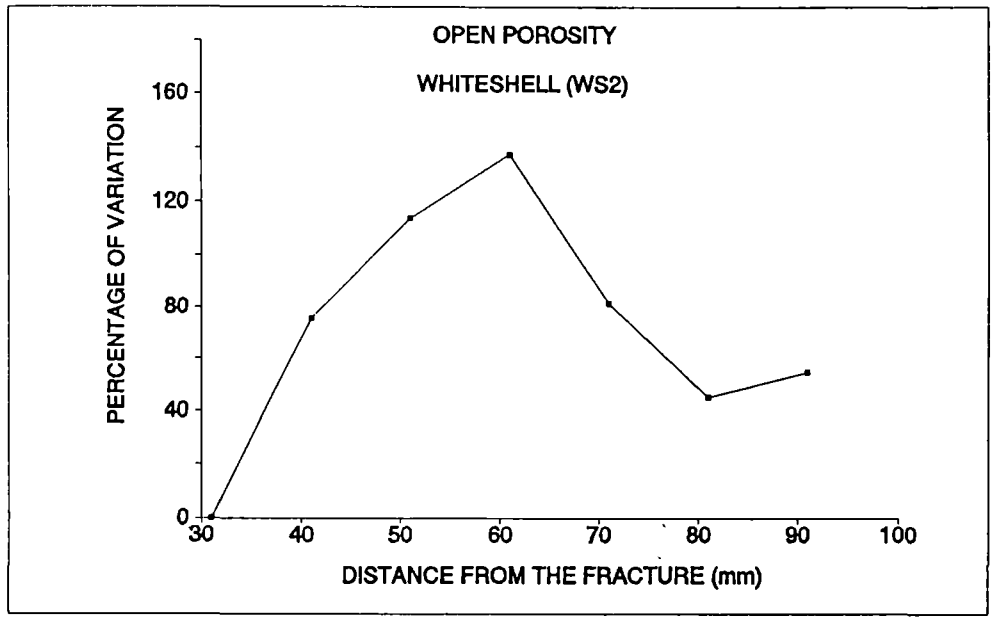

a

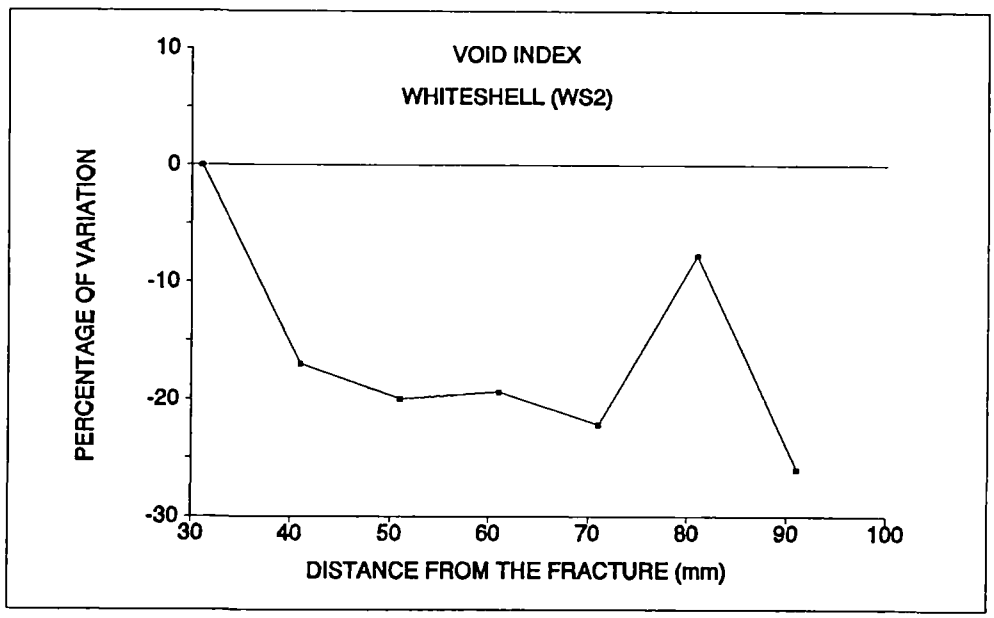

b

Fig. 36.-Variation of the properties with regard to the distance to the main fracture: a) open porosity, b) void index. Whiteshell granite, core WS2.

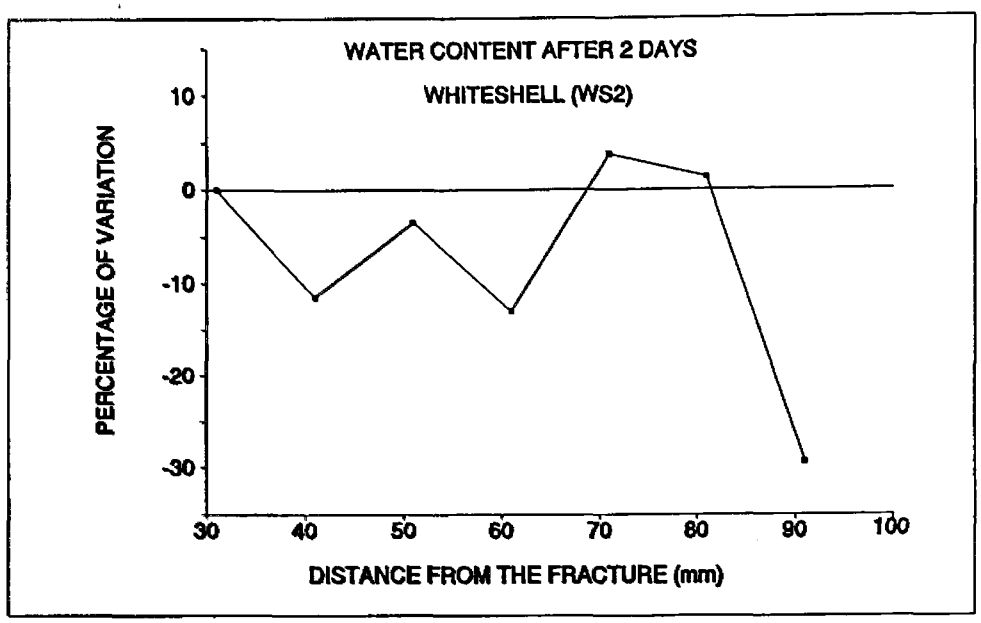

c

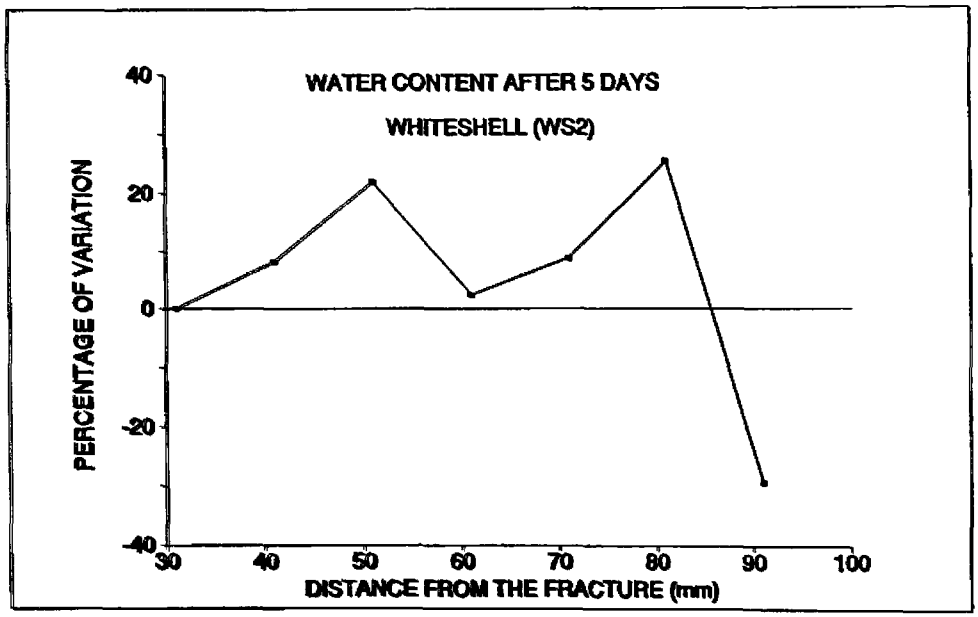

d

Fig. 36.-Variation of the properties with regard to the distance to the main fracture: c) water content after 2 days, d) water content after 5 days. Whiteshell granite, core WS2.

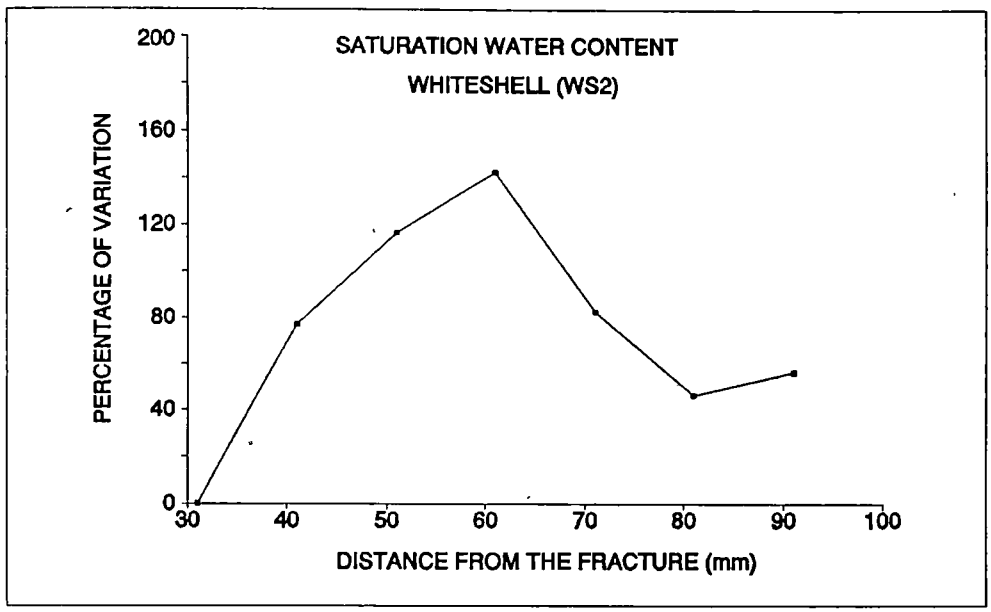

e

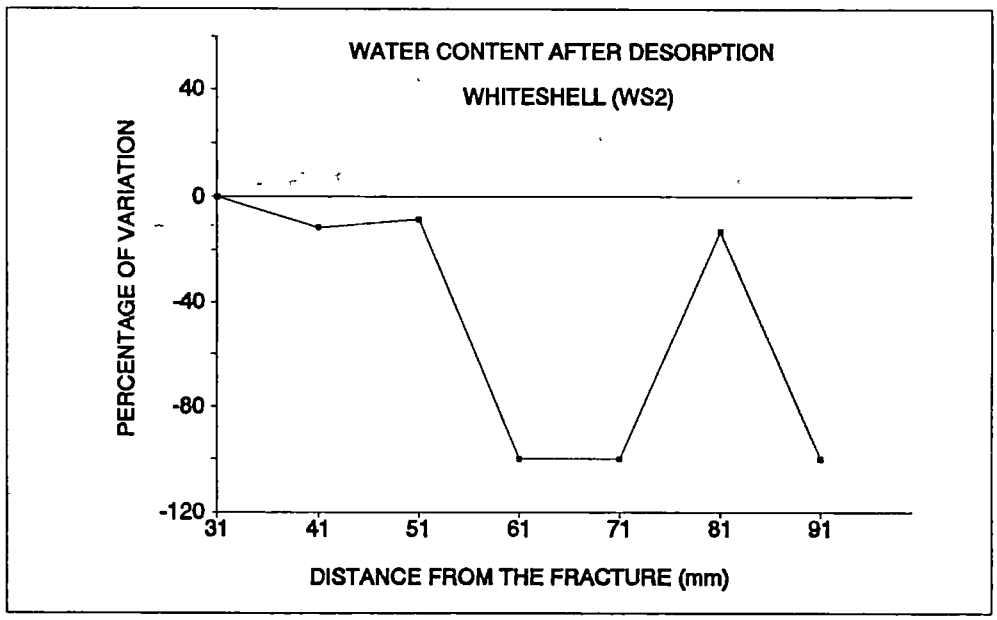

f

Fig. 36.-Variation of the properties with regard to the distance to the main fracture: e) saturation water content, f) water content after desorption. Whiteshell granite, core WS2.

TABLE VI

WS1:	
Dry density, ρ_d (kg/m^3)	2607 ± 9.16
Grain density, ρ_s (kg/m^3)	-
Accessible porosity, n_o (%)	2.03 ± 0.40
Total porosity, n (%)	-
Degree of saturation, Sr (%)	-
Saturation water content, Ws (%)	0.78 ± 0.15
Void index, Iv (%)	0.44 ± 0.12
Water content after 2 days, W_2 (%)	0.65 ± 0.16
Water content after 5 days, W_5 (%)	0.72 ± 0.18
Water content after desorption, W_d (%)	0.08 ± 0.03
WS2:	
Dry density, ρ_d (kg/m^3)	2608 ± 12.72
Grain density, ρ_s (kg/m^3)	-
Accessible porosity, n_o (%)	1.96 ± 0.52
Total porosity, n (%)	-
Degree of saturation, Sr (%)	-
Saturation water content, Ws (%)	0.75 ± 0.20
Void index, Iv (%)	0.30 ± 0.03
Water content after 2 days, W_2 (%)	0.38 ± 0.04
Water content after 5 days, W_5 (%)	0.43 ± 0.07
Water content after desorption, W_d (%)	0.01 ± 0.01

TABLE VI.- Mean values of physical properties of the intact rock for samples WS1 and WS2. The maximum error corresponds to a confidence interval of 95%.

4.3.5. Mercury porosimetry.

Mercury porosimetry has been carried out on samples of El Berrocal granite (EB1) using a Coultronics 9310 porosimeter operating at a maximum pressure of 2,000 atmospheres, producing a vacuum of 0.33 atmospheres and with sample volumes of 6.23 - 7.13 cm^3. The technique employed provides information not only on the total porosity but also on pore size. In the granite samples studied, however, the porosity is of a microfissure type and the pore dimensions provided would not represent actual fissure dimensions. An estimate of the pore size has, therefore, been determined indirectly, and is expressed as a function of injection pressure, providing a measure by which different samples can be compared.

Results obtained from core EB1F are presented in Figure 37 in which the volumetric percentage of penetrated pores is plotted as a function of injection pressure. It appears that, for each pressure employed, the porosity increases with increasing distance from the fracture. Porosities determined at pressures of 7 - 70 kp/cm², 70 - 700 kp/cm² and 700 - 2,100 kp/cm² are presented in Figure 38. If the cores were cylindrical (which they are not), these pressures would correspond to pore radii of 1.0 - 0.1, 0.1 - 0.01 and 0.01 - 0.004 μm respectively. It can be seen that the rock slice nearest to the fracture has fewer large pores but more small and medium sized pores than the other slices.

The porosity values obtained by mercury porosimetry (between 1.2% and 1.4%) are similar to those obtained by water saturation.

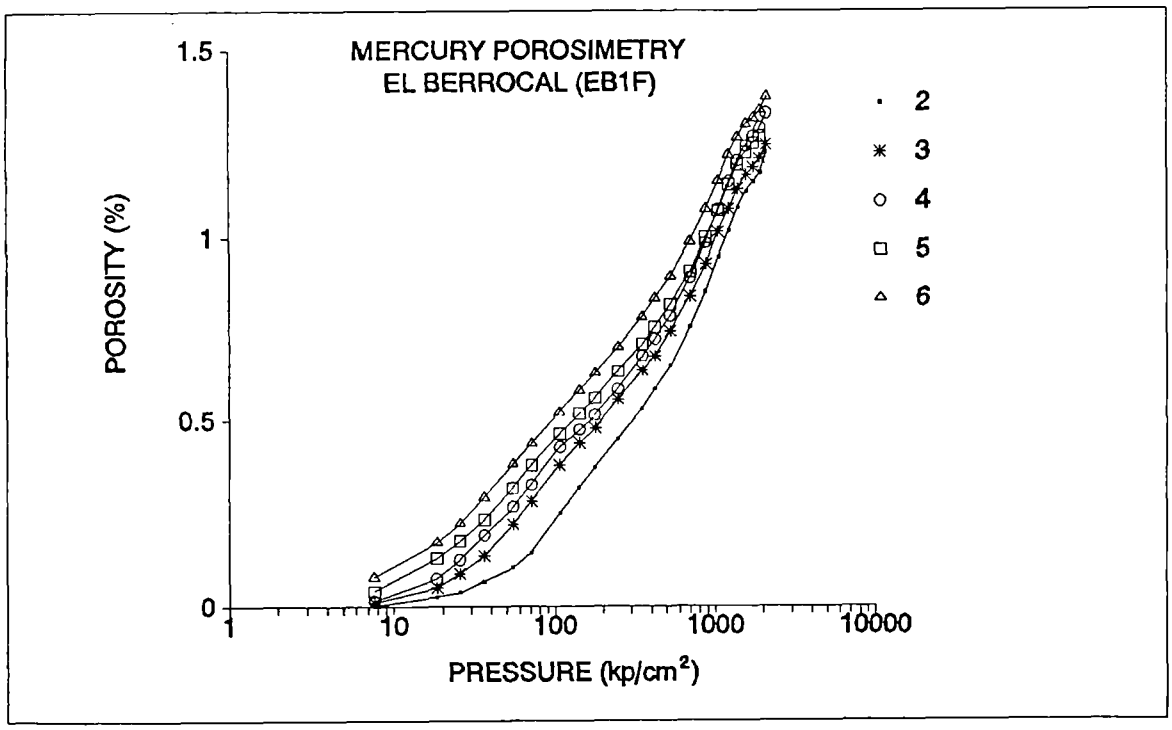

Fig. 37.- Cumulative porosity plots for the different slices (2, 3, 4..., see page 11) of core EB1F. El Berrocal granite.

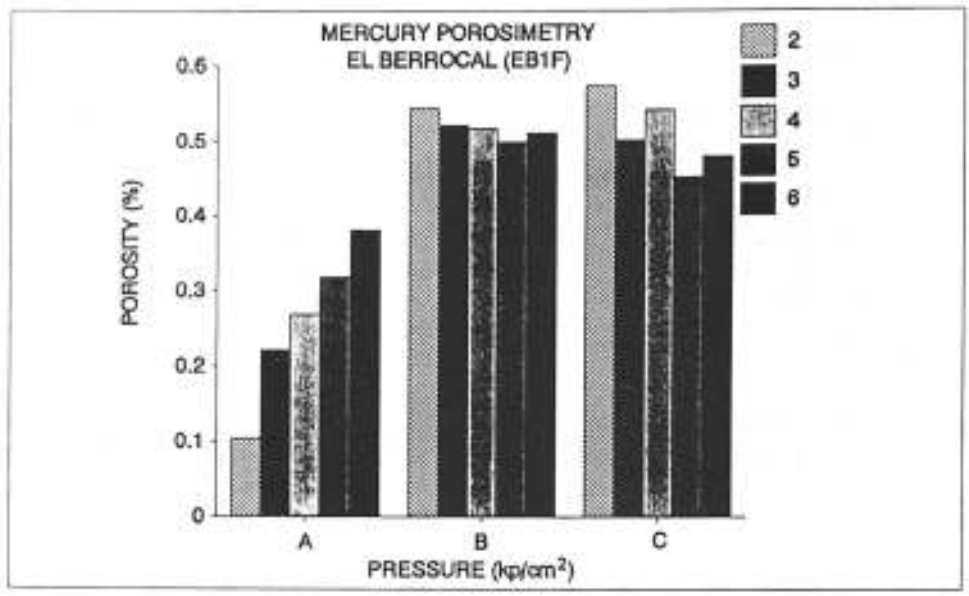

Fig. 38.- Distribution histograms for porosity in three ranges (a = 7-70 kp/cm², b = 70-700 kp/cm², c = 700-2100 kp/cm²) for the different slices of core EB1F. El Berrocal granite.

4.4. DYNAMIC PROPERTIES: VELOCITY OF LONGITUDINAL WAVES.

One of the more interesting non-destructive techniques for the petrophysical characterisation of granites is the study of the transmission of elastic waves through rocks. Ultrasonic parameters such as wave energy, amplitude, count number, longitudinal wave velocity etc. provide information about mineralogical composition, density, texture, porosity and the nature of the microfractographic network, since ultrasonic waves are modified by these petrographic parameters.

Most measurements have been carried out in the transparence mode in a direction parallel to the axis of the cores on each of the slices cut from the cores. The results for both dry and water saturated conditions are presented in Annexes 1 - 5.

4.4.1. Experimental procedure.

Two commercially-available instruments have been used in the study (Figure 39).

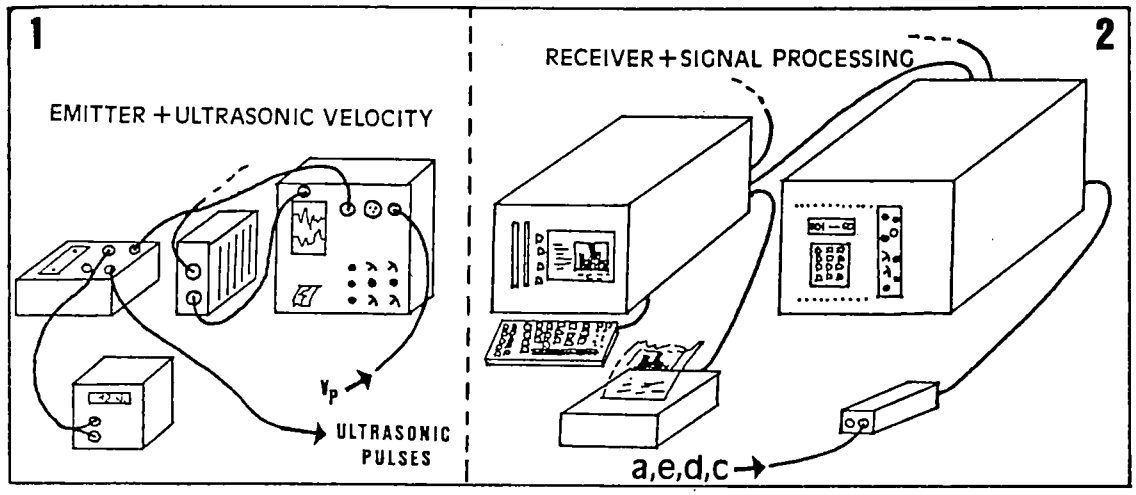

Fig. 39.- Ultrasonic system arrangement.

(1) The "New Sonicviewer", model 5217-A (Oyo Co., Japan): a pulse emitter/receiver to measure the velocity of propagation of longitudinal waves (Vp);

(2) The "Spartan 3000" system, with a "3000 Microcomputer", receiver transducers and preamplifiers designed to monitor and process acoustic emission signals but used here to analyse the ultrasonic signals generated by the "New Sonicviewer" after travelling through rock samples.

Both surface transmission and transparence modes have been used. In both cases, the signal is generated by the "New Sonicviewer", and is introduced into the rock sample by an emitter-transducer (45 kHz resonant frequency). After travelling through the rock, the signal is picked up by two receiver-transducers from the acoustic emission equipment (150 kHz resonant frequency). One of these transducers (A) sends the signal to the "New Sonicviewer" in order to calculate Vp (Figures 40 and 41); the other transducer (B) sends the signal to the "Spartan 3000" where the ultrasonic parameters - amplitude (a), number of counts (c), duration (d) and energy (e) - are recorded and processed (Figures 40 and 41).

No couplant was used between sample and transducer; to guarantee a good contact, a constant pressure of 70 bars was applied. Semicylindrical samples sawn parallel to the core axis were used.

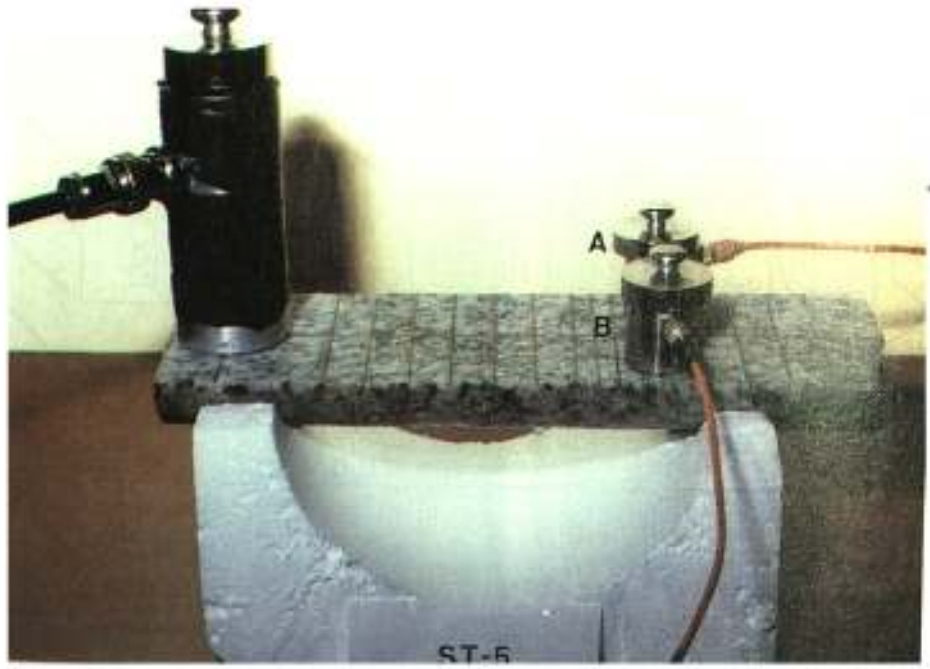

Fig. 40.- Experimental arrangement for ultrasonics measurements in the surface transmission mode.

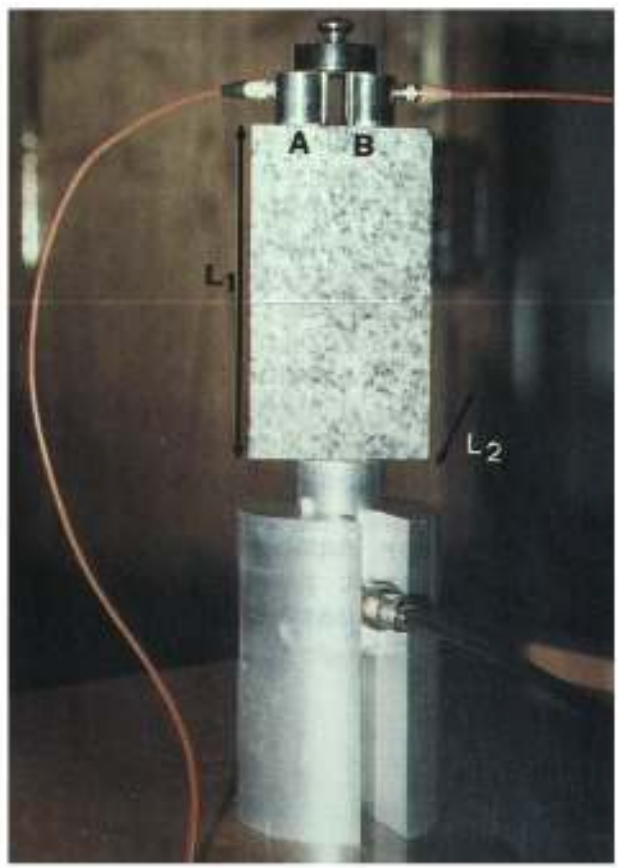

Fig. 41.- Experimental arrangement for ultrasonics measurements in the transparence mode.

4.4.2. Results.

Initial work was carried out on samples of Stripa granite. 13 pairs of surface transmission measurements were carried out on

samples ST6 and ST7, keeping the emitter fixed at one end of the planar sample surface and varying the positions of receivers between constant intervals (Figure 40). Ten measurements were also made in transparence mode, 5 in direction L_1 and 5 in direction L_2 (Figure 41). Measurements in transparence mode were also carried out on cubes of sample ST5.

In surface transmission studies, Vp is calculated from the slope of the regression line between emitter-receiver distances and arrival time. In Figure 42, for example, Vp is 4,874 m/s for sample ST6 and 4,848 m/s for sample ST7.

TABLE VII

	Sample ST6		Sample ST7	
	L_1 (m/s)	L_2 (m/s)	L_1 (m/s)	L_2 (m/s)
	3942	4921	3750	4843
	3660	5000	3750	4769
	3942	4921	4038	4679
	3416	4921	3750	4843
	3660	5000	3750	4843
Mean	3724	4952	3807	4795

TABLE VII.- Vp values in transparence mode in L_1 and L_2 directions for Stripa samples ST6 and ST7.

In the transparence mode, Vp is the average value obtained from the 5 measurements carried out in each of the L_1 and L_2 directions (Table VII). Comparison of the values for each direction shows an anisotropy in the behaviour of longitudinal waves: Vp is smaller along L_1 than along L_2 in both ST6 and ST7.

In Table VIII, the mean values of Vp (dry) and Vp (saturated) obtained for El Berrocal and Whiteshell cores are presented. As expected, the Vp values for saturated samples are greater than those for dry samples., while sample WS1 (Whiteshell altered) show values lower than those for sample WS2 (Whiteshell unaltered).

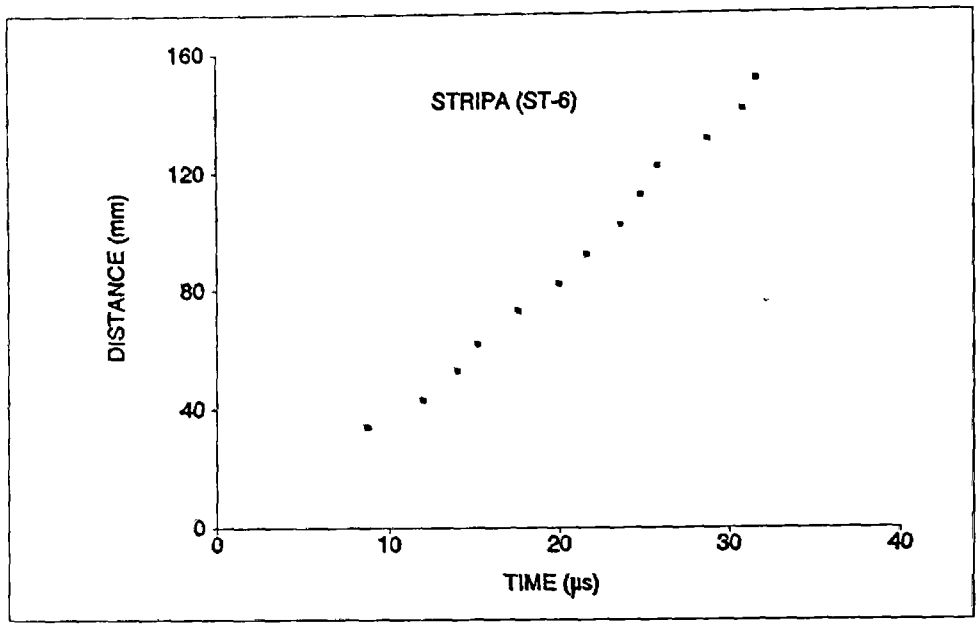

a

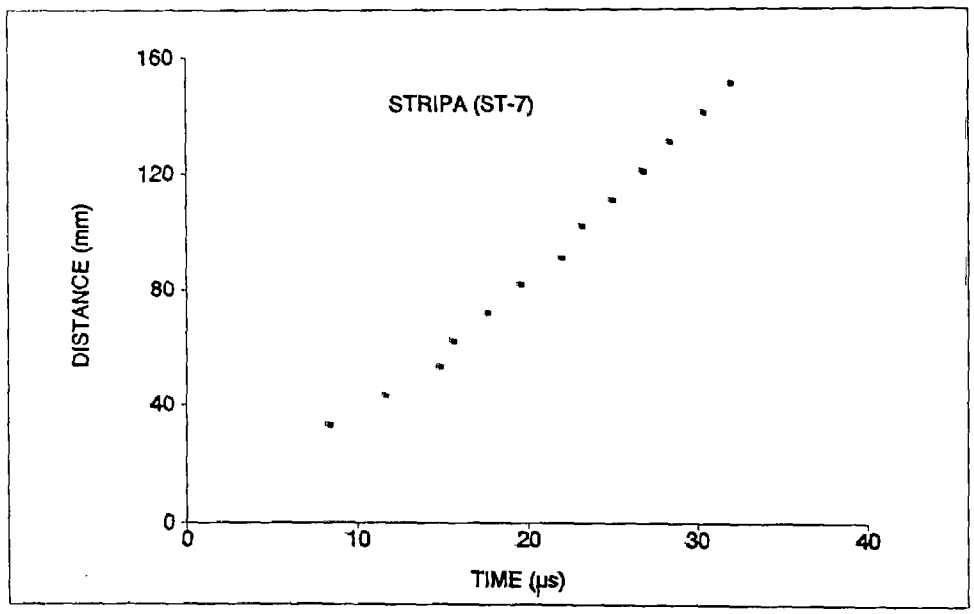

b

Fig. 42.- Arrival times for the different distances both for samples ST-6 (a) and ST-7 (b). Vp is calculated as the slope of regression lines. Stripa granite.

TABLE VIII

Sample No.	Vp (dry) (m/s)	Vp (sat) (m/s)
EB1A	5597 ± 526	6278 ± 590
EB1B	5327 ± 325	6452 ± 711
EB1E	5108 ± 607	6024 ± 632
EB1F	4967 ± 776	6135 ± 478
EB1J	5325 ± 850	6240 ± 558
Mean, EB1A-EB1J	5262 ± 231	6225 ± 206
EB3A	3711 ± 260	5322 ± 312
WS1	3675 ± 766	4352 ± 813
WS2	3864 ± 397	4902 ± 643

TABLE VIII. - Vp values in transparence mode in direction L_1.

The variation in values of Vp(dry) for cores from El Berrocal sample block EB1, expressed as a percentage of the value for the rock slice closest to the fracture surface, is plotted against distance from the fracture in Figure 43. The solid line joins the points corresponding to the mean values of Vp. The variation of Vp(sat) and [Vp(sat)-Vp(dry)]/Vp(dry) are presented for these samples in Figures 44 and 45 respectively.

The variation in Vp(dry) values for sample block EB1 seems rather erratic in many cases. Values of Vp(sat), however, seem to increase with increasing distance from the fracture as do values for [Vp(sat)-Vp(dry)]/Vp(dry).

The variation in Vp values (dry and saturated) with increasing distance from the fracture surface (expressed as a percentage of the value obtained for the slice closest to the fracture) is plotted for El Berrocal sample EB3 and for Whiteshell samples WS1 and WS2 in Figures 46(a) - 46(g).

In the El Berrocal samples (Figure 46(a) and 46(b)), an erratic variation of Vp values can be seen in both dry and saturated samples, but with a general increase in values with increasing distance from the fracture; this is interpreted in terms of increased microfracture density close to the fracture. Due to the positioning of the transducers in the centre of the samples, the fracture present in core EB3 that clearly affected the porosity, did not show any obvious effect on Vp values.

In the unaltered Whiteshell samples (WS2) (Figure 46(c) and 46(d)), the variation in Vp (dry and saturated) is erratic, though there is a slight decrease overall in Vp(dry) with increasing distance from the fracture which can be interpreted as reflecting an increase in porosity. In the altered Whiteshell samples (WS1) (Figure 46(e) and 46(f)), however, Vp values increase with increasing distance from the fracture in both dry and saturated samples; again, this is interpreted in terms of decreasing microfracture density, though much more clearly developed than in El Berrocal sample EB3.

The ratio Vp(sat)/Vp(dry) decreases with increasing distance from the fracture (Figure 46(g)); that is, the difference between the values obtained for each parameter is greater close to the fracture than it is far from the fracture. This is due to the increased microfracture density close to the fracture surface, which reduces the difference between Vp values obtained for dry and saturated samples.

Velocity measurements have also been carried out along three orthogonal directions in cubic specimens of El Berrocal granite (Figure 47). Comparison of the results for each of these directions (Table IX) reveals an anisotropy: the value of Vp(dry) along L_1 (parallel to the axis of the cores) is smaller than along L_2 and L_3.

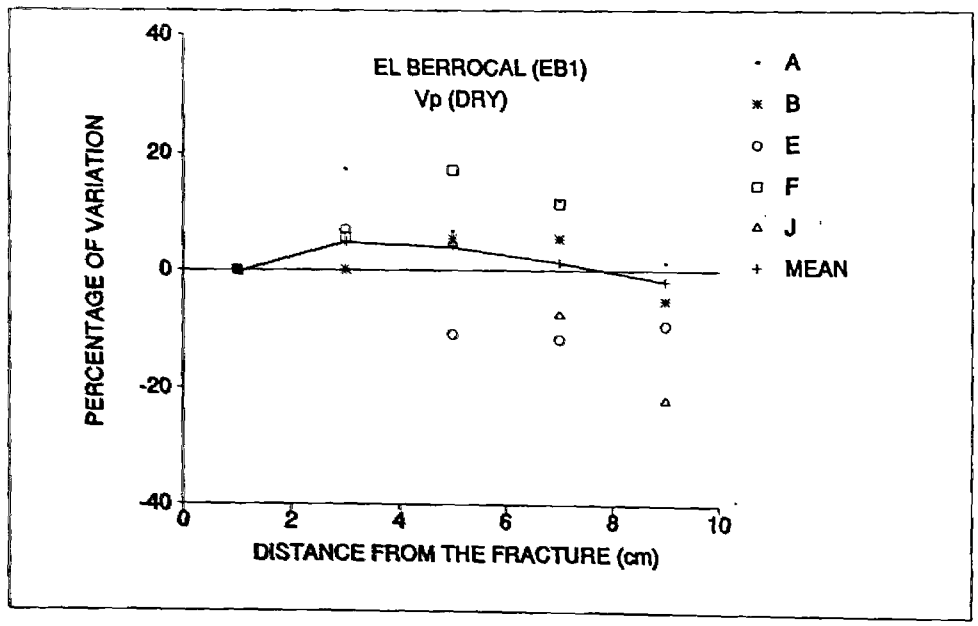

Fig. 43.- Variation of Vp values in dry conditions with respect to the distance from the fracture. El Berrocal granite (EB1), cores A to J.

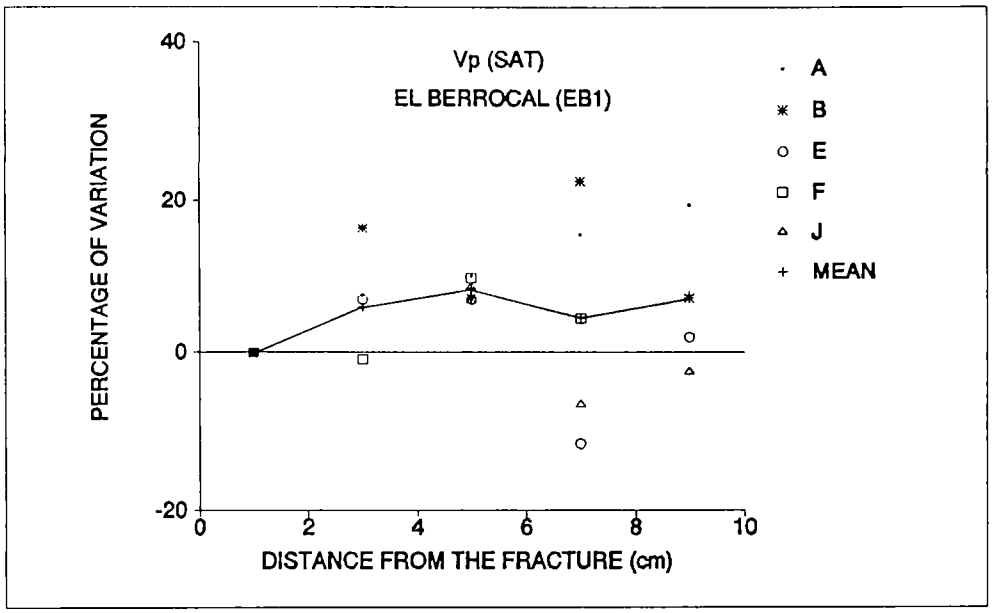

Fig. 44.- Variation of Vp values in saturated specimens with respect to the distance from the fracture. El Berrocal granite (EB1), cores A to J.

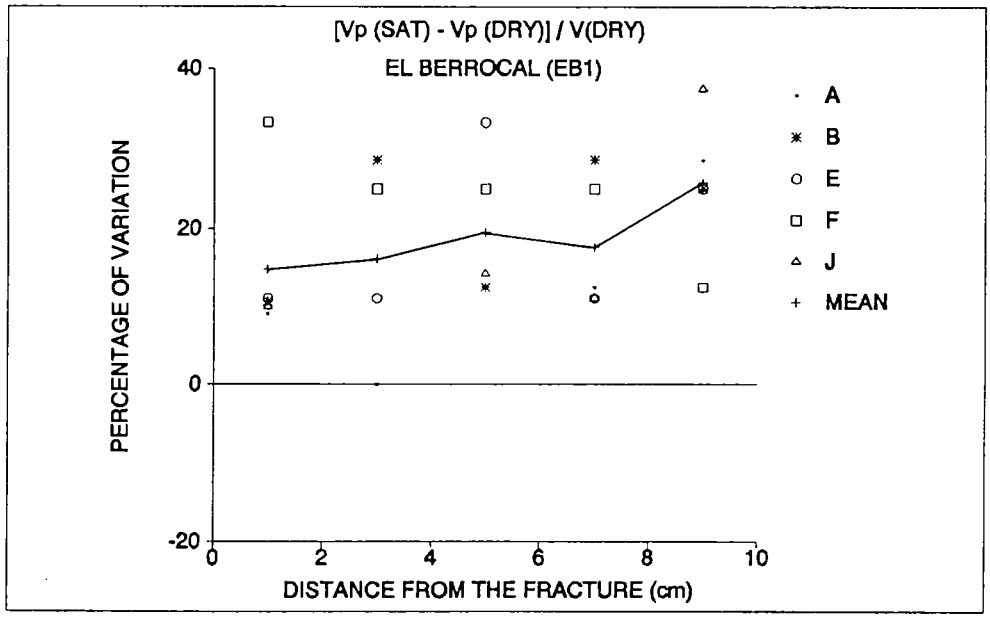

Fig. 45.- Variation of [Vp(sat)-Vp(dry)]/Vp(dry) ratio with respect to the distance from the fracture. El Berrocal granite (EB1), cores A to J.

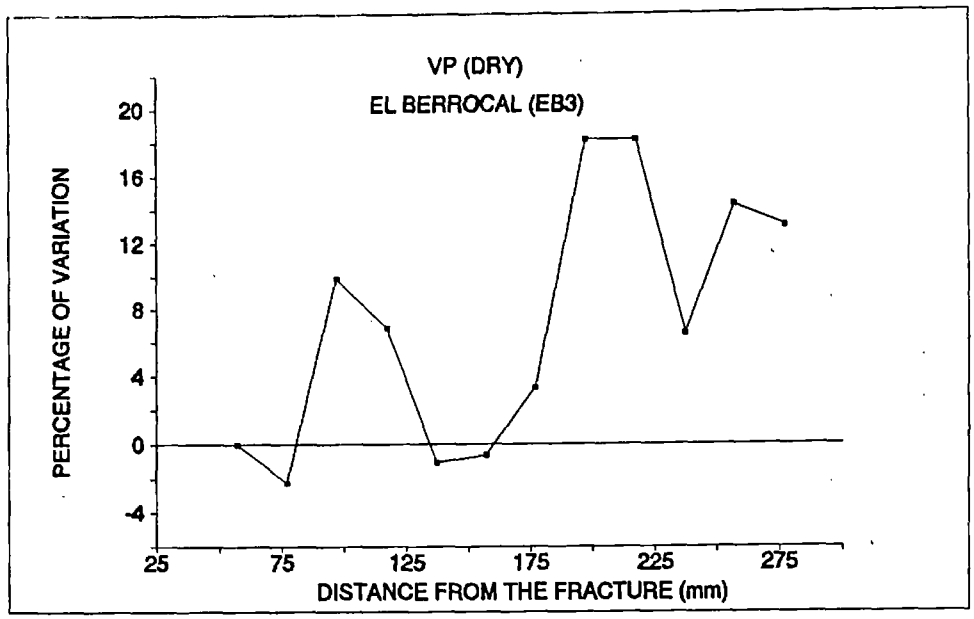

a

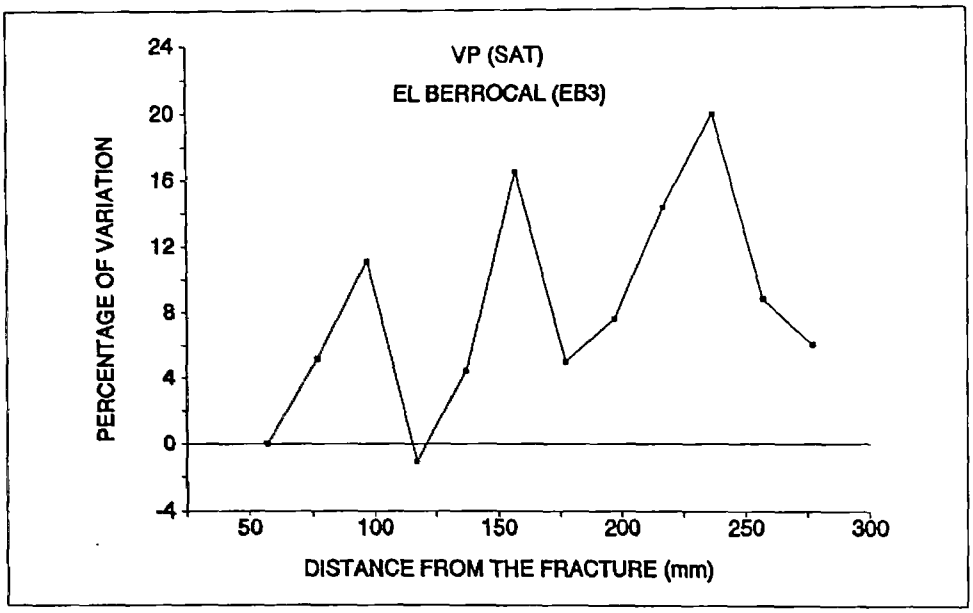

b

Fig. 46.- Variation of Vp values with respect to the distance from the fracture: a) dry conditions, b) saturated specimens. El Berrocal granite, core EB3.

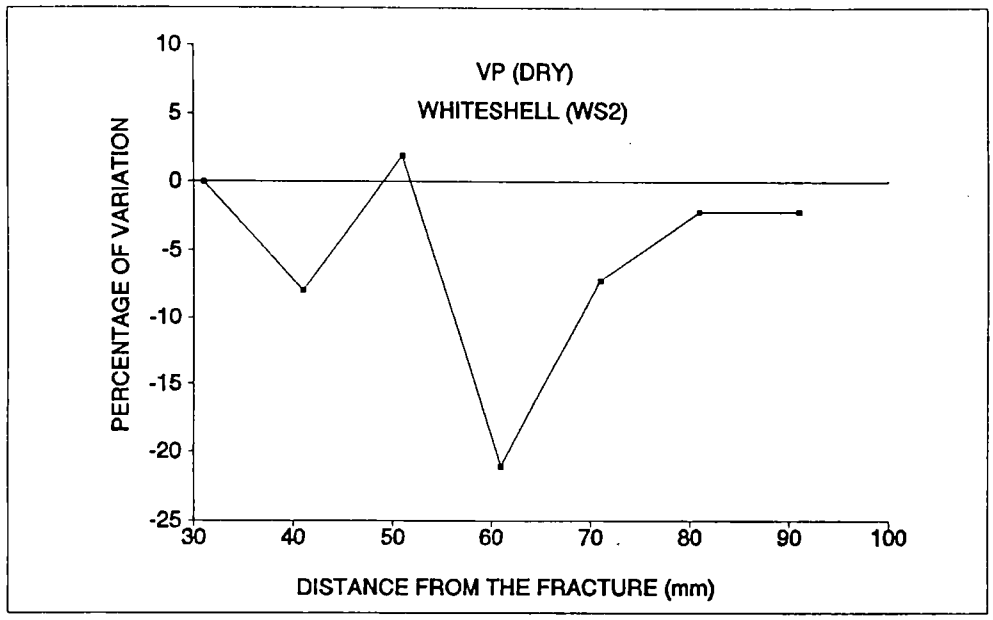

c

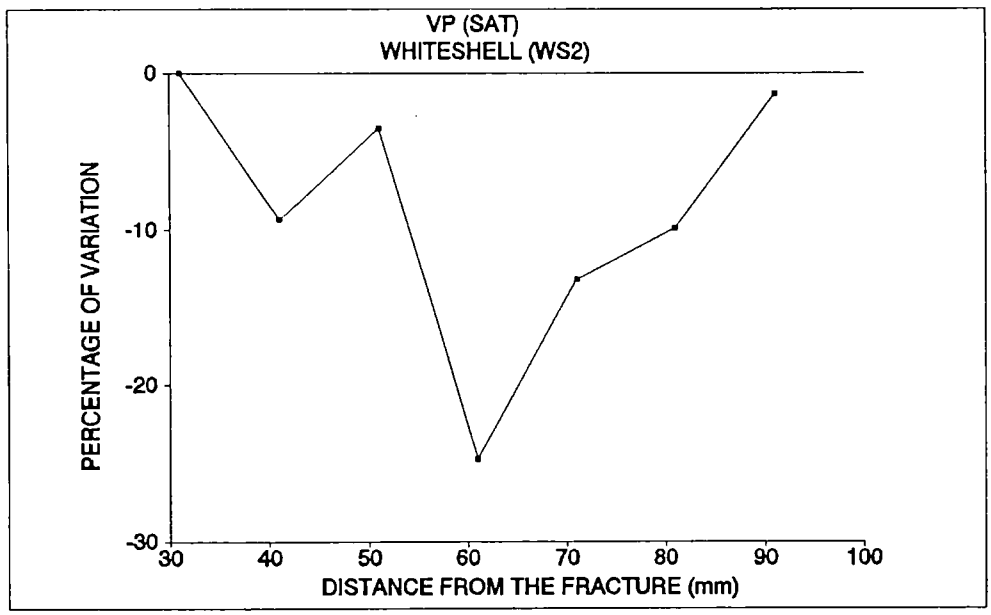

d

Fig. 46.- Variation of Vp values with respect to the distance from the fracture: c) dry conditions, d) saturated specimens. Whiteshell granite, core WS2.

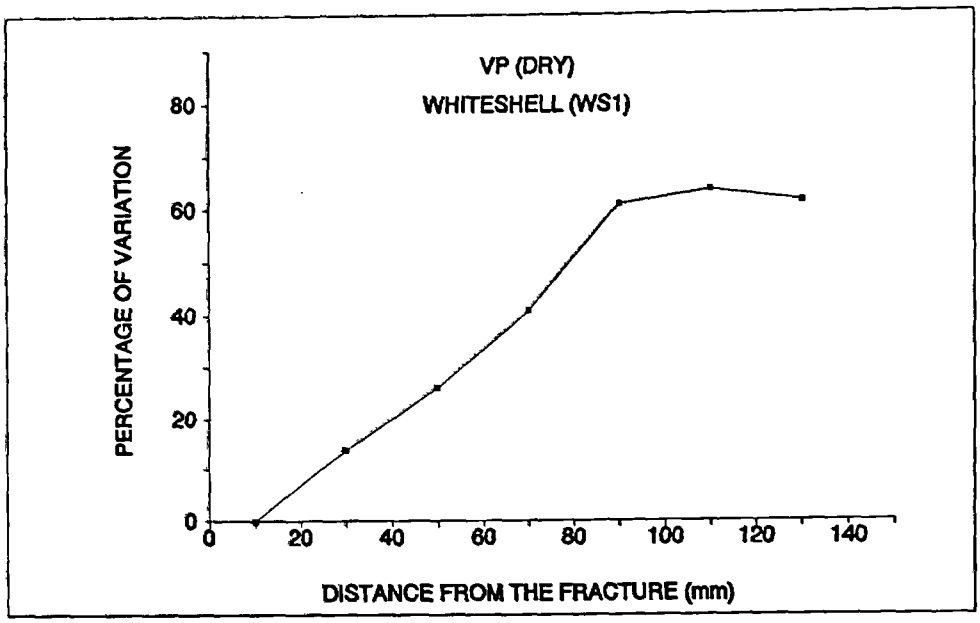

e

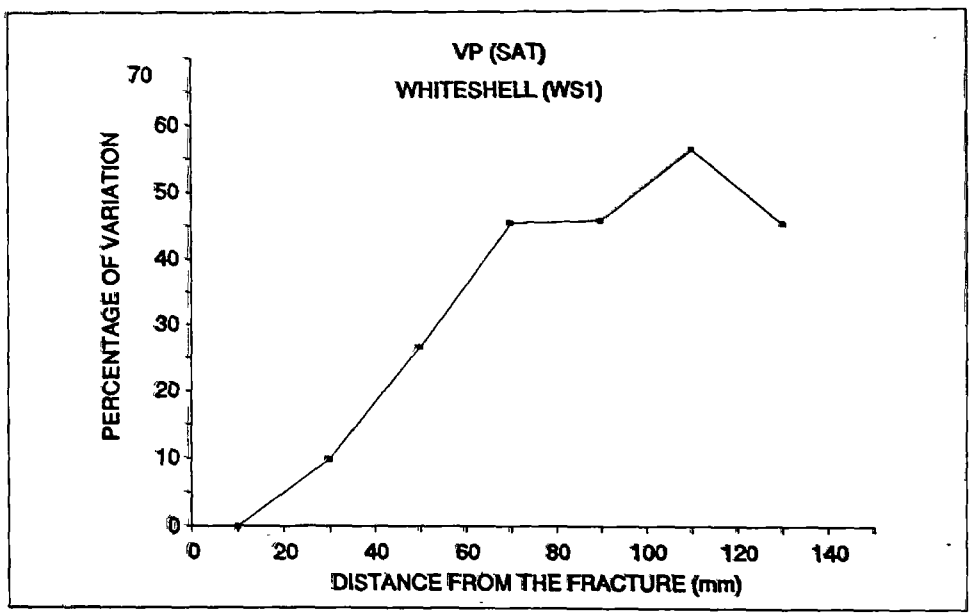

f

Fig. 46.- Variation of Vp values with respect to the distance from the fracture: e) dry conditions, f) saturated specimens. Whiteshell granite, core WS1.

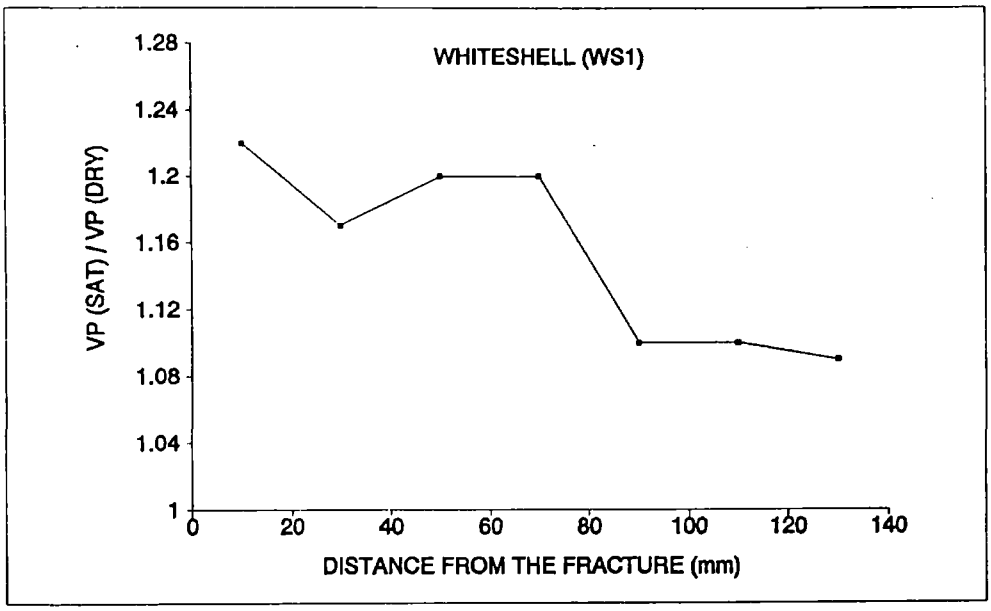

g

Fig. 46 g.- Variation of Vp(sat)/Vp(dry) ratio with respect to the distance from the fracture. Whiteshell granite, core WS1.

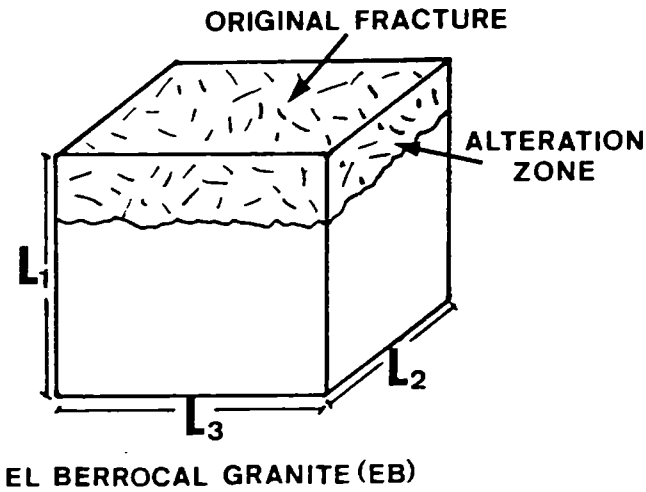

Fig. 47.- Scheme of the cube shaped specimens and directions of Vp measurements. El Berrocal granite.

TABLE IX

Direction	Vp (dry)
L_1	4642 m/s
L_2	5441 m/s
L_3	5416 m/s

TABLE IX.- Values of Vp(dry) in three orthogonal directions in cubic specimen of El Berrocal granite (Sample EB2).

Regarding the remaining ultrasonic parameters, it has been observed that not all are particularly useful in assessing mineralogical and textural changes in rocks. This is illustrated in Figure 48, where values for each ultrasonic parameter measured along two orthogonal directions in a cube of Stripa sample ST5 are presented.

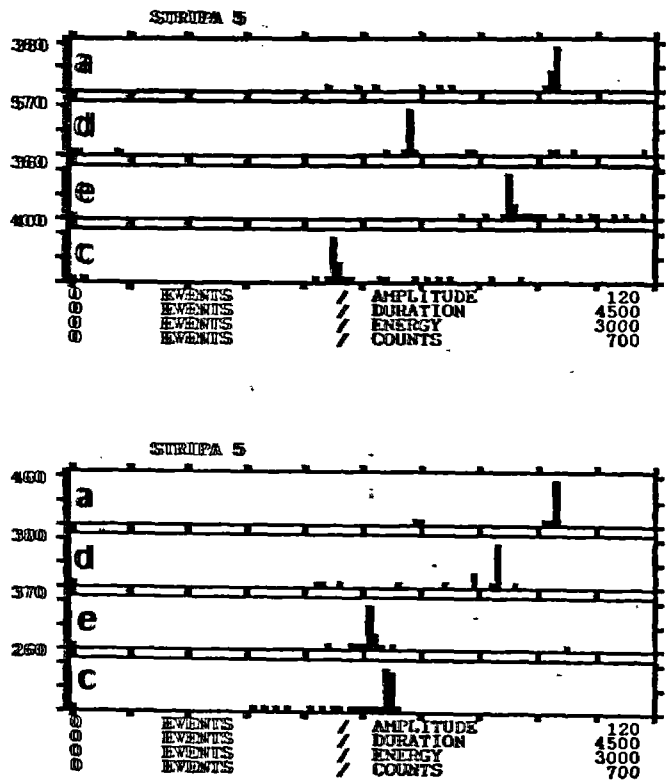

Fig. 48.- Ultrasonic parameters (amplitude, a; duration, d; energy, e; number of counts, c) versus number of events for two orthogonal directions in the cube-shaped sample ST-5. Stripa granite.

4.5. EVALUATION OF VARIOUS SYSTEMS FOR THE DETERMINATION OF INTACT ROCK PERMEABILITY AND THEIR APPLICABILITY TO THIS PROJECT.

In order to understand the relative importance of the various factors influencing the flux of radionuclides from a fracture into the rock matrix, the permeability of intact rock samples adjacent and remote from water-conducting fractures, and the permeability of fracture walls, were to be determined in the laboratory. In view of cost considerations and the need for special expertise in operating permeability systems, it was not possible to pursue this aspect of the study beyond an initial appraisal of the available techniques. A brief overview is presented here.

4.5.1. Available techniques.

Existing methods for the determination of permeability on intact rock samples are based upon Darcy's equation, and require either the measurement of the flow of water across a sample while the injection pressure is held constant (steady state methods), or measurement of pressure decay following small pressure changes (non-steady state methods). Both methods have been assessed for the determination of intact rock permeabilities down to nanodarcy levels, thus encompassing the full permeability range likely to be encountered in granites (Brace, 1980).

4.5.2. Steady state methods.

In steady state methods, permeability is determined by measuring the velocity of flow of fluid across a sample while maintaining a constant pressure gradient. Steady state permeameters include those in which the load to which the sample is subjected during the test is constant (used for materials of relatively high permeability) and those in which the confining pressure is varied (used for low permeability materials down to 10^{-18} m^2).

4.5.3. Non-steady state methods.

Transient or pulse decay methods are based upon the measurement of pressure decay following the introduction of small pressure changes at one end of a sample. Two variations of this method have been described.

In a simple analytical technique described by Brace et al. (1968), following the introduction of a pressure pulse, pressure decays exponentially with time and permeability is determined from the slope of the curve representing pressure decay, assuming that there is no storage of fluid in the sample. This

technique is suitable for materials with permeabilities in the range 10^{-17} - 10^{-20} m^2.

In a numerical version described by Lin (1977, 1981) and Trimmer et al. (1980), the equation governing pressure decay is resolved using a finite differentiation mathematical model, and permeability is obtained by comparing experimental pressure decay curves with curves obtained numerically. This is applicable in the permeability range 10^{-20} - 10^{-24} m^2. For materials with permeabilities of less than 10^{-19} m^2, non-steady methods are most suitable. According to Trimmer (1981) and Lin (1982), the technique of Brace et al. (1968) is most suitable for the determination of rock permeabilities; the technique requires that the pore volume of the sample is small, as there is a systematic error associated with the technique which is proportional to the pore volume. If the experimental parameters cannot be adjusted as required by the technique of Brace et al. (1968), or if the rock has such a low permeability (10^{-20} - 10^{-24} m^2) that the time required for pressure to re-equilibrate is excessively long, the numerical version can be used. This method does not suffer the systematic error of the simple analytical technique.

Given that the rocks of interest are granitic and of low permeability (10^{-17} - 10^{-21} m^2), the non-steady state (transient or pulse decay) method is most appropriate. If samples have permeability values that permit the experimental parameters to be adjusted as required by the simple analytical technique, the method of Brace et al. (1968) can be used; otherwise, the numerical version is more appropriate.

The most suitable permeameter for the present study appears to be that described by Bernabe (1987), which is capable of determining permeabilities over a range of 8 orders of magnitude (10^{-15} - 10^{-22} m^2) under high confining pressure. This permeameter can use either the steady state or non-steady state method depending upon the permeability of the sample.

4.6. URANIUM SERIES DISEQUILIBRIUM STUDIES.

The penetration of modern waters (the last million years) into the rock adjacent to fractures has been investigated by measuring the state of radioactive disequilibrium in the U-238 decay series. Alpha spectrometry has been employed following separation of uranium and thorium by ion exchange techniques. An existing method employed in work on the distribution of natural uranium in the granites of south west England was modified, with particular regard to the choice of tracer (spike) added before ion exchange separation to determine recovery. The modifications were aimed at reducing the need for complex corrections, which are required when using spikes of short half-life, and to minimise contamination of detector surfaces by

alpha-recoil mechanisms (which occurs when U-232 is used as the uranium tracer, Th-228 generated in the detector tending to become embedded in the detector surface). From each of the fractures, cores or blocks studied, 'slices' of rock at increasing distance from the fracture surface were obtained for analysis, allowing the construction of disequilibrium profiles from fracture surfaces into the rock matrix; these disequilibrium profiles have been compared with the geochemical, microstructural and petrophysical profiles obtained using the other techniques employed in the study.

4.6.1. Alpha spectrometry system and ion exchange separation of uranium and thorium.

The alpha spectrometry system consisted of apparatus for the ion exchange separation of uranium and thorium from rock samples, their electrodeposition as 'infinitely thin' sources onto stainless steel planchettes, and the collection of alpha particle energy spectra from which the required isotopic ratios were obtained.

Granite samples were first ground to a powder and 0.4 - 1.0 g was pressure digested in aqua regia and hydrofluoric acid. The acid was then evaporated almost to dryness and the residue taken up in deionised water to make a sample solution. To this sample solution was added U-236 (half-life 23.9 million years) and Th-229 (half-life 7340 years) tracers to enable recovery to be determined. Tracer solutions with activities of 20 dpm/g (disintegrations per minute per gram) were prepared in 0.1 M hydrochloric acid from 5 ml standards containing 370 Bq of U-236 and 950 Bq of Th-229.

Following addition of the spikes, the sample solutions were evaporated to dryness and, if shown by a yellow colour to contain excessive iron, the iron was removed by solvent extraction using the solvent isobutyl methyl ketone (MIBK).

The sample solution was then passed through ion exchange columns containing the quaternary ammonium styrene resin 'Dowex'. The columns were generated either (1) with hydrochloric acid to produce a 'chloride column' for the separation of U, Pa and Fe(III) from Th and other cations; or (2) with nitric acid to produce a 'nitrate column' for the separation of U from Pa and Fe(III) and of Th from the other cations.

Early work carried out using 20 mm diameter ion exchange columns produced a poor separation of uranium from thorium. Later work, however, using slim (10 mm) columns provided a more complete separation and allowed more economic use of resins.

The solutions recovered from the ion exchange columns were

evaporated to dryness and the residue dissolved in concentrated sulphuric acid before being placed in a furnace for 1 hour at 360°C to remove chloride ions which cause corrosion of the platinum electrode in the electrodeposition cell. The residue from the furnace was then dissolved in ammonium sulphate solution and passed to an electrodeposition cell in which the uranium and thorium are deposited onto stainless steel planchettes. The uranium and thorium deposited onto these planchettes act as 'infinitely thin' alpha sources (in which there is negligible internal absorption of alpha particle energies) that were placed in a vacuum chamber beneath a silicon surface barrier detector (Canberra P200-20-100M). The alpha particle energy spectrum obtained was displayed on a Canberra 35 multi-channel analyzer.

4.6.2. Alpha spectra.

As the alpha particle energies of U-234 and Th-230 are very similar, uranium and thorium must be separated and two spectra are subsequently collected for each sample. A sample spectrum is shown in Figure 49. As uranium recovery is some 50% more efficient than that for thorium, the number of counts in each thorium channel has been adjusted in Figure 49 to allow direct comparison of the uranium and thorium spectra. The thorium spectrum in shows a number of peaks corresponding to Th-232 and its daughter Th-228, the multiple peaked profile of the tracer nuclide, Th-229, and the nuclide of interest, the U-238 daughter Th-230. The uranium spectrum shows U-238, its daughter, U-234, and the tracer, U-236. Also present in this spectrum is a little Th-229 indicating that, in this case, the separation of uranium from thorium was not entirely successful. Subsequent use of slim columns (10 mm internal diameter instead of 20 mm) improved the separation considerably producing much 'cleaner' spectra.

4.6.3. Calibration.

Alpha sources were prepared for the U-236 and Th-229 tracers, passing a mixture of the two tracers through the ion exchange columns in the usual way, but without samples, to enable recovery and the degree of separation of U and Th to be determined. From the alpha spectra collected from these sources, one prominent peak from each tracer spectrum was used to calibrate the multi-channel analyzer:

Tracer	Peak energy
U-236	4.493 MeV
Th-229	4.842 MeV.

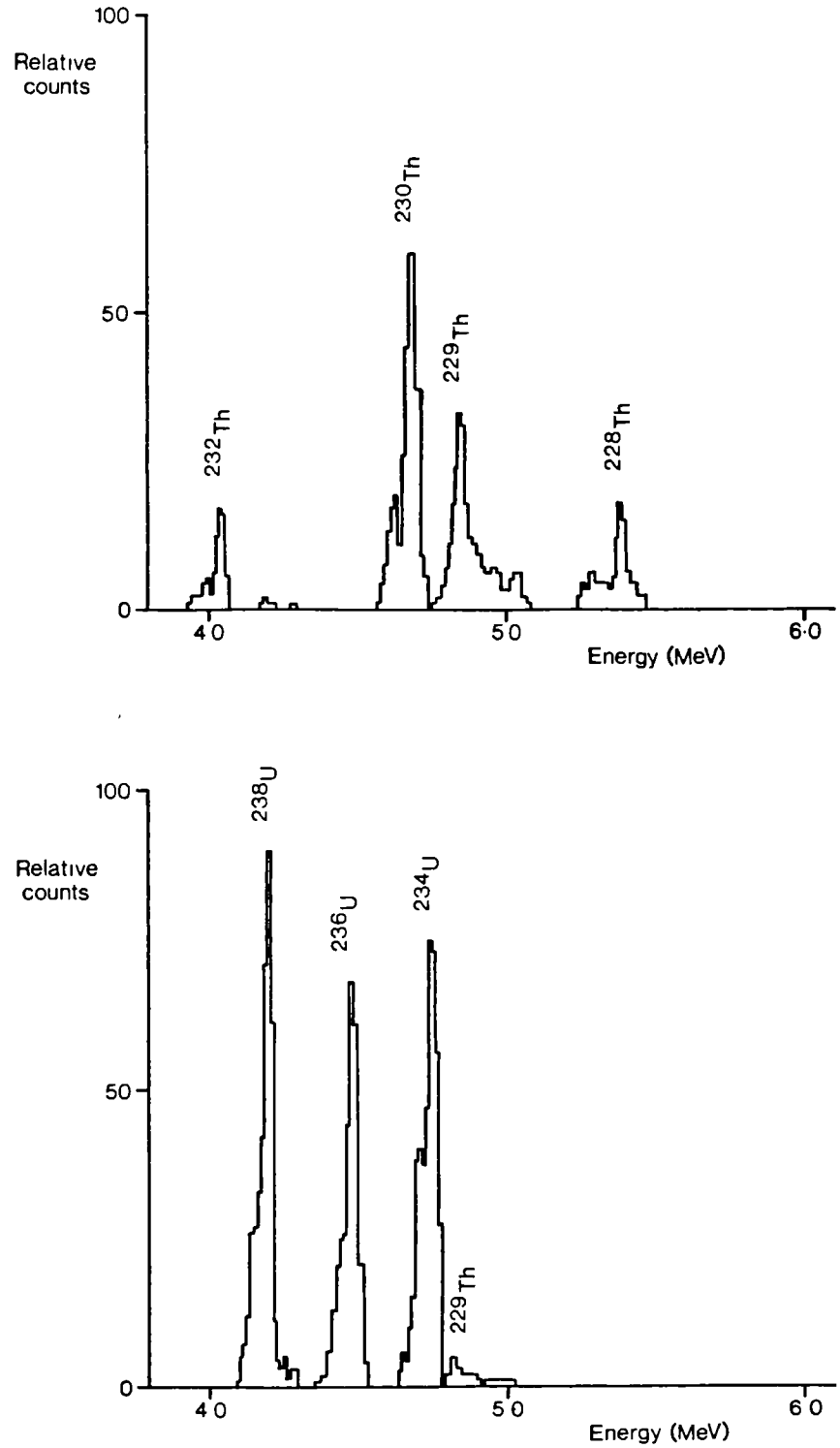

Fig. 49.- Alpha spectrum for Stripa samples ST6.0.

4.6.4. Reliability of alpha spectrometry data.

The reliability of the alpha spectrometry data obtained during the study has been assessed, firstly, by repeating the analysis of each of the seven rock slices from core EB1F and, secondly, by comparing the uranium concentrations obtained for each sample by alpha spectrometry with the values obtained by X-ray fluorescence spectrometry.

4.6.4.1. Results of repeat analysis, sample EB1F.

The mean isotopic ratios obtained for sample EB1F are shown with the analytical error, expressed as one standard deviation, in Figure 50. The greatest analytical variation is shown by the Th-230/U-234 ratios, reflecting the poorer and more variable recovery of thorium during ion exchange separation. In interpreting the observed variations in isotopic ratios, therefore, only the clearest and best-developed patterns have been noted, particularly where Th-230/U-234 ratios are concerned.

The isotopic data presented for sample EB1F in Figure 52 were obtained from the first analysis; the mean values from the two analyses (Figure 50) differ little from those illustrated and the interpretation is not affected.

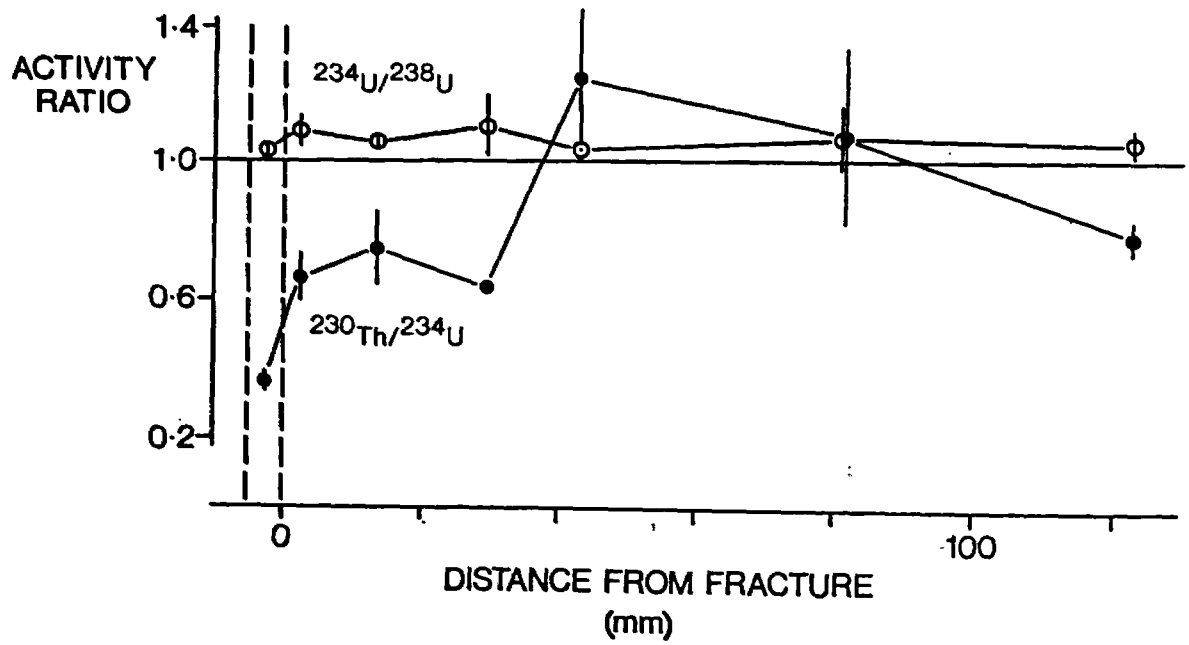

Fig. 50.- Analytical error for alpha spectrometry, sample EB1F; error bars represent one standard deviation.

4.6.4.2. Comparison of uranium values obtained by alpha spectrometry and X-ray fluorescence spectrometry.

The results of uranium determinations by alpha spectrometry are compared with those obtained by X-ray fluorescence spectrometry in Figure 51, where an excellent correlation can be observed ($r = 0.997$, $N = 32$). The values obtained by alpha spectrometry are a little lower that those obtained by XRF (by about 10%), but this does not affect the interpretation of the data obtained in the study.

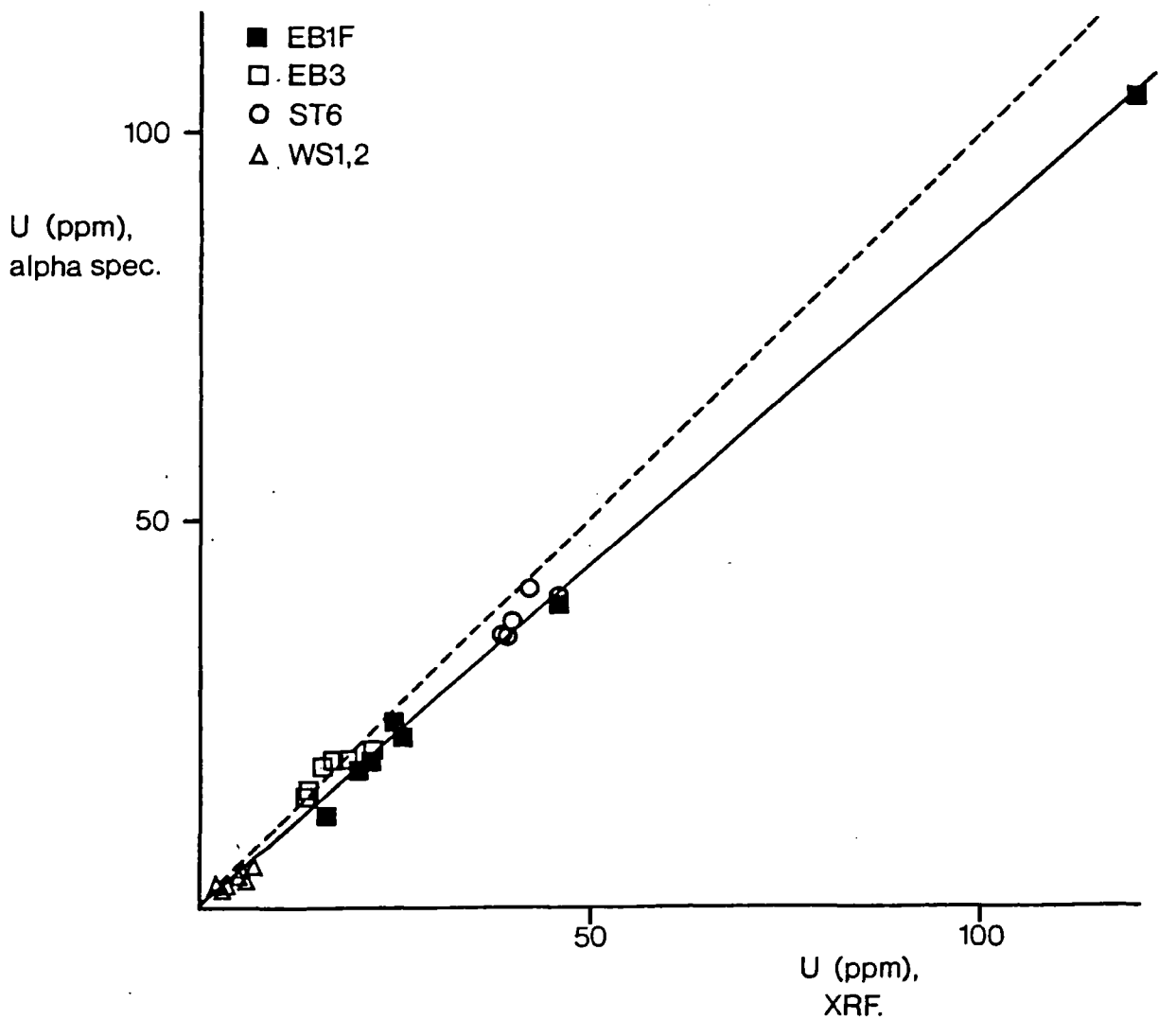

Fig. 51.- Comparison of uranium values obtained by alpha spectrometry and X-ray fluorescence spectometry. The solid line is the reduced major axis; the broken line represents unity.

4.6.5. Results of alpha spectrometric analysis.

4.6.5.1. El Berrocal samples.

Uranium series data have been obtained for samples EB1F and EB3. These data are presented in Figures 52 and 53 where they can be compared with selected geochemical and petrophysical data.

EL BERROCAL SAMPLE EB1F (Figure 52): Distributions of U-234/U-238 and Th-230/U-234 ratios show a clearly-defined zone of uranium enrichment (U-234/U-238 greater than 1.0 and Th-230/U-234 less than 1.0) extending from the fracture surface to a depth of about 35 mm, with a zone of uranium depletion (Th-230/U-234 greater than 1.0) extending from 35 mm to about 100 mm. This is consistent with the observed limit of chemical uranium enrichment (see Section 4.7.2.1).

EL BERROCAL SAMPLE EB3 (Figure 53): The distribution of U-234/U-238 ratios shows a zone of U-234 depletion extending approximately 80 mm into the rock from the fracture. At greater depth into the rock, equilibrium appears to be established. Interestingly, this zone of recent uranium depletion coincides approximately with a zone of chemical uranium enrichment, suggesting older uranium deposition, accompanied by limited diffusion of uranium into the rock, followed by a later and probably still active, uranium leaching. Th-230/U-234 ratios show an erratic distribution which is difficult to interpret overall. The Th-230 excess shown in the rock closest to the fracture is consistent with the observed uranium depletion; deeper into the rock the Th-230/U-234 data are more difficult to interpret, though the apparent correlation with the distribution of total iron, Zn, W and Mn is interesting.

U-234/U-238 activity ratios for El Berrocal groundwater vary between 1.14 and 2.80,. Detailed data have been presented by Dearlove et al. (1990).

4.6.5.2. Stripa samples.

Alpha spectrometry data were obtained for sample ST6 and are presented with geochemical and petrophysical data for the sample in Figure 54.

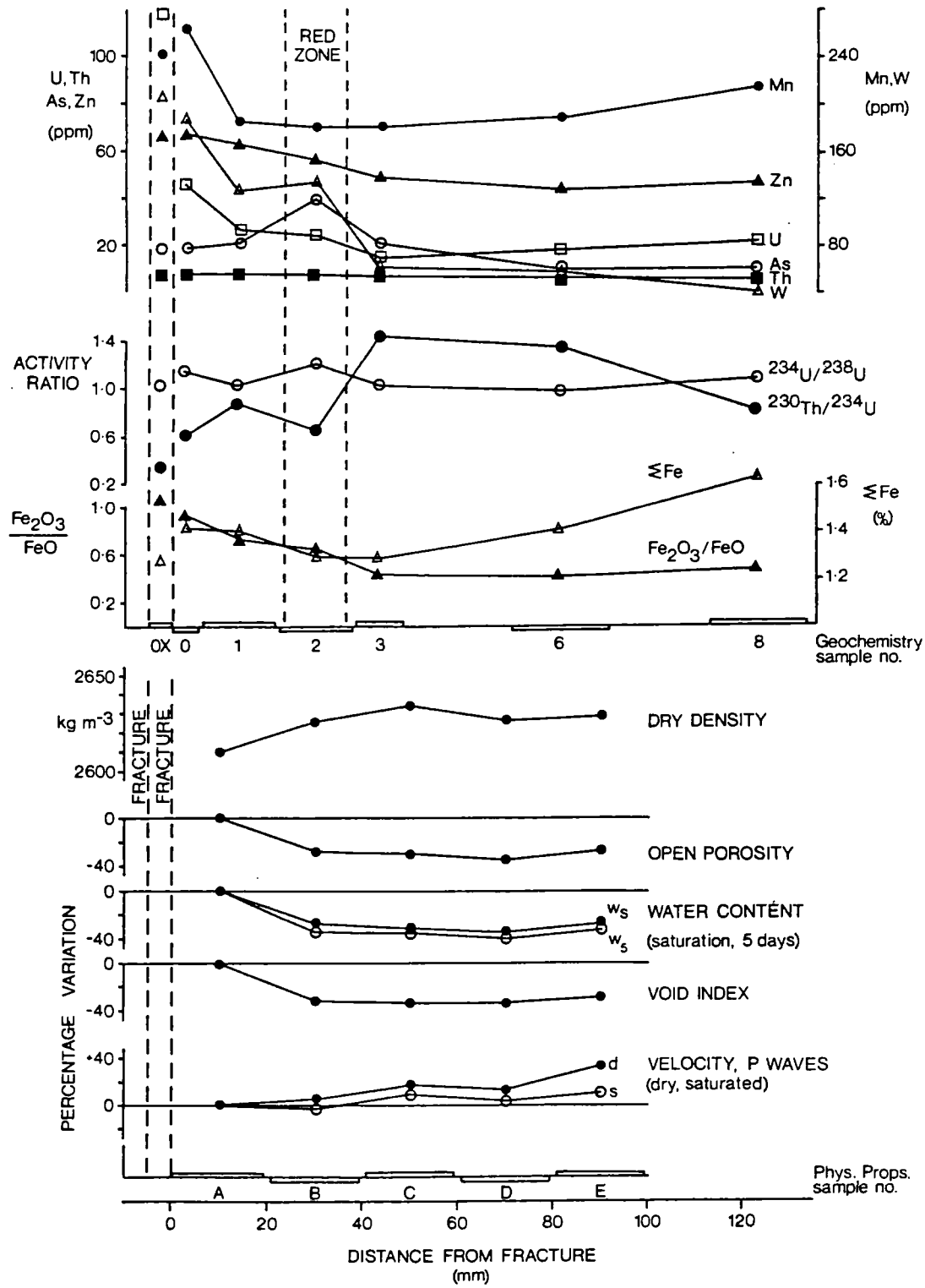

Fig. 52.- Variation in selected parameters with distance from the fracture surface. El Berrocal sample EB1F.

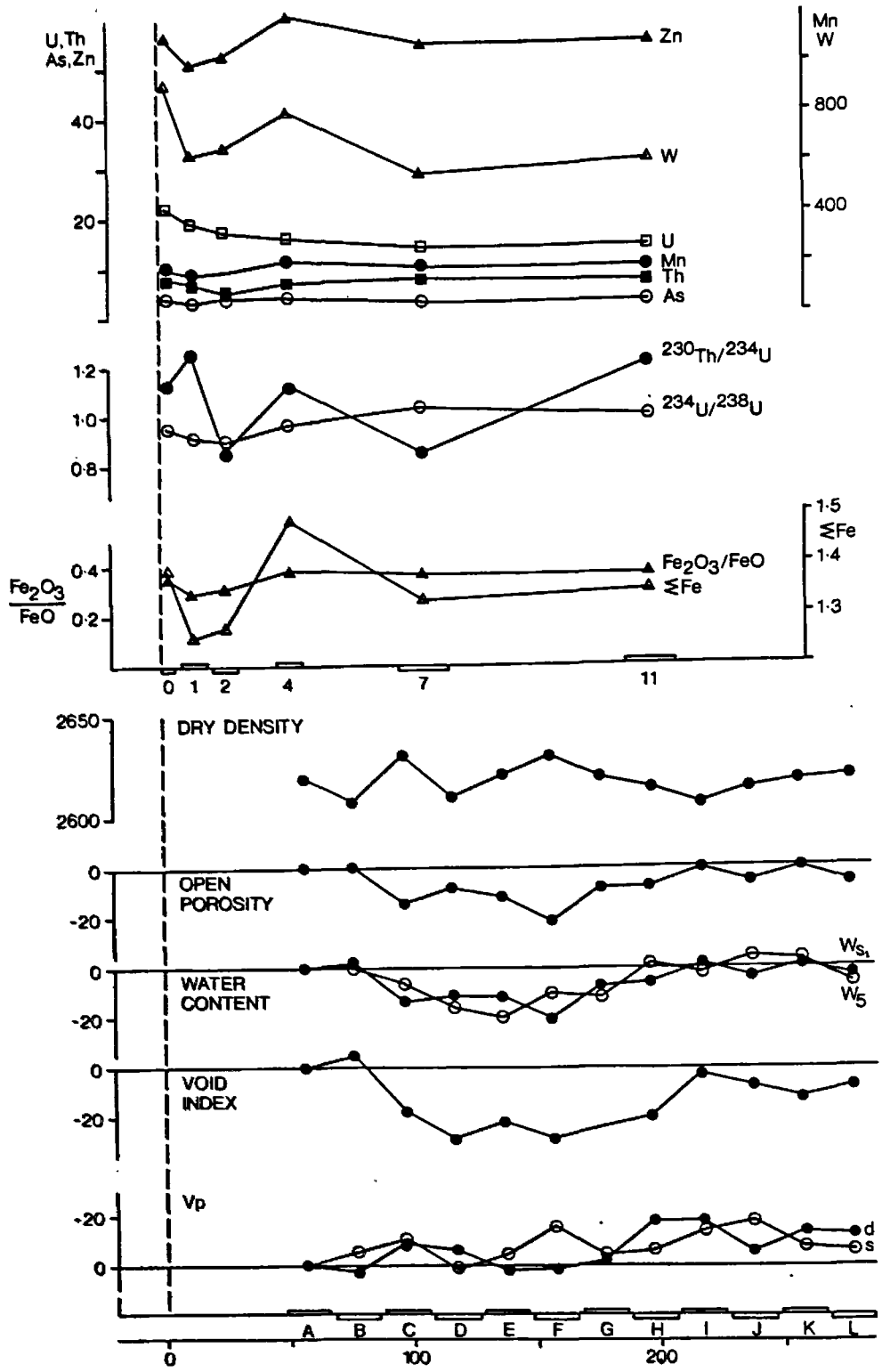

Fig. 53.- Variation in selected parameters with distance from the fracture surface. El Berrocal sample EB3. (See fig. 52 for further explanation).

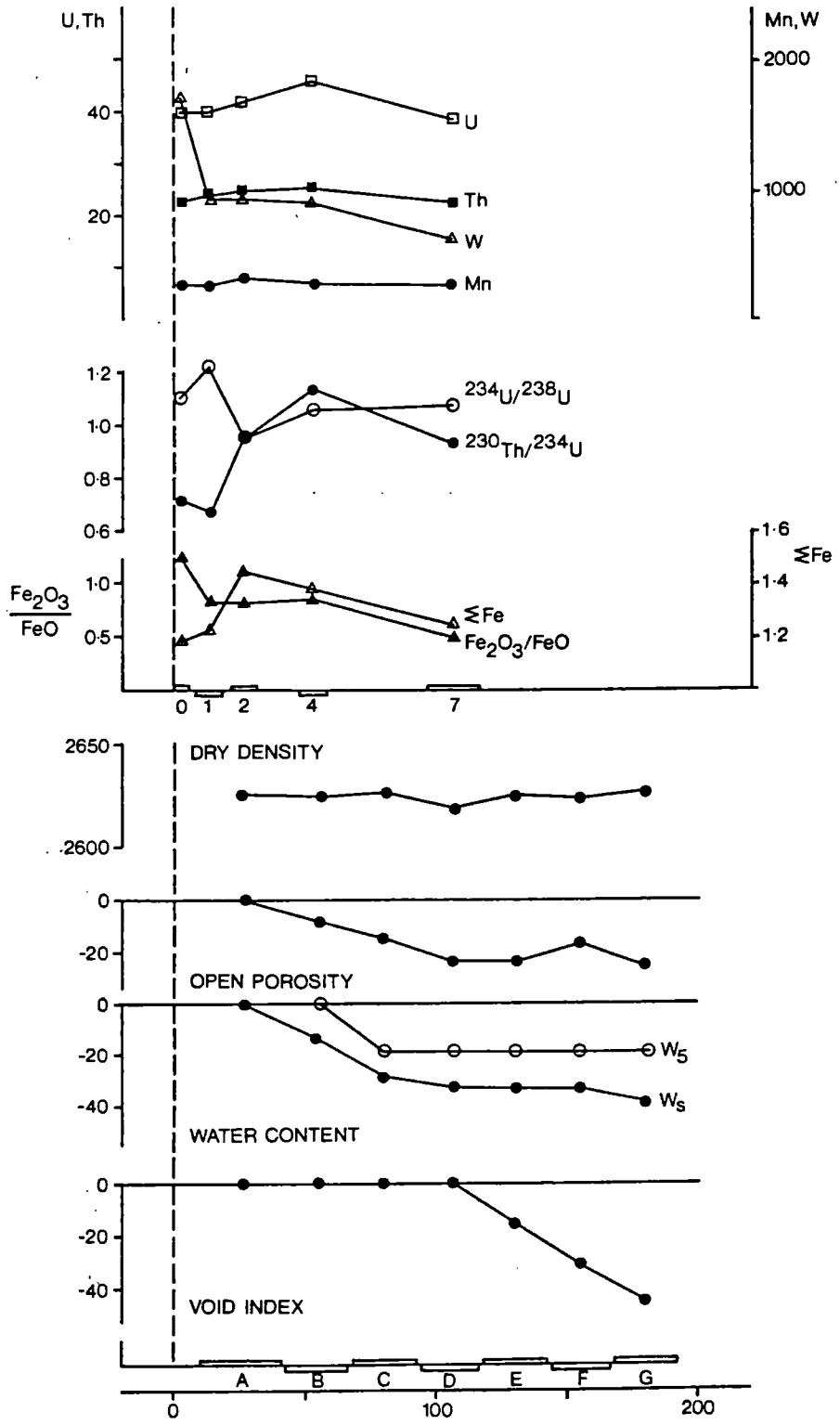

Fig. 54.- Variation in selected parameters with distance from the fracture surface. Stripa sample ST6. (See fig. 52 for further explanation).

The U-234/U-238 activity ratios obtained for sample ST6 show a zone of recent uranium enrichment extending some 20 mm from the fracture surface (U-234/U-238 greater than 1.0). This uranium enrichment is reflected in the Th-230/U-234 activity ratios, which show an excess of U-234 over Th-230 (Th-230/U-234 less than 1.0).

The isotopic composition of Stripa groundwaters, in which U-234/U-234 ratios are around 1.60, has been described by Nordstrom et al. (1985).

4.6.5.3. Whiteshell samples.

Uranium series data were obtained for both samples WS1 and WS2. These data are presented with the results of geochemical and petrophysical analysis of these samples in Figures 55 and 56.

WHITESHELL SAMPLE WS1 (Figure 55): The uranium series data for sample WS1, the altered granite, show evidence of uranium migration both into and away from the fracture surface. U-234/U-238 ratios show an excess of U-234 extending some 50 mm into the rock. Th-230/U-234 ratios show a more marked zone of recent uranium depletion (Th-230/U-234 greater than 1.0) extending some 50 mm into the rock from the fracture face. Interpretation of these data is difficult as the history of the sample is clearly complex with both loss and gain of uranium by the rock adjacent to the fracture. Ancient heavy leaching of uranium from the rock (producing a Th-230/U-234 activity ratio considerably greater than 1.0), followed by more recent deposition of U-234-enriched uranium from solution (producing a U-234/U-238 activity ratio greater than 1.0), would explain the observed activity ratios. The complexity of the processes taking place in the rock preclude any attempt to date these two uranium migration episodes.

WHITESHELL SAMPLE WS2 (Figure 56): In contrast to the altered granite, the uranium series data for the unaltered sample WS2 is more straightforward. U-234/U-238 activity ratios reveal a zone of recent uranium enrichment extending some 50 mm from the fracture surface. This is reflected in Th-230/U-234 ratios of less than 1.0, and coincides with a zone of slight chemical uranium enrichment (Section 4.7.2.3). At depths greater than 50 mm, the Th-230/U-234 ratio is greater than 1.0, suggesting uranium depletion in this part of the rock.

Gascoyne and Cramer (1987) reported U-234/U-238 ratios of between 1.98 and 6.47 in Whiteshell groundwaters.

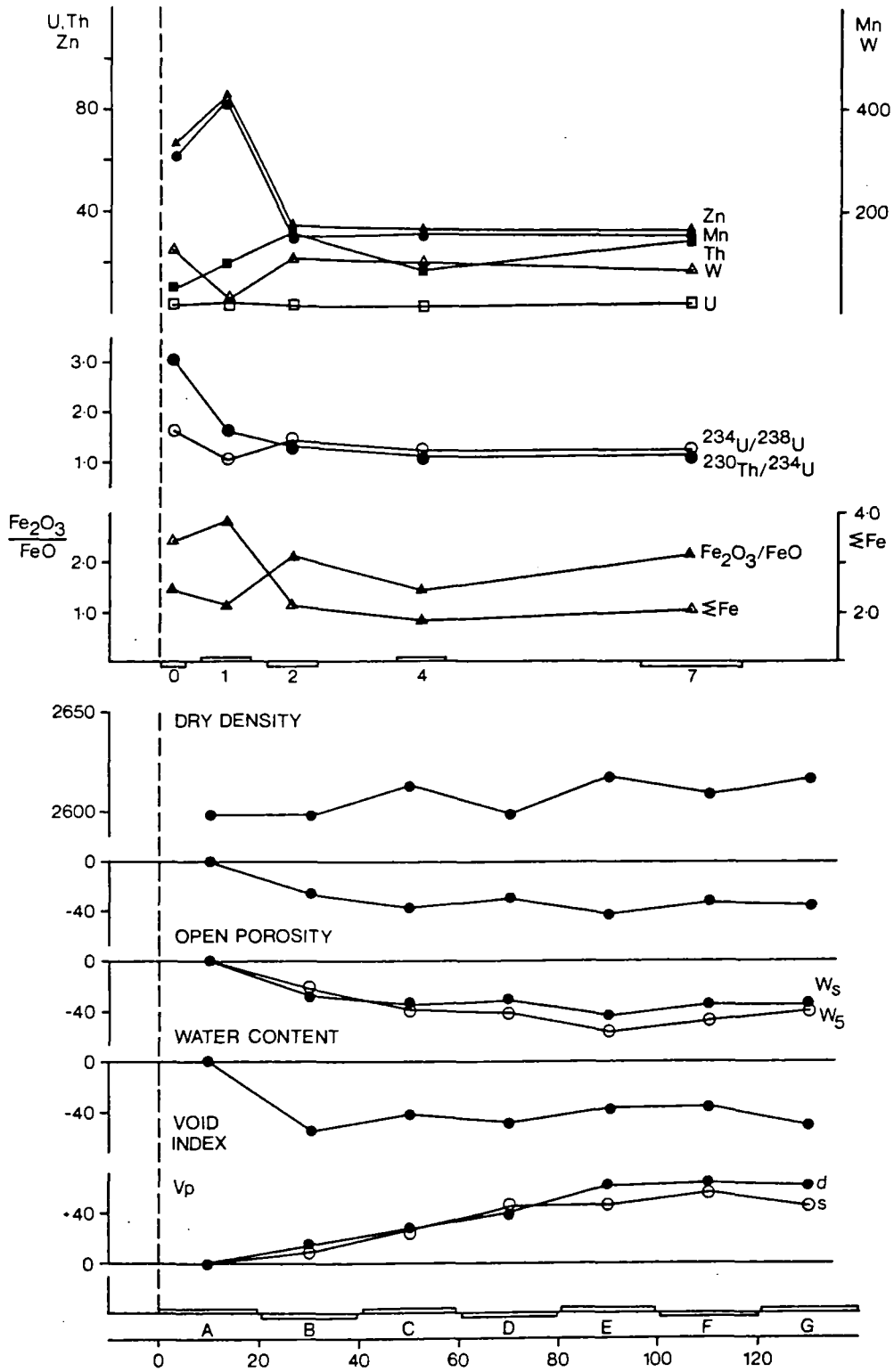

Fig. 55.- Variation in selected parameters with distance from the fracture surface. Witeshell sample WS1. (See fig. 52 for further explanation).

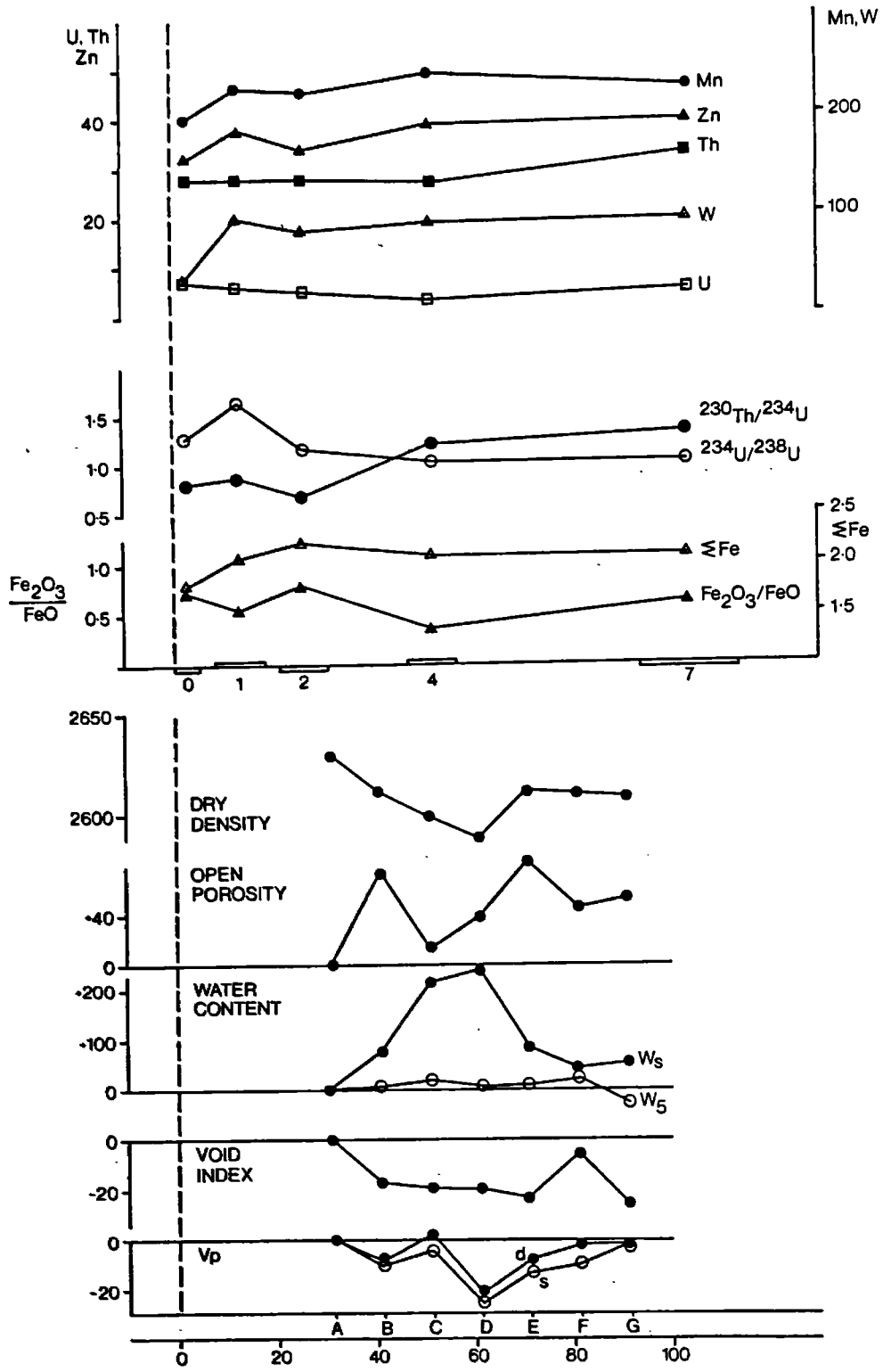

Fig. 56.- Variation in selected parameters with distance from the fracture surface. Witeshell sample WS2. (See fig. 52 for further explanation).

4.6.5.4. Grimsel samples.

Alpha spectrometry data have been obtained for two rock slices from each of samples GR1 and GR2 (results are presented in Annex 5). No petrophysical or microstructural work was carried out on these samples. The results of the uranium series studies are difficult to interpret as, although earlier studies of Grimsel granite (e.g. Smellie et al. (1986) and Alexander et al. (1990)) show U-234/U-238 and Th-230/U-238 to be generally close to equilibrium, and although the rocks studied were apparently unaltered, many of the activity ratios determined on samples GR1 and GR2 deviate considerably from unity, particularly those away from the fracture. As in the case of Whiteshell sample WS1, a complex history is suggested.

4.7. GEOCHEMICAL ANALYSIS.

4.7.1. Analytical techniques.

The geochemistry of the samples studied has been determined primarily by X-ray fluorescence spectrometry (XRF), supplemented where necessary by other techniques. Ferrous iron (as FeO) has been determined by a traditional titration technique. The geochemical analysis undertaken has provided data for some nine major and 22 trace elements, including both Fe(III) as Fe_2O_3 and Fe(II) as FeO.

Geochemical analysis has been carried out for each of the rock slices for which uranium series disequilibrium data have been obtained, allowing the U series characteristics to be related to geochemical changes in the rock. Some additional geochemical analyses were carried out on El Berrocal samples EB1A, EB1B and EB1E, and Stripa sample ST7, though alpha spectrometric data are not available for these samples.

4.7.2. Results of geochemical analysis.

The full results of the geochemical analyses carried out are presented in Annexes 1 - 5. In establishing the relation between geochemistry and uranium series characteristics, and with regard to evidence for diffusion having taken place in the rock adjacent to the fractures studied, most of the elements analysed show no systematic variation in concentration with respect to distance from the fracture.

A number of elements, however, do show a systematic variation in some samples that can be interpreted in terms of element migration (i.e. diffusion) from the fracture surface into the rock matrix. Of particular interest are uranium, thorium, iron and iron oxidation characteristics, manganese, tungsten, arsenic and zinc.

4.7.2.1. El Berrocal samples.

Geochemical and uranium series data for El Berrocal samples are presented in Figures 52 and 53 where they can be compared with petrophysical data from the same core.

Uranium and thorium.

The El Berrocal site is a disused uranium mine with primary pitchblende and secondary uranium mineralisation. The mine water is reported to contain up to 65 ppb uranium (Ivanovich, 1990).

EL BERROCAL SAMPLE EB1: Geochemical analysis of Core EB1F shows a clear uranium enrichment at the fracture surface (nearly 120 ppm in rock slice '0X'), but the zone of enrichment is limited and does not extend beyond about 35 mm from the fracture surface. Thorium concentrations are constant (7 - 8 ppm) throughout the core.

EL BERROCAL SAMPLE EB3: The uranium distribution in core EB3 also shows a clear uranium enrichment extending some 60 - 80 mm from the fracture into the rock. Thorium values vary between 5 ppm and 8 ppm, the single low value being 13 mm from the fracture, though this is not considered to be significant.

Iron and iron oxidation characteristics.

EL BERROCAL SAMPLE EB1: The Fe_2O_3/FeO ratio, an indicator of iron oxidation, increases close to the fracture surface, but again this is limited to a zone extending only 40 mm into the rock. Total iron (Fe_2O_3 + FeO) first decreases with increasing distance from the fracture, and then increases. Interestingly, the 'red zone' is not a zone of oxidation or iron enrichment, but seems to be due to a redistribution of iron within the rock fabric.

EL BERROCAL SAMPLE EB3: The Fe_2O_3/FeO ratio falls slightly immediately adjacent to the fracture, compared with the value at the fracture face, then rises to a fairly constant value approximately 50 mm into the rock. Total iron falls sharply in the rock immediately adjacent to the fracture, then rises to a peak concentration approximately 50 mm from the fracture, then falls to reach what appears to be a fairly constant value within 100 mm of the fracture surface.

Other trace metals.

EL BERROCAL SAMPLE EB1: Most of the trace elements determined in the sample show no systematic variation with distance from the fracture. Mn, Zn and W, however, do show a marked enrich-

ment close to the fracture but, as with uranium, this is limited to a zone only 35 mm into the rock. As and, to a lesser extent, Pb show enhanced values in the red zone.

EL BERROCAL SAMPLE EB3: A number of other trace metals in the rock follow the same distribution pattern as total iron; thus Mn, Zn and W all fall in the rock immediately adjacent to the fracture face, then rise to a peak concentration approximately 50 mm from the fracture before falling to what appear to be fairly constant concentrations within 100 mm of the fracture face. There is a marked surface enrichment in W, but this is confined to the fracture face. As also appears to follow this pattern, but values are too low to permit any significant variation to be identified.

Major element variation.

EL BERROCAL SAMPLE EB1: It is worth noting that some major element variations are observed with increasing distance from the fracture surface. Concentrations of Ca, Mg, K and Na (elements commonly mobilised during weathering) are lower immediately adjacent to the fracture surface (slice '0'), while Ca, Mg and P are significantly depleted in slice '0X' (as is total iron). No clearly-defined distribution pattern has been identified deeper into the rock.

EL BERROCAL SAMPLE EB3: As in sample EB1, K and Na show some depletion at the fracture surface, but this depletion does not extend into the rock. Other major elements show no systematic distribution pattern.

4.7.2.2. Stripa samples.

The results of geochemical analysis of Stripa samples ST6 and ST7 show remarkable similarities in the distribution of elements. Geochemical and uranium series data for Stripa sample ST6 are presented in Figure 54 where they can be compared with petrophysical data from the same core.

Uranium and thorium.

The Stripa granite is unusually enriched in uranium, both samples ST6 and ST7 containing around 40 ppm uranium. (A detailed account of the radiogeology of the stripa pluton was presented by Wollenberg et al., 1980.) In terms of their chemical concentrations, neither uranium nor thorium show any significant variation with respect to distance from the fracture surface in either sample ST6 or ST7. This is in contract with the uranium series evidence which shows uranium enrichment near the fracture (Section 4.6.4.2).

Iron and iron oxidation characteristics.

In sample ST6, the Fe_2O_3/FeO ratio rises sharply (to a value of 1.25) at the fracture surface where the rock has been in contact with oxidising groundwater, but this highly oxidised zone does not extend into the rock. Iron oxidation levels remain fairly constant between about 10 mm and 50 mm from the fracture (around 0.75), then fall to a value of 0.5 100 mm from the fracture. This pattern is also observed in sample ST7. Total iron is fairly constant through core ST7, but shows a peak concentration some 25 mm from the fracture in ST6, a feature that is not considered to be significant.

Other trace metals.

The only trace metal the distribution of which appears to be related to the fracture is W, which shows a marked surface enrichment in both samples ST6 and ST7; concentrations then fall to a fairly constant level between about 10 mm and 50 mm from the fracture, then fall again about 100 mm from the fracture. This distribution pattern is identical to that of the Fe_2O_3/FeO ratio, to which it is probably related, W deposition being controlled by oxidation conditions.

Major element variation.

Apart from some apparent Ca depletion at the fracture surface in sample ST7, there seems to be no systematic major element variation related to the fracture.

4.7.2.3. Whiteshell samples.

Geochemical and uranium series data for Whiteshell samples are presented in Figures 55 and 56 where they can be compared with petrophysical data from the same cores.

Two very different samples of Whiteshell granite have been studied, one highly altered (WS1), the other apparently unaltered (WS2). Their geochemical characteristics are very different.

Uranium and thorium.

WHITESHELL SAMPLE WS1: Uranium values are low (3 - 4 ppm) and are constant throughout the core. Thorium values vary between 10 and 32 ppm, the lowest values being closest to the fracture; as thorium is immobile in most geochemical environments, this probably reflects its primary distribution in the rock and is not considered to be significant in terms of near-fracture processes.

WHITESHELL SAMPLE WS2: Again, uranium values are low (3 - 7 ppm), but there does seem to be a slight increase in uranium content close to the fracture (within a few centimetres). Thorium values are fairly constant throughout the core (27 - 33 ppm).

Iron and iron oxidation characteristics.

WHITESHELL SAMPLE WS1: The Fe_2O_3/FeO ratios determined for sample WS1 are high throughout the core compared with the other rocks studied (not unexpectedly in such a highly altered rock). Close to the fracture (within about 20 mm of the fracture face), values are actually a little lower than deeper into the rock, a feature that may be significant in view of other element variations observed in the core. There is an enrichment in total iron in the rock adjacent to the fracture, but it is confined to a zone extending about 20 mm from the fracture surface.

WHITESHELL SAMPLE WS2: Fe_2O_3/FeO ratios are lower in the unaltered sample WS2 than in the altered sample WS1, and there is no well-defined distribution of values with respect to the fracture face. Total iron concentrations are fairly constant except at the fracture face, where there is a lower concentration. Again, this may be significant in view of a similar variation in other metal concentrations (Mn, Zn and W), which show a similar distribution reflecting leaching of these metals from the fracture surface (though the leached zone does not extend into the rock).

Other trace metals.

WHITESHELL SAMPLE WS1: Both Zn and Mn show the same distribution in the rock as total iron, with a marked enrichment in the 20 mm or so nearest to the fracture and peak concentrations 12 - 13 mm from the fracture face. The W concentration actually falls at the point of highest Zn/Mn concentration, but is otherwise fairly constant.

WHITESHELL SAMPLE WS2: The concentrations of Zn, Mn and W follow that of total iron, with a marked depletion at the fracture surface. This zone of leaching does not, however, extend into the rock.

Major element variation.

WHITESHELL SAMPLE WS1: Both Ca and Na are depleted at the fracture surface; this suggests a narrow zone of leaching, though some of the Ca appears to have been redistributed inwards into the rock immediately adjacent to the fracture. There is some enrichment in K on the fracture surface; as there is no similar K enrichment in the unaltered sample (WS2), this high K value

may be due to the presence of clay minerals (notably illite) on the altered fracture surface.

WHITESHELL SAMPLE WS2: Sample WS2 also shows Ca and Na depletion on the fracture surface, but there is no accompanying increase in K concentration in this unaltered sample.

4.7.2.4. Grimsel samples.

Geochemical and uranium series data for Grimsel samples are presented in Annex 5 where they can be compared with petrophysical data from the same cores. Insufficient time was available to complete the analysis of a full set of Grimsel samples, only two rock slices being analysed from each of two cores. On the basis of the limited data obtained, it is not possible to identify any trends in element concentrations with respect to the fracture. It is hoped to complete this work in the near future.

4.8. PETROPHYSICAL AND GEOCHEMICAL VARIATION IN ROCK ADJACENT TO FRACTURES IN GRANITE AND ITS INTERPRETATION IN TERMS OF ROCK MATRIX DIFFUSION.

The results of uranium series, geochemical and petrophysical analyses are presented in full in Annexes 1 - 5. For each of the five main samples studied (EB1, EB3, ST6, WS1 and WS2), the following observations can be made. In view of known analytical uncertainties (with regard, for example, to Th-230/U-234 values, as described in Section 4.6.4.2), only broad patterns of variation have been included in the overall interpretation of the data obtained.

4.8.1. El Berrocal samples.

The cores obtained from block EB1 were obtained from a granite block collected from a shallow mine adit (20 - 30 m depth) and showing clear evidence of water movement through open fractures. In such an environment, and with high levels of uranium in the groundwater, deep penetration of uranium into the rock matrix from water-conducting fractures might be expected. Such free diffusion does not appear to have taken place, however, there being a clearly-defined zone, extending only 35 mm into the rock, to which diffusion from the fracture appears to have been limited. Beyond this zone of uranium enrichment, and extending up to 100 mm into the rock, is a zone of uranium depletion. Iron oxidation also increases in the nearest 40 mm to the fracture, while the penetration of zinc and tungsten is also confined to this zone.

Physical changes in the rock have also been observed within this zone of uranium enrichment. Open porosity, water content

after five days and at saturation, void index, p-wave velocity in dry rock and dry density all show significant changes in the 30 mm or so nearest the fracture. Uranium and other metal mobility appears, therefore, to have been enhanced by these microstructural changes immediately adjacent to the fracture.

Results for the deep core, EB3, reveal a similar picture, though in this case the zone of enhanced uranium mobility (characterised by U-234 depletion) is rather wider, extending some 80 mm or so into the rock from the fracture studied. Variation in physical properties is rather erratic, the greatest variation appearing to occur within 210 mm of the fracture.

4.8.2. Stripa sample.

Unlike the shallow sample EB1, Stripa sample ST6 is a deep core (350 m). The uranium series, geochemical and petrophysical studies have, however, revealed a remarkably similar picture of uranium mobility limited to a narrow zone extending only a few centimetres from the fracture.

Uranium series data show a marked uranium enrichment in the 25 mm or so nearest to the fracture. Iron oxide evidence suggests changes extending more than 50 mm into the rock, while petrophysical changes (notably in accessible porosity, water content after two and five days, and saturation water content) continue up to 80 mm from the fracture, beyond which key properties reach constant values. Results for sample ST7 are very similar. In this case, uranium mobility is confined to the zone in which the greatest microstructural changes have taken place.

Here, at depths of interest for repository construction, the potential for radionuclide retardation by rock matrix diffusion seems to be very limited, most of the rock mass between water-conducting fractures appearing to be unavailable for diffusion.

4.8.3. Whiteshell samples.

In Whiteshell sample WS1 (the altered granite) there is a clearly-defined zone of enhanced uranium mobility extending up to about 50 mm from the fracture. Iron enrichment is confined to a slightly narrower zone (30 mm). Petrophysical changes continue to about 80 mm from the fracture, where key properties (e.g. velocity of p-waves in dry rock) reach constant values. As in the Stripa samples, the enhanced uranium mobility appears to be confined to the region of greatest microstructural change.

In the unaltered granite (sample WS2), a similar zone of enhanced uranium mobility can be observed, again extending some

50 mm from the fracture. Owing to practical difficulties in cutting core WS2, the petrophysical data are more difficult to interpret, though values for key parameters appear to become less erratic 70 - 80 mm from the fracture.

4.8.4. Grimsel samples.

Insufficient data are available to draw any conclusions from the limited study of Grimsel samples. In contrast to the other rocks studied, uranium mobility seems to have affected the entire length of each of the two cores, but further data are required before any firm conclusions can be offered.

5. DISCUSSION AND CONCLUSIONS

The objective of the study has been to explore the possibility that radionuclide (specifically, uranium) retardation by rock matrix diffusion will be limited in granitic rocks by geological factors that constrain other fracture-related processes (alteration, mineralisation etc.), and that diffusion will be confined in many cases to a zone extending only a limited distance from water-conducting fractures (perhaps a few centimetres).

In pursuit of this objective, data of two types have been collected from granites of different ages, from different depths, with different histories and with different structural and alteration characteristics. Firstly, uranium series and geochemical analyses have been carried out in order to estab- lish whether or not there is any record of diffusion of uranium (a natural analogue of many of the actinides in radioactive waste), its daughters, or other elements in the rock adjacent to fractures. Secondly, petrophysical measurements have been performed in order to establish the extent of fracture-related microstructural changes that might influence the potential for diffusion in the rock adjacent to fractures. In each case, the emphasis has been on observation rather than experiment.

During the study, a considerable quantity of data has been accumulated, all of which is presented for reference in this report. Not all of the data collected has been useful in identifying evidence for diffusion, however, and only selected data, showing changes that can be interpreted in terms of diffusion, have been discussed.

In each of the main rocks studied, the granites of El Berrocal (Spain), Stripa (Sweden) and Whiteshell (Canada), the results obtained suggest that:

- a zone of enhanced uranium mobility exists adjacent to the fractures studied;
- this zone is, mainly in weathered rocks with hidrologically-active fractures, associated to microstructural changes in the rock that are related to the fracture;
- the evidence for diffusion having taken place in the rock is confined largely to this zone, or part of it; and
- that the zone of enhanced element mobility extends only a few centimetres from the fracture:

    - 35 mm in the shallow El Berrocal granite;
    - 80 mm in the deep El Berrocal granite;
    - 25 mm in the Stripa granite;
    - 50 mm in the altered Whiteshell granite;
    - 50 mm in the unaltered Whiteshell granite.

The limited data obtained for the Grimsel granite samples suggest uranium series disequilibrium throughout the cores examined, but further evidence is required.

The results of the study have shown that the rock adjacent to hydrologically-active fractures is very different from the intact rock distant from fractures, mainly in cases of weathered rock. In sound rocks (sound Whiteshell or El Berrocal deep sample) erratic variations of the physical properties are observed. The zone of microstructural alteration associated with the fracture is fairly narrow (generally less than 100 mm). As the evidence for diffusion is confined to the zone of microstructural alteration, it appears that diffusivity determinations on rock collected away from the influence of fractures will not give representative data for diffusion modelling; this is in addition to the problems associated with the de-stressing of samples when they are removed from the ground.

The approach adopted has proved to be very effective in identifying both the extent to which natural diffusion of the actinides studied (and other trace metals) has taken place in the rock and the physical characteristics of the rock which have facilitated that diffusion.

In radionuclide migration models for deep, fractured crystalline rock formations, rock matrix diffusion must be considered as a retardation mechanism. A good geological host should, therefore, allow diffusion to take place freely, thus allowing radionuclides to be retained in the rock mass, and released slowly later, rather than be transported away rapidly from the repository by fracture flow. The results of the study suggest, however, that diffusion will be of limited effectiveness as a retardation mechanism for uranium in many granitic rocks; this will be particularly important where water movement is confined to narrow channels in which flow velocity may be high and access by nuclides to the walls of fractures is restricted. These factors should be taken into account in establishing

radionuclide migration models for potential repository sites.

6. ACKNOWLEDGEMENTS

For their kind cooperation and provision of samples, thanks are due to Carlos del Olmo and Julio Astudillo and his colleagues at Empresa Nacional de Residuos Radiactivos S.A. (ENRESA) and Pedro Rivas, Berta de la Cruz, Luis Pérez del Villar and Julio Pardillo from Centro de Investigaciones, Energeticas, Medio Ambientales y Tecnologicas (CIEMAT), Spain; to SKB, and Gunnar Ramqvist and his colleagues at Stripa Mine Service AB, Sweden; to Tjalle 'Chuck' Vandergraaf, Mel Gascoyne and Peter Sargent of Atomic Energy of Canada Ltd. (AECL); to Russell Alexander of the Paul Scherrer Institute (now at the University of Bern) and his colleagues at NAGRA, Switzerland. Thanks are also extended to Alain Chambaudet at the Laboratoire de Microanalyses Nucleaires, University of Franche-Comte, Besançon, France, for use of the LMN porosimetry laboratory, and to Andrew Briggs at the Department of Materials, University of Oxford, for use of the acoustic microscopy laboratory.

7. REFERENCES

ALEXANDER, W. R., MACKENZIE, A. B., SCOTT, R. D. and MCKINLEY, I. G. (1990). Natural analogue studies in crystalline rock: the influence of water-bearing fractures on radionuclide immobilization in a granitic rock repository. NAGRA Technical Report 87-08.

ALEXANDER, W. R., SCOTT, R. D., MACKENZIE, A. B. and McKINLEY, I. G. (1988). A natural analogue study of radionuclide migration in a water conducting fracture in crystalline rock. Radiochimica Acta.

ARRIBAS, A. (1964). Mineralogia y metalogenia de los yacimientos de uranio: El Berrocal, Escalona (Toledo). Not. y Com. IGME, Vol. 1, No. 77, 67-92.

A.S.T.M. (1988). ASTM Standards. Vol. 04.08. Soil and Rock, Building Stones; Geotextiles. American Society for Testing and Materials. Philadelphia. 953 pp.

BAUER, S. J. and JOHNSON, B. (1979). Effects of slow uniform heating on the physical properties of the Westerly and Charcoal granites. Proc. 20th Symp. Rock Mech., Austin, Texas, 7-18.

BELIKOV, B. P., ZALESSKII, B. V., ROZANOV, Y. A., SANINA, E. and TIMCHENKO, I. P. (1967). Methods of studying the physicochemical properties of rocks. In: Zalesskii, B. V. (Ed.), Israel Program for Scientific Translations, Jerusalem, 1-58.

BERNABE, Y. (1987). A wide range permeameter for use in rock physics (technical note). Int. J. Rock Mech. Min. Sci. & Geomech. Abstr. Vol. 24, No 5, 309-315.

BRACE, W.F., WALSH, J.B. and FRANGUS, W.F. (1968). Permeability of granite under high pressure. J. Geophysical Research, Vol. 73, No 6, 2225-2236.

BRACE, W.F. (1980). Permeability of crystalline and argillaceous rocks. Int. J. Rock Mech., Min. Sci. & Geomech. Abst.17, 241-251.

BRIGGS, G. A. D. (1985). An introduction to scanning acoustic microscopy. Royal Microscopical Society. Oxford University Press.

C.N.R.-I.C.R. (1981). Assorbimento d'acqua per immersione totale. Capacita di imbibizione. Doc. Normal: 7/81. Istituto Centrale del Restauro. Roma, 5 pp.

DEARLOVE, J. P. L., LONGWORTH, G. and IVANOVICH, M. (1990). Improvement of colloid sampling techniques in groundwater and actinide characterisation of the groundwater systems at Gorleben (FRG) and El Berrocal (E). AEA Technology Report AEA D&R 0066.

ENRESA. Characterisation of actinides, complex and colloid migration in granite (El Berrocal). CEC Contract No. FI1W.230.

ENRESA (1987). IPES Project. Empresa Nacional de Residuos Radiactivos, S.A.. Proc. 7th Information Meeting AECL/Euratom. Pinawa, Canada, October 1987.

GALE, J., MACLEOD, R., WELHAN, J., COLE, C. and VAIL, L. (1987). Hydrogeological characterisation of the Stripa site. Stripa Project Tech. Rept. 87-15. SKB, Stockholm.

GASCOYNE, M. AND CRAMER, J. J. (1987). History of actinide and minor element mobility in an Archaen granitic batholith in Manitoba, Canada. Applied Geochem., 2, 37-53.

GRISAK, G. E. and PICKENS, J. F. (1981). An analytical solution for matrix transport through fractured media with matrix diffusion. J. Hydrol., 52, 47-57.

HADERMANN, J. and ROESEL, F. (1985). Radionuclide chain transport in inhomogeneous crystalline rocks: limited matrix diffusion and effective surface sorption. NAGRA Technical Report 85-40.

HEATH, M. J. (1988). Natural analogue and microstructural studies in relation to radionuclide retardation by rock matrix dif-

fusion in granite. Progress report to CEC, April 1988, 6 pp.

HEATH, M. and MONTOTO, M. (1990). Natural analogue and microstructural studies in relation to radionuclide retardation by rock matrix diffusion in granite: progress report, December 1989 - May 1990. 9 pp.

HOPPE, M. and BEREITER-HAHN, J. (1985). Applications of scanning acoustic microscopy - survey and new aspects. IEEE Trans. on Sonics and Ultrasonics, Vol. SU-32, 2, 289-301.

HOWARTH, D. F. and ROWLANDS, J. C. (1987). Quantitative assessment of rock texture and correlation with drillability and strength properties. Rock mechanics and Rock Engineering, 20, 57-85.

ILETT, C., SOMEKH, M. G. and BRIGGS, G. A. D. (1984). Acoustic microscopy of elastic discontinuities. Proc. R. Soc. Lond., A393, 171-183.

I.S.R.M. (1981). Rock characterisation, testing and monitoring. E. T. Brown (Ed.). International Society for Rock Mechanics: Suggested Methods, 211 pp.

IVANOVICH, M. (1990). El Berrocal Project. Interim report to the 10th Coco Club meeting, Harwell Laboratory, 5-7 February 1990.

IVANOVICH, M., LONGWORTH, G., WILKINS, M. A. and HASLER, S. E. (1987). A study of uranium series disequilibrium in core profiles and mineral separates from the samples of Lac de Bonnet granite from the URL site, Pinawa, Manitoba, Canada. Harwell Report AERE G 4307.

K.B.S. (1983). Final storage of spent nuclear fuel - KBS-3. Swedish Nuclear Supply Co./Division KBS (SKBF/KBS), Vol. III, p. 14.10.

LEVER, D. A., BRADBURY, M. H. and HEMINGWAY, S. J. (1982).Modelling the effect of diffusion into the rock matrix on radionuclide migration. Harwell Report AERE-R 10614.

LIN, W. (1977). Compressible fluid flow through rocks of variable permeability. Rept. UCRL-52304, p. 15. Lawrence Livermore Lab., Livermore, California.

LIN, W. (1981). Parametric analysis of the transient method of measuring permeability. Rept. UCRL-84290. Lawrence Livermore Lab., Livermore, California.

LIN, W. (1982). Parametric analysis of the transient method of measuring permeability. J. Geophysical Research, Vol. 87, No.

B2, pp. 1055-1060.

LOTZE, F. (1945). Observaciones respecto a las Variscides de la Meseta Iberica. Public. Extr. sobre Geologia de España. T. V, 149-166.

MONTOTO, M. and HEATH, M. J. (1989). Natural analogue and microstructural studies in relation to radionuclide retardation by rock matrix diffusion in granite: progress report, December 1988 - May 1989. Report to CEC. 30 pp.

MONTOTO, M. and HEATH, M. J. (1990). Natural analogue and microstructural studies in relation to radionuclide retardation by rock matrix diffusion in granite: progress report, June 1989 -November 1989. Report to CEC. 33 pp.

MONTOTO, M., MONTOTO, L., ROSHOFF, K. and LEIJON, B. (1980). Microfractographic study of heated and non-heated Stripa granite. Proc. int. Symp. on Subsurface Space (Rockstore '80), Stockholm. Vol. 3, 1357-1368.

NAGRA (1985). Project Gewahr 1985. Nuclear waste management in Switzerland: feasibility studies and safety analysis. NAGRA Project Report NGB 85-09, p. 11.20.

NERETNIEKS, I. (1980). Diffusion in the rock matrix: an important factor in radionuclide migration? J. Geophys res., 85, 4379-4397.

NERETNIEKS, I., ABELIN, H. and BIRGERSSON, L. (1987). Some recent observations of channelling in fractured rocks - its potential impact on radionuclide migration. Proc. DOE/AECL Conf., Sept. 1987. San Francisco, USA.

NORDSTROM, D. K., ANDREWS, J. N., CARLSSON, L., FONTES, J-C., FRITZ, P., MOSER, H. and OLSSON, T. (1985). Hydrogeological and hydrogeochemical investigations in boreholes - final report of the Phase 1 geochemical investigations of the Stripa groundwaters. Stripa Project Tech. Rept. 85-06, SKB, Stockholm.

NORTON, D. and KNAPP, R. (1977). Transport phenomena in hydrothermal systems: the nature of porosity. Am. J. Sci., 277, 913-936.

PELTONEN, E. et al. (1985). Safety analysis of disposal of spent nuclear fuel - normal and disturbed evolution scenarios. Nuclear Waste Commission of Finnish Power Companies, Report YJT-85-22, Helsinki.

PEREZ DEL VILLAR, L. and DE LA CRUZ, B. (1989). Caracterizacion mineralogica y geoquímica del granito sano y alterado del macizo de "El Berrocal" (Sierra de Gredos, Provincia de Toledo). Studia Geologica Salmanticensia, XXVI, 47-80.

R.I.L.E.M. (1980). Essais recommandes pour mesurer l'alteration des pierres et evaluer l'efficacite des methodes de traitement. Materiaux et Constructions. Bull. RILEM, 13 (75), 216-220.

RODRIGUEZ REY, A., BRIGGS, G. A. D., FIELD, T. and MONTOTO, M. (1990). Acoustic microscopy of rocks. J. Microscopy, 160, 21-29.

RODRIGUEZ REY, A., RUIZ DE ARGANDOÑA, V. G., MONTOTO, M. and HEATH, M. J. (1988). Natural analogue and microstructural studies in relation to radionuclide retardation by rock matrix diffusion in granite: progress report, May - November 1988. Report to CEC, 29 pp.

SKAGIUS, K. and NERETNIEKS, I. (1986). Diffusivity measurements and electrical resistivity measurements in rock samples under mechanical stress. Water Resources Research, 22, No.4, 570-580.

SMELLIE, J. A. T., MACKENZIE, A. B. and SCOTT, R. D. (1986). An analogue validation study of natural radionuclide migration in crystalline rocks using uranium-series disequilibrium studies. Chem. Geol., 55, 233-254.

STRECKEISEN, A. (1974). Classification and nomenclature of plutonic rocks. Geol. Rdsch., 63, 773-786.

TRIMMER, D.A. (1981). Design criteria for laboratory measurements of low permeability rocks. Geophysical Research Letters, Vol. 8, No. 9, 973-975.

TRIMMER, D.A., BONNER, B., HEARD, H.C. and DUBA, A. (1980). Effect of pressure and stress on water transport in intact and fractured gabbro and granite. J. Geophysical Research, Vol. 85, No. B 12, 7059-7071.

WOLLENBERG, H. A., FLEXSER, S. and ANDERSON, L. (1981). Petrology and radiology of the Stripa Pluton. Lawrence Berkeley Lab. Rept. LBL-11654; Swedish-American Cooperative Program on Radioactive Waste Storage in Mined Caverns in Crystalline Rock, Rept. SAC-36.

8. RESEARCH TEAM

Modesto Montoto, Vicente G. Ruiz de Argandoña, Angel Rodríguez Rey, Lope Calleja Escudero, Beatriz Menendez and Antonio Martínez (Department of Geology, University of Oviedo); Mike Heath, John Merefield, Ian Stone, Brian Bews and Eric Durrance (Earth Resources Centre, University of Exeter). The contribution of Angel M. Nistal in Oviedo to the digital image processing work described in this report is also gratefully acknowledged.

Annex 1A. GEOCHEMICAL AND URANIUM SERIES DATA, EL BERROCAL SAMPLE EB1A

Sample No.	1A.0	1A.1	1A.2	1A.3	1A.6
Distance from fracture (mm)	0-5	6-21	22-37	38-48	71-91
Major elements (%)					
SiO_2	71.70	77.53	72.48	73.43	75.22
TiO_2	0.20	0.16	0.18	0.16	0.18
Al_2O_3	15.02	14.50	14.82	14.14	13.64
Fe_2O_3	0.79	0.59	0.63	0.41	0.45
FeO	0.88	0.75	0.90	0.93	1.11
MgO	0.50	0.50	0.50	0.49	0.54
CaO	0.53	0.53	0.59	0.62	0.57
Na_2O	3.50	3.48	3.63	4.18	3.47
K_2O	5.06	4.58	4.81	4.04	3.99
P_2O_5	0.30	0.30	0.32	0.31	0.30
Total	98.48	102.92	98.86	98.71	99.47
Trace elements (ppm)					
U	47	24	27	13	21
Th	10	8	8	7	7
Nb	24	23	22	21	25
Zr	67	56	59	62	58
Y	31	25	28	27	26
Sr	15	10	14	9	11
Rb	557	498	525	470	482
Cs	21	18	18	18	17
Sn	18	14	16	15	14
V	nd	nd	nd	nd	nd
Cr	11	13	12	12	12
Mn	253	194	196	189	212
Ba	55	29	44	26	26
La	7	6	13	8	12
Ce	23	24	25	23	22
Pb	3	1	4	Tr	nd
As	20	20	35	19	12
Ga	26	24	25	23	24
Zn	77	61	60	48	49
Cu	3	3	3	3	3
Ni	9	8	9	8	8
W	146	155	107	66	51
Total Fe (%)	1.67	1.34	1.53	1.34	1.56
Fe_2O_3/FeO	0.90	0.79	0.70	0.44	0.41
Th/U	0.21	0.33	0.30	0.54	0.33
U-234/U-238	-	-	-	-	-
Th-230/U-234	-	-	-	-	-
Th-230/U-238	-	-	-	-	-

Annex 1A continued. PETROPHYSICAL DATA, EL BERROCAL SAMPLE EB1A

Sample No.	1A.A	1A.B	1A.C	1A.D	1A.E
Distance from fracture (mm)	0-20	22-32	44-64	66-86	88-108
Dry density (kg/m^3)	2629	2629	2614	2624	2625
Total porosity (%)	1.32	1.23	1.63	1.35	1.31
Open porosity (%)	1.31	1.20	1.25	1.18	1.17
Degree of saturation (%)	99.24	97.56	76.78	87.41	89.31
Water content after desorption (%)	0.12	0.10	0.09	0.10	0.11
Void index (%)	0.36	0.37	0.37	0.33	0.34
Water content after 2 days (%)	0.40	0.37	0.39	0.37	0.36
Water content after 5 days (%)	0.43	0.38	0.42	0.41	0.38
Saturation water content (%)	0.49	0.42	0.41	0.43	0.42
Vp, dry (m/s)	5208	6111	5555	5833	5277
Vp, saturated (m/s)	5681	6111	6250	6562	6785

Annex 1B. GEOCHEMICAL AND URANIUM SERIES DATA, EL BERROCAL SAMPLE EB1B

Sample No.	1B.0	1B.1	1B.2	1B.3	1B.6
Distance from fracture (mm)	0-5	6-21	22-37	38-48	71-91
Major elements (%)					
SiO_2	74.38	71.37	72.15	73.76	73.65
TiO_2	0.18	0.19	0.18	0.17	0.16
Al_2O_3	13.89	13.70	15.04	14.53	14.49
Fe_2O_3	0.65	0.59	0.53	0.42	0.29
FeO	0.77	0.82	0.99	0.96	1.00
MgO	0.54	0.48	0.53	0.55	0.51
CaO	0.57	0.57	0.59	0.59	0.59
Na_2O	3.67	3.68	3.90	3.96	3.74
K_2O	4.16	4.09	4.76	4.21	4.44
P_2O_5	0.32	0.31	0.33	0.30	0.32
Total	99.13	95.80	99.00	99.45	99.19
Trace elements (ppm)					
U	85	28	28	15	23
Th	7	8	7	6	6
Nb	18	23	24	24	23
Zr	56	63	59	63	61
Y	26	27	27	27	27
Sr	11	11	11	10	11
Rb	477	496	529	494	505
Cs	18	16	20	19	16
Sn	15	13	14	18	17
V	nd	nd	nd	nd	nd
Cr	11	12	12	13	12
Mn	279	207	199	193	194
Ba	32	34	28	23	25
La	5	12	7	11	7
Ce	18	22	23	21	22
Pb	nd	nd	2	nd	Tr
As	21	20	39	23	12
Ga	23	24	25	25	24
Zn	72	62	65	51	45
Cu	3	4	3	4	3
Ni	8	9	9	9	8
W	149	108	116	55	60
Total Fe (%)	1.42	1.41	1.52	1.38	1.29
Fe_2O_3/FeO	0.84	0.72	0.54	0.44	0.29
Th/U	0.08	0.29	0.25	0.40	0.26
U-234/U-238	-	-	-	-	-
Th-230/U-234	-	-	-	-	-
Th-230/U-238	-	-	-	-	-

Annex 1B continued. PETROPHYSICAL DATA, EL BERROCAL SAMPLE EB1B

Sample No.	1B.A	1B.B	1B.C	1B.D	1B.E
Distance from fracture (mm)	0-20	22-32	44-64	66-86	88-108
Dry density (kg/m^3)	2623	2621	2628	2620	2633
Total porosity (%)	1.50	1.46	1.21	1.50	1.10
Open porosity (%)	1.49	1.27	1.13	1.13	1.09
Degree of saturation (%)	99.33	86.98	93.39	75.33	99.09
Water content after desorption (%)	0.12	0.14	0.11	0.12	0.13
Void index (%)	0.42	0.38	0.33	0.33	0.33
Water content after 2 days (%)	0.44	0.40	0.37	0.37	0.34
Water content after 5 days (%)	0.46	0.40	0.39	0.39	0.38
Saturation water content (%)	0.58	0.48	0.42	0.45	0.40
Vp, dry (m/s)	5250	5277	5555	5555	5000
Vp, saturated (m/s)	5833	6785	6250	7142	6250

Annex 1C. GEOCHEMICAL AND URANIUM SERIES DATA, EL BERROCAL SAMPLE EB1E

Sample No.	1E.0	1E.1	1E.2	1E.3	1E.6
Distance from fracture (mm)	0-5	6-21	22-37	38-48	71-91
Major elements (%)					
SiO_2	76.90	73.10	73.56	75.10	74.77
TiO_2	0.16	0.17	0.18	0.17	0.18
Al_2O_3	12.69	13.50	13.99	13.54	14.42
Fe_2O_3	0.70	0.55	0.46	0.38	0.59
FeO	0.78	0.92	0.91	0.93	1.03
MgO	0.54	0.55	0.52	0.55	0.60
CaO	0.51	0.53	0.56	0.54	0.53
Na_2O	3.18	3.46	3.76	3.63	3.71
K_2O	3.84	4.20	4.17	4.03	4.51
P_2O_5	0.29	0.29	0.31	0.31	0.31
Total	99.59	97.27	98.42	99.18	100.65
Trace elements (ppm)					
U	84	26	26	16	20
Th	8	7	7	7	6
Nb	19	24	23	24	22
Zr	53	61	55	56	57
Y	25	27	25	25	28
Sr	9	12	11	10	12
Rb	459	520	489	476	506
Cs	16	18	17	16	17
Sn	15	17	15	16	15
V	nd	nd	nd	nd	nd
Cr	13	13	12	12	12
Mn	239	203	186	176	183
Ba	24	23	25	23	32
La	10	7	7	10	7
Ce	28	19	19	22	21
Pb	nd	nd	2	nd	Tr
As	18	19	35	19	11
Ga	22	25	24	24	24
Zn	64	64	58	47	43
Cu	4	3	3	3	4
Ni	8	8	8	8	9
W	135	74	70	86	84
Total Fe (%)	1.48	1.47	1.37	1.31	1.62
Fe_2O_3/FeO	0.90	0.60	0.51	0.41	0.57
Th/U	0.10	0.27	0.27	0.44	0.30
U-234/U-238	-	-	-	-	-
Th-230/U-234	-	-	-	-	-
Th-230/U-238	-	-	-	-	-

Annex 1C continued. PETROPHYSICAL DATA, EL BERROCAL SAMPLE EB1E

Sample No.	1E.A	1E.B	1E.C	1E.D	1E.E
Distance from fracture (mm)	0-20	22-32	44-64	66-86	88-108
Dry density (kg/m^3)	2622	2619	2623	2627	2634
Total porosity (%)	1.43	1.54	1.39	1.24	1.10
Open porosity (%)	1.15	1.25	1.16	1.07	1.08
Degree of saturation (%)	80.41	81.17	83.45	86.29	98.18
Water content after desorption (%)	0.10	0.11	0.09	0.10	0.11
Void index (%)	0.32	0.35	0.33	0.32	0.31
Water content after 2 days (%)	0.34	0.38	0.34	0.32	0.31
Water content after 5 days (%)	0.34	0.39	0.35	0.32	0.31
Saturation water content (%)	0.44	0.49	0.45	0.41	0.40
Vp, dry (m/s)	5375	5750	4792	4750	4875
Vp, saturated (m/s)	5972	6388	6388	5277	6093

Annex 1D. GEOCHEMICAL AND URANIUM SERIES DATA, EL BERROCAL SAMPLE EB1F

Sample No.	1F.0X	1F.0	1F.1	1F.2	1F.3	1F.6	1F.8
Distance from fracture (mm)	-5-0	0-5	6-21	22-37	38-48	71-91	113-133
Major elements (%)							
SiO_2	75.56	74.62	74.33	73.92	74.93	73.36	73.70
TiO_2	0.18	0.18	0.18	0.18	0.17	0.17	0.19
Al_2O_3	13.68	13.50	14.21	13.89	13.77	13.80	14.56
Fe_2O_3	0.65	0.68	0.59	0.51	0.40	0.43	0.55
FeO	0.62	0.73	0.79	0.80	0.89	0.98	1.09
MgO	0.56	0.59	0.60	0.55	0.59	0.59	0.58
CaO	0.42	0.53	0.56	0.53	0.53	0.51	0.62
Na_2O	3.54	3.63	3.72	3.72	3.44	3.47	3.77
K_2O	4.22	4.05	4.32	4.23	4.35	4.35	4.23
P_2O_5	0.24	0.31	0.31	0.31	0.30	0.28	0.33
Total	99.67	98.82	99.61	98.64	99.37	97.94	99.62
Trace elements (ppm)							
U	119	46	26	25	16	20	22
Th	7	8	7	7	7	8	7
Nb	15	21	23	22	23	23	26
Zr	60	54	58	61	59	58	60
Y	25	25	27	26	26	25	26
Sr	9	10	11	10	10	9	9
Rb	494	477	498	493	493	509	510
Cs	17	17	18	16	17	20	21
Sn	16	12	14	18	15	18	19
V	nd	nd	nd	nd	nd	nd	nd
Cr	12	12	12	11	12	13	13
Mn	241	265	186	181	182	191	217
Ba	18	26	18	26	23	29	20
La	6	7	8	5	7	7	9
Ce	25	23	21	22	24	17	21
Pb	Tr	nd	nd	nd	nd	Tr	nd
As	18	20	22	40	21	11	10
Ga	24	24	24	24	23	23	25
Zn	66	66	63	57	50	45	48
Cu	3	3	2	3	3	3	3
Ni	8	8	8	8	7	8	8
W	205	187	126	135	63	59	40
Total Fe (%)	1.27	1.41	1.38	1.31	1.29	1.41	1.64
Fe_2O_3/FeO	1.05	0.93	0.75	0.64	0.45	0.44	0.50
Th/U	0.06	0.17	0.27	0.28	0.44	0.40	0.32
U-234/U-238	1.03	1.14	1.04	1.20	1.04	0.98	1.10
Th-230/U-234	0.34	0.60	0.86	0.65	1.45	1.34	0.83
Th-230/U-238	0.35	0.68	0.90	0.78	1.51	1.31	0.75

Annex 1D continued. PETROPHYSICAL DATA, EL BERROCAL SAMPLE EB1F

Sample No.	1F.A	1F.B	1F.C	1F.D	1F.E
Distance from fracture (mm)	0-20	22-32	44-64	66-86	88-108
Dry density (kg/m^3)	2610	2626	2634	2627	2629
Total porosity (%)	1.87	1.28	1.25	1.24	1.20
Open porosity (%)	1.64	1.18	1.14	1.08	1.19
Degree of saturation (%)	87.70	92.18	91.20	87.09	99.16
Water content after desorption (%)	0.10	0.12	0.11	0.10	0.11
Void index (%)	0.49	0.34	0.33	0.33	0.35
Water content after 2 days (%)	0.53	0.36	0.35	0.34	0.38
Water content after 5 days (%)	0.57	0.38	0.37	0.34	0.38
Saturation water content (%)	0.62	0.45	0.43	0.40	0.45
Vp, dry (m/s)	4375	4625	5125	4875	5833
Vp, saturated (m/s)	5833	5781	6406	6093	6562

Annex 1E. PETROPHYSICAL DATA, SAMPLE EB1J

GEOCHEMICAL AND URANIUM SERIES DATA NOT DETERMINED.

Sample No.	1J.A	1J.B	1J.C	1J.D	1J.E
Distance from fracture (mm)	0-20	22-32	44-64	66-86	88-108
Dry density (kg/m^3)	2625	2631	2628	2624	2619
Total porosity (%)	1.31	1.18	1.21	1.25	1.34
Open porosity (%)	1.23	1.16	1.12	1.10	1.26
Degree of saturation (%)	93.89	98.30	92.56	88.00	94.02
Water content after desorption (%)	0.11	0.09	0.12	0.10	0.11
Void index (%)	0.38	0.34	0.32	0.30	0.36
Water content after 2 days (%)	0.41	0.38	0.34	0.34	0.39
Water content after 5 days (%)	0.42	0.39	0.35	0.34	0.40
Saturation water content (%)	0.47	0.45	0.43	0.41	0.50
Vp, dry (m/s)	5681	-	5937	5250	4431
Vp, saturated (m/s)	6250	-	6785	5833	6093

Annex 1F. MEAN VALUES OF PETROPHYSICAL DATA, EL BERROCAL SAMPLES EB1A,B,E,F,J

Rock slice no.	A	B	C	D	E
Distance from fracture (mm)	0-20	22-32	44-64	66-86	88-108
Dry density (kg/m^3)	2622	2625	2625	2624	2628
Total porosity (%)	1.50	1.34	1.34	1.32	1.21
Open porosity (%)	1.36	1.20	1.16	1.11	1.15
Degree of saturation (%)	92.11	91.24	87.48	84.82	95.95
Water content after desorption (%)	0.11	0.11	0.10	0.10	0.11
Void index (%)	0.39	0.36	0.34	0.32	0.34
Water content after 2 days (%)	0.42	0.38	0.36	0.35	0.36
Water content after 5 days (%)	0.44	0.39	0.38	0.36	0.37
Saturation water content (%)	0.52	0.46	0.43	0.42	0.43
Vp, dry (m/s)	5178	5441	5393	5253	5083
Vp, saturated (m/s)	5914	6266	6416	6181	6357

Annex 2. GEOCHEMICAL AND URANIUM SERIES DATA, EL BERROCAL SAMPLE EB3

Sample No.	3.0	3.1	3.2	3.4	3.7	3.11
Distance from fracture (mm)	0-5	8-18	21-31	47-57	96-116	188-208
Major elements (%)						
SiO_2	76.74	74.62	75.41	75.08	75.50	75.17
TiO_2	0.17	0.15	0.15	0.17	0.15	0.15
Al_2O_3	13.60	14.62	13.87	14.54	14.17	14.53
Fe_2O_3	0.36	0.27	0.29	0.41	0.35	0.36
FeO	1.03	0.98	0.98	1.08	0.98	0.99
MgO	0.61	0.57	0.57	0.59	0.59	0.52
CaO	0.56	0.58	0.61	0.60	0.58	0.66
Na_2O	3.43	3.71	3.60	3.72	3.72	3.94
K_2O	4.08	4.84	4.23	4.47	4.28	4.35
P_2O_5	0.31	0.31	0.31	0.31	0.31	0.32
Total	100.89	100.65	100.02	100.97	100.63	100.99
Trace elements (ppm)						
U	22	19	17	16	14	14
Th	8	7	5	7	8	7
Nb	17	17	16	20	19	18
Zr	53	56	55	57	55	54
Y	27	27	27	28	27	27
Sr	10	11	11	12	10	12
Rb	435	488	449	472	468	465
Cs	17	18	18	20	21	18
Sn	13	11	14	15	11	13
V	3	3	2	3	4	Tr
Cr	11	11	12	11	11	11
Mn	198	177	183	212	197	194
Ba	48	50	31	54	34	36
La	11	12	11	13	10	6
Ce	23	22	24	24	25	22
Pb	11	14	10	12	12	13
As	4	3	4	4	3	3
Ga	23	23	23	25	24	23
Zn	56	51	53	61	55	55
Cu	7	6	6	6	6	7
Ni	6	7	6	6	7	6
W	932	646	678	831	571	615
Total Fe (%)	1.39	1.25	1.27	1.49	1.33	1.35
Fe_2O_3/FeO	0.35	0.28	0.30	0.38	0.36	0.36
Th/U	0.36	0.37	0.29	0.44	0.57	0.50
U-234/U-238	0.94	0.91	0.89	0.96	1.03	0.99
Th-230/U-234	1.13	1.26	0.86	1.13	0.85	1.21
Th-230/U-238	1.07	1.14	0.76	1.08	0.88	1.20

Annex 2 continued. PETROPHYSICAL DATA, EL BERROCAL SAMPLE EB3

Sample No.	3.A	3.B	3.C	3.D	3.E	3.F	3.G
Mean distance from fracture (mm)	57	77	97	117	137	157	177
Dry density (kg/m^3)	2621	2609	2631	2611	2622	2632	2620
Total porosity (%)	1.58	1.88	1.31	1.83	1.39	1.21	1.47
Open porosity (%)	1.48	1.49	1.28	1.37	1.32	1.17	1.37
Degree of saturation (%)	93.7	79.3	97.7	74.9	94.2	96.7	93.2
Water content after desorption (%)	0.03	0.04	0.04	0.03	0.03	0.03	0.03
Void index (%)	0.47	0.49	0.39	0.34	0.37	0.34	0.36
Water content after 2 days (%)	0.48	0.49	0.39	0.37	0.37	0.38	0.38
Water content after 5 days (%)	0.51	0.51	0.48	0.43	0.41	0.46	0.45
Saturation water content (%)	0.56	0.57	0.49	0.50	0.50	0.45	0.52
Vp, dry (m/s)	3462	3384	3804	3700	3425	3440	3576
Vp, saturated (m/s)	4921	5176	5468	4868	5139	5733	5166

Annex 2 continued. PETROPHYSICAL DATA, EL BERROCAL SAMPLE EB3

Sample No.	3.H	3.I	3.J	3.K	3.L
Mean distance from fracture (mm)	197	217	237	257	277
Dry density (kg/m^3)	2615	2608	2615	2618	2621
Total porosity (%)	1.65	1.91	1.65	1.54	1.43
Open porosity (%)	1.38	1.48	1.41	1.48	1.40
Degree of saturation (%)	83.6	77.5	85.5	96.1	97.9
Water content after desorption (%)	0.04	0.02	0.03	0.03	0.03
Void index (%)	0.38	0.46	0.44	0.42	0.44
Water content after 2 days (%)	0.42	0.50	0.44	0.42	0.44
Water content after 5 days (%)	0.52	0.50	0.54	0.53	0.48
Saturation water content (%)	0.53	0.57	0.54	0.57	0.54
Vp, dry (m/s)	4091	4091	3687	3956	3916
Vp, saturated (m/s)	5294	5625	5900	5353	5222

The position of each sample is shown graphically in Figure 28.

Annex 3A. GEOCHEMICAL AND URANIUM SERIES DATA, STRIPA SAMPLE ST6

Sample No.	ST6.0	ST6.1	ST6.2	ST6.4	ST6.7
Distance from fracture (mm)	0-5	8-18	21-31	47-57	96-116
Major elements (%)					
SiO_2	74.21	74.37	74.04	74.85	74.97
TiO_2	0.08	0.08	0.08	0.09	0.07
Al_2O_3	13.83	13.91	13.56	13.59	14.26
Fe_2O_3	0.66	0.56	0.66	0.65	0.42
FeO	0.53	0.67	0.79	0.73	0.83
MgO	0.20	0.20	0.21	0.18	0.16
CaO	0.56	0.54	0.56	0.60	0.72
Na_2O	3.93	3.98	3.77	3.75	4.06
K_2O	4.72	4.70	4.57	4.63	4.86
P_2O_5	0.03	0.03	0.04	0.03	0.03
Total	98.75	99.04	98.28	99.10	100.38
Trace elements (ppm)					
U	40	40	42	46	39
Th	23	24	25	26	23
Nb	43	43	49	50	44
Zr	78	85	88	90	85
Y	73	84	85	90	86
Sr	24	26	27	25	27
Rb	237	254	246	256	265
Cs	3	2	3	4	4
Sn	11	13	13	14	11
V	Tr	nd	Tr	nd	1
Cr	13	13	12	13	12
Mn	281	277	343	311	293
Ba	262	259	250	244	255
La	30	30	35	30	21
Ce	64	66	73	68	60
Pb	24	26	24	27	25
As	2	2	2	2	2
Ga	20	20	20	20	20
Zn	9	11	12	13	11
Cu	3	9	5	5	6
Ni	8	8	8	8	7
W	1709	968	951	920	633
Total Fe (%)	1.19	1.23	1.45	1.38	1.25
Fe_2O_3/FeO	1.25	0.84	0.84	0.89	0.51
Th/U	0.58	0.60	0.60	0.57	0.59
U-234/U-238	1.11	1.23	0.96	1.07	1.09
Th-230/U-234	0.72	0.68	0.96	1.15	0.94
Th-230/U-238	0.79	0.84	0.93	1.23	0.98

Annex 3A continued. PETROPHYSICAL DATA, STRIPA SAMPLE ST6

Sample No.	6.A	6.B	6.C	6.D	6.E	6.F	6.G
Mean distance from fracture (mm)	25	55	80	105	130	155	180
Dry density (kg/m^3)	2625	2624	2627	2619	2625	2624	2627
Total porosity (%)	0.69	0.53	0.41	0.82	0.48	Q.52	0.41
Open porosity (%)	0.47	0.43	0.40	0.36	0.36	0.39	0.35
Degree of saturation (%)	68	81	97	58	74	74	85
Water content after desorption (%)	0.00	0.03	0.00	0.00	0.02	0.02	0.00
Void index (%)	0.13	0.13	0.13	0.13	0.11	0.09	0.08
Water content after 2 days (%)	0.16	0.16	0.13	0.13	0.13	0.13	0.13
Water content after 5 days (%)	0.16	0.16	0.13	0.13	0.13	0.13	0.13
Saturation water content (%)	0.21	0.18	0.15	0.14	0.14	0.14	0.13
Vp, dry (m/s)	-	-	-	-	-	-	-
Vp, saturated (m/s)	-	-	-	-	-	-	-

Annex 3B. GEOCHEMICAL AND URANIUM SERIES DATA, STRIPA SAMPLE ST7

Sample No.	ST7.0	ST7.1	ST7.2	ST7.4	ST7.7
Distance from fracture (mm)	0-5	8-18	21-31	47-57	96-116
Major elements (%)					
SiO_2	73.12	74.09	73.36	74.05	73.44
TiO_2	0.08	0.07	0.09	0.08	0.08
Al_2O_3	13.61	13.81	13.48	13.74	13.53
Fe_2O_3	0.61	0.55	0.55	0.59	0.39
FeO	0.61	0.65	0.67	0.69	0.86
MgO	0.03	0.02	0.04	0.04	0.06
CaO	0.61	0.76	0.73	0.80	0.81
Na_2O	3.82	3.82	3.75	3.91	3.72
K_2O	4.78	4.73	4.64	4.56	4.64
P_2O_5	0.03	0.04	0.03	0.04	0.03
Total	97.30	98.54	97.34	98.50	97.56
Trace elements (ppm)					
U	39	41	42	42	40
Th	23	23	23	25	25
Nb	44	43	45	45	47
Zr	80	86	86	89	91
Y	78	82	85	87	87
Sr	24	26	26	26	26
Rb	260	265	261	257	272
Cs	4	4	5	4	5
Sn	13	13	11	11	14
V	2	2	1	Tr	2
Cr	13	12	13	13	12
Mn	467	289	302	335	321
Ba	279	240	239	239	230
La	33	27	30	35	29
Ce	71	67	65	67	66
Pb	31	25	26	28	28
As	1	3	2	2	3
Ga	20	20	20	20	20
Zn	13	14	15	16	16
Cu	4	4	4	5	6
Ni	8	7	7	8	7
W	1403	971	892	862	639
Total Fe (%)	1.22	1.20	1.22	1.28	1.25
Fe_2O_3/FeO	1.00	0.85	0.82	0.86	0.45
Th/U	0.59	0.56	0.55	0.60	0.63
U-234/U-238	-	-	-	-	-
Th-230/U-234	-	-	-	-	-
Th-230/U-238	-	-	-	-	-

Annex 3B continued. PETROPHYSICAL DATA, STRIPA SAMPLE ST7

Sample No.	7.A	7.B	7.C	7.D	7.E	7.F	7.G
Mean distance from fracture (mm)	25	55	80	105	130	155	180
Dry density (kg/m^3)	2625	2624	2629	2623	2620	2623	2628
Total porosity (%)	0.67	0.53	0.34	0.56	0.81	0.56	0.37
Open porosity (%)	0.41	0.38	0.34	0.40	0.34	0.40	0.33
Degree of saturation (%)	61	71	100	71	56	71	89
Water content after desorption (%)	0.00	0.02	0.00	0.00	0.00	0.00	0.00
Void index (%)	0.11	0.07	0.09	0.07	0.09	0.09	0.09
Water content after 2 days (%)	0.14	0.12	0.12	0.12	0.12	0.12	0.12
Water content after 5 days (%)	0.14	0.12	0.12	0.12	0.12	0.12	0.12
Saturation water content (%)	0.18	0.16	0.14	0.15	0.13	0.15	0.13
Vp, dry (m/s)	-	-	-	-	-	-	-
Vp, saturated (m/s)	-	-	-	-	-	-	-

Annex 4A. GEOCHEMICAL AND URANIUM SERIES DATA, WHITESHELL SAMPLE WS1

Sample No.	WS1.0	WS1.1	WS1.2	WS1.4	WS1.7
Distance from fracture (mm)	0-5	8-18	21-31	47-57	96-116
Major elements (%)					
SiO_2	70.00	68.08	73.18	72.36	71.34
TiO_2	0.33	0.41	0.23	0.20	0.21
Al_2O_3	14.16	15.20	14.14	14.43	15.12
Fe_2O_3	2.01	2.05	1.48	1.07	1.42
FeO	1.42	1.78	0.70	0.75	0.65
MgO	1.41	1.65	0.88	0.85	0.71
CaO	0.93	1.71	1.38	1.38	1.43
Na_2O	2.56	3.96	3.93	3.93	4.05
K_2O	5.83	4.09	3.63	4.41	4.65
P_2O_5	0.11	0.29	0.05	0.06	0.06
Total	98.76	99.22	99.60	99.44	99.64
Trace elements (ppm)					
U	3	4	3	3	4
Th	10	19	32	17	29
Nb	13	12	9	6	7
Zr	87	219	214	208	238
Y	13	18	14	13	13
Sr	178	224	227	240	261
Rb	204	181	123	150	158
Cs	1	3	2	1	Tr
Sn	6	10	6	7	6
V	nd	nd	nd	nd	2
Cr	24	30	17	17	17
Mn	301	415	152	156	154
Ba	599	378	438	518	578
La	40	28	58	24	38
Ce	60	57	110	51	71
Pb	4	Tr	Tr	5	6
As	9	9	9	9	9
Ga	18	21	17	17	18
Zn	66	85	34	33	33
Cu	6	6	5	5	5
Ni	12	15	9	8	8
W	123	27	109	99	85
Total Fe (%)	3.43	3.83	2.18	1.82	2.07
Fe_2O_3/FeO	1.42	1.15	2.11	1.43	2.18
Th/U	3.33	4.75	10.67	5.67	7.25
U-234/U-238	1.60	1.05	1.42	1.26	1.29
Th-230/U-234	3.08	1.62	1.36	1.16	1.21
Th-230/U-238	4.92	1.70	1.93	1.47	1.56

Annex 4A continued. PETROPHYSICAL DATA, WHITESHELL SAMPLE WS1

Sample No.	1.A	1.B	1.C	1.D	1.E	1.F	1.G
Mean distance from fracture (mm)	10	30	50	70	90	110	130
Dry density (kg/m^3)	2598	2597	2613	2599	2618	2609	2617
Total porosity (%)	-	-	-	-	-	-	-
Open porosity (%)	2.87	2.13	1.80	2.00	1.64	1.90	1.86
Degree of saturation (%)	-	-	-	-	-	-	-
Water content after desorption (%)	0.15	0.10	0.09	0.04	0.05	0.05	0.08
Void index (%)	0.71	0.33	0.41	0.37	0.45	0.46	0.36
Water content after 2 days (%)	1.00	0.66	0.61	0.52	0.59	0.57	0.59
Water content after 5 days (%)	1.09	0.84	0.65	0.64	0.61	0.57	0.65
Saturation water content (%)	1.11	0.84	0.69	0.77	0.63	0.73	0.71
Vp, dry (m/s)	2723	3100	3433	3833	4380	4452	4392
Vp, saturated (m/s)	3325	3652	4206	4833	4842	5194	4823

The position of each sample is shown graphically in Figure 31.

Annex 4B. GEOCHEMICAL AND URANIUM SERIES DATA, WHITESHELL SAMPLE WS2

Sample No.	WS2.0	WS2.1	WS2.2	WS2.4	WS2.7
Distance from fracture (mm)	0-5	8-18	21-31	47-57	94-114
Major elements (%)					
SiO_2	73.30	70.71	71.72	71.72	71.65
TiO_2	0.27	0.30	0.34	0.34	0.30
Al_2O_3	13.60	14.51	14.66	14.47	14.77
Fe_2O_3	0.75	0.74	0.99	0.80	0.80
FeO	1.03	1.33	1.23	1.30	1.28
MgO	0.74	0.83	0.84	0.79	0.87
CaO	1.36	1.59	1.59	1.60	1.71
Na_2O	3.79	4.13	4.18	4.08	4.34
K_2O	4.28	4.15	4.27	4.32	4.05
P_2O_5	0.07	0.08	0.07	0.09	0.09
Total	99.19	98.37	99.89	99.51	99.86
Trace elements (ppm)					
U	7	6	5	3	5
Th	28	28	28	27	33
Nb	6	7	8	7	7
Zr	193	226	214	218	227
Y	10	12	12	11	14
Sr	197	207	211	211	214
Rb	151	155	148	158	150
Cs	1	nd	Tr	nd	Tr
Sn	6	5	4	4	8
V	nd	nd	nd	nd	nd
Cr	19	14	14	14	13
Mn	200	231	227	246	230
Ba	423	423	439	439	410
La	46	42	43	37	45
Ce	79	66	71	66	74
Pb	9	13	10	11	13
As	9	7	7	8	7
Ga	15	16	17	17	17
Zn	32	38	34	39	39
Cu	5	5	5	5	5
Ni	7	8	7	8	7
W	35	100	88	95	96
Total Fe (%)	1.78	2.07	2.22	2.10	2.08
Fe_2O_3/FeO	0.73	0.56	0.80	0.38	0.63
Th/U	4.00	4.67	5.60	9.00	6.60
U-234/U-238	1.26	1.65	1.17	1.04	1.01
Th-230/U-234	0.81	0.88	0.70	1.22	1.32
Th-230/U-238	1.01	1.44	0.82	1.26	1.34

Annex 4B continued. PETROPHYSICAL DATA, WHITESHELL SAMPLE WS2

Sample No.	2.A	2.B	2.C	2.D	2.E	2.F	2.G
Mean distance from fracture (mm)	31	41	51	61	71	81	91
Dry density (kg/m^3)	2630	2611	2598	2589	2612	2610	2609
Total porosity (%)	-	-	-	-	-	-	-
Open porosity (%)	1.14	2.00	2.44	2.71	2.07	1.65	1.76
Degree of saturation (%)	-	-	-	-	-	-	-
Water content after desorption (%)	0.02	0.02	0.02	0.00	0.00	0.02	0.00
Void index (%)	0.36	0.30	0.29	0.29	0.28	0.34	0.27
Water content after 2 days (%)	0.41	0.36	0.40	0.36	0.43	0.42	0.29
Water content after 5 days (%)	0.41	0.44	0.50	0.42	0.45	0.51	0.29
Saturation water content (%)	0.43	0.77	0.94	1.05	0.79	0.63	0.68
Vp, dry (m/s)	3773	3472	3845	2977	3500	3692	3692
Vp, saturated (m/s)	4611	4182	4450	3469	4000	4156	4550

The position of each sample is shown graphically in Figure 32.

Annex 5. GEOCHEMICAL AND URANIUM SERIES DATA, GRIMSEL SAMPLES

PETROPHYSICAL DATA NOT DETERMINED.

Sample No.	GR1.0	GR1.5	GR2.0	GR2.5
Distance from fracture (mm)	0-5	60-70	0-5	60-70
Major elements (%)				
SiO_2	67.57	68.22	68.67	71.19
TiO_2	0.54	0.52	0.54	0.53
Al_2O_3	16.81	16.43	15.41	16.32
Fe_2O_3	1.10	0.89	1.38	1.57
FeO	2.13	2.65	2.22	1.87
MgO	2.00	1.94	1.87	1.60
CaO	0.93	1.03	1.35	2.18
Na_2O	4.45	5.21	4.44	4.92
K_2O	4.87	4.21	4.07	3.47
P_2O_5	0.16	0.16	0.15	0.16
Total	100.56	101.26	100.10	103.81
Trace elements (ppm)				
U	3	3	7	6
Th	11	8	13	12
Nb	28	26	32	31
Zr	287	284	287	288
Y	48	45	59	60
Sr	118	162	143	247
Rb	195	183	207	177
Cs	3	2	3	3
Sn	11	7	8	9
V	39	43	42	41
Cr	4	5	4	5
Mn	562	616	661	545
Ba	716	652	768	767
La	39	20	27	40
Ce	82	62	64	83
Pb	6	4	29	16
As	3	3	nd	2
Ga	18	18	18	18
Zn	40	42	61	45
Cu	8	8	10	10
Ni	6	6	7	6
W	489	427	609	464
Total Fe (%)	3.23	3.54	3.60	3.44
Fe_2O_3/FeO	0.52	0.34	0.62	0.84
Th/U	3.67	2.67	1.86	2.00
U-234/U-238	1.06	1.22	1.06	1.12
Th-230/U-234	1.01	1.25	1.15	1.11
Th-230/U-238	1.07	1.53	1.15	1.25

(Tr = trace; nd = not detected)

European Communities – Commission

EUR 14352 – Natural analogue and microstructural studies in relation to radionuclide retardation by rock matrix diffusion in granite

M. Montoto, M. J. Heath, A. Rodríguez Rey, V. G. Ruiz de Argandoña, L. Calleja, B. Menéndez

Luxembourg: Office for Official Publications of the European Communities

1992 – V, 124 pp., num. tab., fig. – 21.0 × 29.7 cm

Nuclear science and technology series

ISBN 92-826-4961-X

Price (excluding VAT) in Luxembourg: ECU 13.50

The possibility that radionuclide retardation by rock matrix diffusion will be limited in granitic rocks by geological factors is studied, as well as the possibility that diffusion will be confined to a narrow zone from water-conducting fractures.

Petrophysical measurements, uranium series and geochemical analyses in the rock adjacent to fractures, have been performed to establish the extent of fracture-related microstructural changes that might influence the potential for diffusion and whether or not there is any record of diffusion of uranium, its daughters, or other elements.

The results obtained from El Berrocal (Spain), Stripa (Sweden) and Whiteshell (Canada) granites, suggest that:

(a) there is a zone adjacent to the fractures (generally less than 100 mm) where microstructural changes and enhanced uranium mobility exist;

(b) the evidence for diffusion having taken place in the rock is confined largely to this zone.

So, it appears that diffusivity determinations on rock collected away from the influence of fractures will not give representative data for diffusion modelling, in addition to the effect of distressing after removing rocks from depth.

It is suggested that diffusion will be of limited effectiveness as a retardation mechanism in many granitic rocks, particularly in water movement confined to narrow channels where access by nuclides to the fracture walls is restricted.

Venta y suscripciones • Salg og abonnement • Verkauf und Abonnement • Πωλήσεις και συνδρομές
Sales and subscriptions • Vente et abonnements • Vendita e abbonamenti
Verkoop en abonnementen • Venda e assinaturas

BELGIQUE / BELGIË

Moniteur belge / Belgisch Staatsblad
Rue de Louvain 42 / Leuvenseweg 42
B-1000 Bruxelles / B-1000 Brussel
Tél. (02) 512 00 26
Fax (02) 511 01 84

Autres distributeurs / Overige verkooppunten

Librairie européenne/ Europese boekhandel
Rue de la Loi 244/Wetstraat 244
B-1040 Bruxelles / B-1040 Brussel
Tél. (02) 231 04 35
Fax (02) 735 08 60

Jean De Lannoy
Avenue du Roi 202 /Koningslaan 202
B-1060 Bruxelles / B-1060 Brussel
Tél. (02) 538 51 69
Télex 63220 UNBOOK B
Fax (02) 538 08 41

Document delivery:
Credoc
Rue de la Montagne 34 / Bergstraat 34
Bte 11 / Bus 11
B-1000 Bruxelles / B-1000 Brussel
Tél. (02) 511 69 41
Fax (02) 513 31 95

DANMARK

J. H. Schultz Information A/S
Herstedvang 10-12
DK-2620 Albertslund
Tlf. (45) 43 63 23 00
Fax (Sales) (45) 43 63 19 69
Fax (Management) (45) 43 63 19 49

DEUTSCHLAND

Bundesanzeiger Verlag
Breite Straße
Postfach 10 80 06
D-W-5000 Köln 1
Tel. (02 21) 20 29-0
Telex ANZEIGER BONN 8 882 595
Fax 2 02 92 78

GREECE/ΕΛΛΑΔΑ

G.C. Eleftheroudakis SA
International Bookstore
Nikis Street 4
GR-10563 Athens
Tel. (01) 322 63 23
Telex 219410 ELEF
Fax 323 98 21

ESPAÑA

Boletín Oficial del Estado
Trafalgar, 29
E-28071 Madrid
Tel. (91) 538 22 95
Fax (91) 538 23 49

Mundi-Prensa Libros, SA
Castelló, 37
E-28001 Madrid
Tel. (91) 431 33 99 (Libros)
431 32 22 (Suscripciones)
435 36 37 (Dirección)
Télex 49370-MPLI-E
Fax (91) 575 39 98

Sucursal:

Librería Internacional AEDOS
Consejo de Ciento, 391
E-08009 Barcelona
Tel. (93) 488 34 92
Fax (93) 487 76 59

Llibreria de la Generalitat de Catalunya
Rambla dels Estudis, 118 (Palau Moja)
E-08002 Barcelona
Tel. (93) 302 68 35
302 64 62
Fax (93) 302 12 99

FRANCE

Journal officiel
Service des publications des Communautés européennes
26, rue Desaix
F-75727 Paris Cedex 15
Tél. (1) 40 58 75 00
Fax (1) 40 58 77 00

IRELAND

Government Supplies Agency
4-5 Harcourt Road
Dublin 2
Tel. (1) 61 31 11
Fax (1) 78 06 45

ITALIA

Licosa SpA
Via Duca di Calabria, 1/1
Casella postale 552
I-50125 Firenze
Tel. (055) 64 54 15
Fax 64 12 57
Telex 570466 LICOSA I

GRAND-DUCHÉ DE LUXEMBOURG

Messageries Paul Kraus
11, rue Christophe Plantin
L-2339 Luxembourg
Tél. 499 88 88
Télex 2515
Fax 499 88 84 44

NEDERLAND

SDU Overheidsinformatie
Externe Fondsen
Postbus 20014
2500 EA 's-Gravenhage
Tel. (070) 37 89 911
Fax (070) 34 75 778

PORTUGAL

Imprensa Nacional
Casa da Moeda, EP
Rua D. Francisco Manuel de Melo, 5
P-1092 Lisboa Codex
Tel. (01) 69 34 14

Distribuidora de Livros Bertrand, Ld.ª
Grupo Bertrand, SA
Rua das Terras dos Vales, 4-A
Apartado 37
P-2700 Amadora Codex
Tel. (01) 49 59 050
Telex 15798 BERDIS
Fax 49 60 255

UNITED KINGDOM

HMSO Books (Agency section)
HMSO Publications Centre
51 Nine Elms Lane
London SW8 5DR
Tel. (071) 873 9090
Fax 873 8463
Telex 29 71 138

ÖSTERREICH

Manz'sche Verlags- und Universitätsbuchhandlung
Kohlmarkt 16
A-1014 Wien
Tel. (0222) 531 61-0
Telex 112 500 BOX A
Fax (0222) 531 61-39

SUOMI

Akateeminen Kirjakauppa
Keskuskatu 1
PO Box 128
SF-00101 Helsinki
Tel. (0) 121 41
Fax (0) 121 44 41

NORGE

Narvesen information center
Bertrand Narvesens vei 2
PO Box 6125 Etterstad
N-0602 Oslo 6
Tel. (2) 57 33 00
Telex 79668 NIC N
Fax (2) 68 19 01

SVERIGE

BTJ
Tryck Traktorvägen 13
S-222 60 Lund
Tel. (046) 18 00 00
Fax (046) 18 01 25

SCHWEIZ / SUISSE / SVIZZERA

OSEC
Stampfenbachstraße 85
CH-8035 Zürich
Tel. (01) 365 54 49
Fax (01) 365 54 11

ČESKOSLOVENSKO

NIS
Havelkova 22
13000 Praha 3
Tel. (02) 235 84 46
Fax 42-2-264775

MAGYARORSZÁG

Euro-Info-Service
Pf. 1271
H-1464 Budapest
Tel./Fax (1) 111 60 61/111 62 16

POLSKA

Business Foundation
ul. Krucza 38/42
00-512 Warszawa
Tel. (22) 21 99 93, 628-28-82
International Fax&Phone
(0-39) 12-00-77

ROUMANIE

Euromedia
65, Strada Dionisie Lupu
70184 Bucuresti
Tel./Fax 0 12 96 46

BULGARIE

D.J.B.
59, bd Vitocha
1000 Sofia
Tel./Fax 2 810158

RUSSIA

CCEC (Centre for Cooperation with the European Communities)
9, Prospekt 60-let Oktyabria
117312 Moscow
Tel. 095 135 52 87
Fax 095 420 21 44

CYPRUS

Cyprus Chamber of Commerce and Industry
Chamber Building
38 Grivas Dhigenis Ave
3 Deligiorgis Street
PO Box 1455
Nicosia
Tel. (2) 449500/462312
Fax (2) 458630

TÜRKIYE

Pres Gazete Kitap Dergi Pazarlama Dağitim Ticaret ve sanayi AŞ
Narlibahçe Sokak N. 15
Istanbul-Cağaloğlu
Tel. (1) 520 92 96 - 528 55 66
Fax 520 64 57
Telex 23822 DSVO-TR

ISRAEL

ROY International
PO Box 13056
41 Mishmar Hayarden Street
Tel Aviv 61130
Tel. 3 498 108
Fax 3 544 60 39

CANADA

Renouf Publishing Co. Ltd
Mail orders — Head Office:
1294 Algoma Road
Ottawa, Ontario K1B 3W8
Tel. (613) 741 43 33
Fax (613) 741 54 39
Telex 0534783

Ottawa Store:
61 Sparks Street
Tel. (613) 238 89 85

Toronto Store:
211 Yonge Street
Tel. (416) 363 31 71

UNITED STATES OF AMERICA

UNIPUB
4611-F Assembly Drive
Lanham, MD 20706-4391
Tel. Toll Free (800) 274 4888
Fax (301) 459 0056

AUSTRALIA

Hunter Publications
58A Gipps Street
Collingwood
Victoria 3066
Tel. (3) 417 5361
Fax (3) 419 7154

JAPAN

Kinokuniya Company Ltd
17-7 Shinjuku 3-Chome
Shinjuku-ku
Tokyo 160-91
Tel. (03) 3439-0121

Journal Department
PO Box 55 Chitose
Tokyo 156
Tel. (03) 3439-0124

SINGAPORE

Legal Library Services Ltd
STK Agency
Robinson Road
PO Box 1817
Singapore 9036

AUTRES PAYS
OTHER COUNTRIES
ANDERE LÄNDER

Office des publications officielles des Communautés européennes
2, rue Mercier
L-2985 Luxembourg
Tél. 499 28 1
Télex PUBOF LU 1324 b
Fax 48 85 73/48 68 17

NOTICE TO THE READER

All scientific and technical reports published by the Commission of the European Communities are announced in the monthly periodical **'euro abstracts'**. For subscription (1 year: ECU 110) please write to the address below.

Price (excluding VAT) in Luxembourg: ECU 13.50

OFFICE FOR OFFICIAL PUBLICATIONS
OF THE EUROPEAN COMMUNITIES

L-2985 Luxembourg

ISBN 92-826-4961-X